

RADC-TR-84-28
Final Technical Report
February 1984

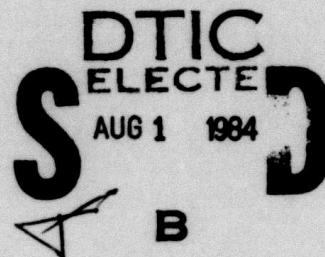


15

ACOSS TWELVE (Active Control of Space Structures)

Lockheed Missiles and Space Company, Inc.

Sponsored by
Defense Advanced Research Projects Agency (DOD)
ARPA Order No. 3654



APPROVED FOR PUBLIC RELEASE; DISTRIBUTION UNLIMITED

The views and conclusions contained in this document are those of the authors and should not be interpreted as necessarily representing the official policies, either expressed or implied, of the Defense Advanced Research Projects Agency or the U.S. Government.

DTIC FILE COPY

ROME AIR DEVELOPMENT CENTER
Air Force Systems Command
Griffiss Air Force Base, NY 13441

84 -7 31 251

This report has been reviewed by the RADC Public Affairs Office (PA) and is releasable to the National Technical Information Service (NTIS). At NTIS it will be releasable to the general public, including foreign nations.

RADC-TR-84-28 has been reviewed and is approved for publication.

APPROVED:



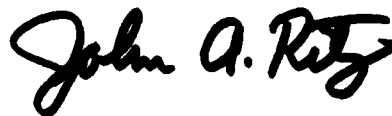
RICHARD W. CARMAN
Project Engineer

APPROVED:



FRANK J. REHM
Technical Director
Surveillance Division

FOR THE COMMANDER:



JOHN A. RITZ
Acting Chief, Plans Office

If your address has changed or if you wish to be removed from the RADC mailing list, or if the addressee is no longer employed by your organization, please notify RADC (OCSE) Griffiss AFB NY 13441. This will assist us in maintaining a current mailing list.

Do not return copies of this report unless contractual obligations or notices on a specific document requires that it be returned.

ACOSS TWELVE
(Active Control of Space Structures)

J.N. Aubrun
J.A. Breakwell
N.K. Gupta
M.G. Lyons

Contractor: Lockheed Missiles and Space Company
Contract Number: F30602-81-C-0260
Effective Date of Contract: 22 July 1981
Contract Expiration Date: 30 May 1983
Short Title of Work: ACOSS TWELVE (Active Control of Space Structures)
Program Code Number: 2E20
Period of Work Covered: September 81 - May 82

Principal Investigator: Arthur A. Woods, Jr.
Phone: (408) 742-2210

RADC Project Engineer: Richard W. Carman
Phone: (315) 330-3148

Approved for public release; distribution unlimited

This research was supported by the Defense Advanced Research Projects Agency of the Department of Defense and was monitored by Richard W. Carman (OCSE) Griffiss AFB NY 13441, under contract F30602-81-C-0260.

DTIC
ELECTE
AUG 1 1984
B

UNCLASSIFIED

SECURITY CLASSIFICATION OF THIS PAGE (When Data Entered)

REPORT DOCUMENTATION PAGE		READ INSTRUCTIONS BEFORE COMPLETING FORM
1. REPORT NUMBER RADC-TR-84-28	2. GOVERNMENT AGENCY AM3829	3. RECIPIENT'S CATALOG NUMBER
4. TITLE (and Subtitle) ACOSS TWELVE (ACTIVE CONTROL OF SPACE STRUCTURES)		5. TYPE OF REPORT & PERIOD COVERED Final Technical Report September 81 - May 82
7. AUTHOR(s) J.N. Aubrun M.G. Lyons J.A. Breakwell N.K. Gupta		6. PERFORMING ORG. REPORT NUMBER LMSC-D883023
8. PERFORMING ORGANIZATION NAME AND ADDRESS Lockheed Missiles and Space Company, Inc. 1111 Lockheed Way Sunnyvale CA 94086		9. CONTRACT OR GRANT NUMBER(s) F30602-S1-C-0260
11. CONTROLLING OFFICE NAME AND ADDRESS Defense Advanced Research Projects Agency 1400 Wilson Blvd Arlington VA 22209		10. PROGRAM ELEMENT, PROJECT, TASK AREA & WORK UNIT NUMBERS 62301E C6540112
14. MONITORING AGENCY NAME & ADDRESS (if different from Controlling Office) Rome Air Development Center (OCSE) Griffiss AFB NY 13441		12. REPORT DATE February 1984
		13. NUMBER OF PAGES 260
		15. SECURITY CLASS. (of this report) UNCLASSIFIED
		16. DECLASSIFICATION/DOWNGRADING SCHEDULE N/A
18. DISTRIBUTION STATEMENT (of this Report) Approved for public release; distribution unlimited		
17. DISTRIBUTION STATEMENT (of the abstract entered in Block 20, if different from Report) Same		
19. SUPPLEMENTARY NOTES RADC Project Engineer: Richard W. Carman (OCSE)		
20. KEY WORDS (Continue on reverse side if necessary and identify by block number) Control Theory Micro-Vibration Suppression Large Space Structures Stability Augmentation Structural Dynamics Low and High Authority Control Flexible Vehicles Steady State Disturbance Rejection (Cont'd)		
21. ABSTRACT (Continue on reverse side if necessary and identify by block number) The theory of steady state and broad band random disturbance rejection for large space structures is developed and tested analytically on a complex optical strawman configuration. It is shown that active control is potentially feasible for micro-vibration stabilization of precision large structures. A number of brassboard experiments have been carried out to illustrate the theory and to address implementation and mechanization of active control systems with both analog and digital approaches.		

DD FORM 1 JAN 73 1473 EDITION OF 1 NOV 65 IS OBSOLETE

UNCLASSIFIED

SECURITY CLASSIFICATION OF THIS PAGE (When Data Entered)

UNCLASSIFIED

SECURITY CLASSIFICATION OF THIS PAGE (When Data Entered)

Item 19. Key Words (Cont'd)

Multivariable Control
Optimal Regulators

UNCLASSIFIED

SECURITY CLASSIFICATION OF THIS PAGE (When Data Entered)

TABLE OF CONTENTS

<u>Section</u>	<u>Page</u>
1 INTRODUCTION	1
1.1 Background	1
1.2 Objectives for Phase II	4
1.3 Scope	5
1.4 Report Format	5
2 TECHNOLOGY ACHIEVEMENTS	6
2.1 Major Findings and Results	6
2.2 Summary of Past Achievements During Phases 1 and 1A	8
2.3 Relationship to Existing Technology	15
2.4 Recommendations for Continuing Studies	18
3 ANALYTICAL ACTIVITIES	19
3.1 Objectives and Approach	19
3.2 Tasks Related to the Statement of Work	20
3.3 Control Design Methodology Summary: Comments on ACOSS 5	22
3.4 New Results on Model Reduction Methodology	28
3.4.1 Introduction	28
3.4.2 Model Reduction Issues	30
3.4.3 Mode-Selection Using Internal Balancing Theory	30
3.4.4 Mode-Selection Methodology	31
3.5 ACOSS Model Results for Disturbance Rejection	34
3.5.1 Modifications of the Disturbance Input	34
3.5.2 Broadband Disturbance Control Design	39
3.5.3 Model Reduction	42
3.5.4 Control Design	42
3.5.5 Full-Spectrum Control Design	54
3.5.6 Principal Conclusions	69
3.6 Robustness Issues and Techniques	69

3.6.1	Some Techniques	70
3.6.2	Robustness Investigation Program	76
3.7	Digital Controller Characteristics and Implementation	79
3.7.1	Multivariable Control Mechanizations	79
3.7.2	Stability Analysis	81
3.7.3	Architecture of the Controller	84
3.7.4	Requirements for Anti-Aliasing Filters	84
3.8	Identification of Control Design Models	90
3.8.1	Identification Requirements	90
3.8.2	Model Forms	93
3.8.2.1	Transfer Function Models	94
3.8.2.2	State Variable Models	95
3.8.3	Identification Algorithms	98
3.8.3.1	Least Squares	99
3.8.3.2	Extended Kalman Filter	99
3.8.3.3	Recursive Prediction Error Methods	99
3.8.3.4	Maximum Likelihood Method	100
3.8.4	Robust Identification	101
3.8.4.1	Nonwhite Noise	102
3.8.4.2	Non-Gaussian Noise	105
3.8.4.3	Selection of Model Order	106
3.8.4.4	Numerical Techniques, Program Architecture and Input/Output Considerations	106
3.8.4.4.1	Numerical Techniques	107
3.8.4.4.2	Convergence Properties	107
3.8.5	Results from Experimental Data	108
3.8.5.2	Closed-Loop Data with Low Gain	113
3.8.5.3	Closed Loop (High Gain)	120
3.8.6	Conclusion and Summary	120
4	EXPERIMENTAL VERIFICATIONS	126
4.1	Objectives and Approach	126
4.2	Experiment Description Overview	127
4.3	Circular Plate Experiment	128

4.3.1	Description	128
4.3.2	Test Plan	138
4.3.3	Results	141
4.4	Truss Wheel Experiment	168
4.4.1	Description	168
4.4.2	Test Plan	174
4.4.3	Results	174
4.5	Proof-of-Concept Experiment	179
4.5.1	Progress	179
REFERENCES		219
APPENDIX A: REDUCTION OF LARGE FLEXIBLE SPACECRAFT MODELS USING INTERNAL BALANCING THEORY		221

Accession For	
NTIS (GAI)	<input checked="checked" type="checkbox"/>
DTIC TAB	<input type="checkbox"/>
Unannounced	<input type="checkbox"/>
Justification	
By	
Distribution/	
Availability Codes	
Dist	Avail and/or Special
A-1	



ILLUSTRATIONS

<u>Figure</u>	<u>Title</u>	<u>Page</u>
2-1	ACOSS Phase I Analytical Results	9
2-2	ACOSS Phase I Experimental Results	11
2-3	ACOSS Phase IA Theoretical Demonstration Model	12
2-4	ACOSS Phase IA Analytical Results - Disturbance Rejection - CSDL No. 2	13
2-5	ACOSS Phase IA Experimental Results	14
2-6	ACOSS Phase IA Experimental Results	16
2-7	ACOSS Phase IA Experimental Results	17
3-1	CSDL No. 2 - Disturbance and Actuator/Sensor Locations	35
3-2	Disturbance PSD	35
3-3	Input PSD Geometrical Relationship at Node No. 37 and Node No. 46	37
3-4	Open-Loop Flexible Nodes	41
3-5	Open-Loop Modal Analysis	43
3-6	Modal Analysis - LOS Breakdown	44
3-7	Open-Loop Modal Cost	45
3-8	26th Order Control Design Spectrum: X-Control, O-Filter	48
3-9	Closed-Loop HAC Spectrum - Broadband Disturbance Control	51
3-10	Closed-Loop HAC/LAC Spectrum - Wideband Disturbance Control	52

ILLUSTRATIONS (Continued)

<u>Figure</u>	<u>Title</u>	<u>Page</u>
3-11	"Component-Cost" for Open-Loop Modal Coordinates	53
3-12	Modal Excitation Due to 8 Hz Sine Disturbance	56
3-13	Closed-Loop Design Spectrum: Wideband + Frequency Shaping	62
3-14	Closed-Loop Spectra for Frequency-Shaped HAC/LAC (X:P0, 0:P2, *:P4)	64
3-15	Closed-Loop HAC/LAC Frequency Response	67
3-16	Sensitivity to Variations in the 8 Hz Sine Disturbance	68
3-17	Singular Values of Return Difference Matrix	72
3-18	$\log_{10} (L(1+L)^{-1})$ State Feedback Only (2-Mode Example)	74
3-19	Adaptive Control with Unmodeled Pole Pair	78
3-20	Minimum Number of Bits for Stable Control Computations	83
3-21	An Architecture for High-Speed Control	83
3-22	Plant and Control Loop Schematic	86
3-23	Maximum Bandwidth vs Bending Frequency	87
3-24	Optimal Design with Prefilter	88
3-25	Maximum Bandwidth vs Bending Frequency for Optimal Controller with Filter	89
3-26	Closed-Loop Frequency Responses	91
3-27	Robust Maximum Likelihood Implementation	104
3-28	Plate Experiment Details	109
3-29	Record 1: Open-Loop Test Data	110

ILLUSTRATIONS (Continued)

<u>Figure</u>	<u>Title</u>	<u>Page</u>
3-30	Input and Output at Channel 5 (Rotation at Right)	110
3-31	Input and Output Spectrum	111
3-32	Measured Transfer Function	111
3-33	Estimated Poles and Zeroes	114
3-34	Measured and Estimated Time History Comparisons	114
3-35	Output Error Spectrum	115
3-36	Comparison of Measured and Estimated Transfer Functions	115
3-37	Closed-Loop Data (Low Gain)	116
3-38	Channel 5 Time History (Closed Loop - Low Gain)	117
3-39	Two Significant Modes	117
3-40	Input Spectrum and Channel 1 Spectrum	118
3-41	Input Spectrum and Channel 5 Output Spectrum	118
3-42	Transfer Function Between Channel 5 and Input	119
3-43	Comparison of Identified and Measured Transfer Functions	119
3-44	Channel 5 Transfer Function Cross Plot	121
3-45	High Gain Closed-Loop Data Time Histories	121
3-46	Input and Output Spectra for High Gain Closed-Loop System	122
3-47	Identified Poles and Zeroes	122
3-48	Measured and Estimated Transfer Functions	123

ILLUSTRATIONS (Continued)

<u>Figure</u>	<u>Title</u>	<u>Page</u>
4-1	Circular Plate Experiment	129
4-2	Proof-of-Concept Experiment	129
4-3	Truss Wheel Experiment	130
4-4	Plate Experiment: General Schematic	131
4-5	Circular Plate Experiment: Angular Optical Sensing System	133
4-6	Circular Plate Experiment Sensors and Actuators Definition	134
4-7	Modal Frequencies (Hz) and Patterns for Circular Plate Experiment	137
4-8	Plate Experiment - Overall Configurations	139
4-9	Control Experiment Procedure	142
4-10	Circular Plate Experiment Response to Excitation at First Bending Frequency	146
4-11	Circular Plate Experiment Optimal State Estimates After Excitation at First Bending Frequency	147
4-12	Circular Plate Experiment - Actual and Estimated Uncontrolled Bending Response to Excitation at the Resonant Frequency	148
4-13	Circular Plate Experiment: Optimal Filter Frequency Discrimination Against Irrelevant Modes	150
4-14	Circular Plate Experiment - Quasi-Static Observer	151
4-15	Circular Plate Experiment - Excitation and Control Inputs	156
4-16	Circular Plate Experiment - Excitation and Sensor Outputs	157
4-17	Circular Plate Experiment - Control and Evaluation Sensors Output	158
4-18	Circular Plate Experiment - Static Observer Output (Chirp Input)	159

ILLUSTRATIONS (Continued)

<u>Figure</u>	<u>Title</u>
4-19	Circular Plate Experiment - Transfer Function Plot Y5/U5
4-20	Circular Plate Experiment - Modal Identification by Curve Fitting (VAMP)
4-21	Circular Plate Experiment - Modal Identification by Curve Fitting (VAMP)
4-22	Circular Plate Experiment - Combined O/L and C/L Frequency Responses of Sensors #5 and 6
4-22a	Wheel Actuators and Sensors
4-22b	Components of the Wheel Finite Element Model
4-22c	Complete Wheel Model
4-23	Truss Wheel Experiment Optical System Model for Truss Wheel
4-24	Wheel Test Matrix
4-25	Sinewave Integration Fourier Transform SWIFT (VAMP Implementation)
4-26	Structure Characterization Configuration
4-27	Truss Wheel Experiment Test Results
4-28	Summary of POC Test Results
4-29	Open Loop State Estimator Output
4-30	Open Loop Test Measurements
4-31	Open Loop Test Measurements (Continued)
4-32	Time History Comparison Yaw Gyro Measurement and Prediction Open Loop Test
4-33	Time History Comparison Pitch Gyro Measurement and Prediction Open Loop Test
4-34	Time History Comparison Roll Gyro Measurement and Prediction Open Loop Test

ILLUSTRATIONS (Continued)

<u>Figure</u>	<u>Title</u>	<u>Page</u>
4-35	Time History Comparison Horizontal LOS Laser Measurement and Prediction Open Loop Test	
4-36	Time History Comparison Vertical LOS Laser Measurement and Prediction Open Loop Test	
4-37	Time History Comparison Horizontal Transverse Laser Measurement and Prediction Open Loop Test	
4-38	Time History Comparison Vertical Transverse Laser Measurement and Prediction Open Loop Test	
4-39	Closed Loop State Estimator Output	
4-40	Closed Loop Test Measurements	
4-41	Closed Loop Test Measurements (Continued)	
4-42	Time History Comparison Yaw Gyro Measurement and Prediction Closed Loop Test	
4-43	Time History Comparison Pitch Gyro Measurement and Prediction Closed Loop Test	
4-44	Time History Comparison Roll Gyro Measurement and Prediction Closed Loop Test	
4-45	Time History Comparison Horizontal LOS Laser Measurement and Prediction Closed Loop Test	
4-46	Time History Comparison Vertical LOS Laser Measurement and Prediction Closed Loop Test	
4-47	Time History Comparison Horizontal Transverse Laser Measurement and Prediction Closed Loop Test	
4-48	Time History Comparison Vertical Transverse Laser Measurement and Prediction Closed Loop Test	
4-49	Software Time Delay Transfer Function CMG Command to CMG Output	
4-50	Rate Gyro Time Delay	
4-51	Caging Loop Dynamics Gimbal Rate Command and Gimbal Position	

ILLUSTRATIONS (Continued)

<u>Figure</u>	<u>Title</u>
4-52	Transfer Function CMG Command to CMG Output
4-53	Rate Gyro Rolloff Transfer Function Magnitude Pitch Accelerometer to Pitch Rate Gyro
4-54	Closed Loop State Estimator Output with Integral States Added

TABLES

<u>Table</u>	<u>Title</u>	<u>Page</u>
I	Disturbance Model	38
II	Rankings Used for Mode Selection	46
III	LQG Design for Wideband Disturbance Rejection	47
IV	Closed-Loop Filter Spectrum	49
V	Stochastic Performance Analysis for Wideband Disturbance Rejection Control (PO)	55
VI	Modal Analysis of Sine Disturbances	57
VII	LOS Effect of Sine Disturbance	59
VIII	Control and Filter Design	61
IX	Filter Design Spectrum	63
X	Wideband Plus Sine Disturbance Rejection: Performance Summary (PO)	65
XI	Wideband Plus Some Disturbance Rejection: Closed-Loop Performance Comparison	66
XII	Robustness Improvements Via Frequency Shaping	72
XIII	Comparison of Closed-Loop Modal Shift (2-Mode Example)	74
XIV	3-Mode Example - Model (Reduced)	77
XV	Propagation of Noise and Vibraton	77
XVI	Selection of Control Algorithm Form	80
XVII	Steady-State LQC Controller Form	80
XVIII	Description of Channels	112
XIX	Results (Using Recursive Maximum Likelihood)	116
XX	Closed-Loop Poles	124

TABLES (Continued)

<u>Table</u>	<u>Title</u>	<u>Page</u>
XXI	Control, Measurement and State Vectors Definition	135
XXII	Circular Plate Test Matrix Control Experiments	140
XXIII	Results of the First Series of Tests	144
XXIV	16 States Control Synthesis Model	153
XXV	16 States HAC Controller	154
XXVI	Closed-Loop Poles	164
XXVII	Circular Plate Experiment Significant Results	167
XXVIII	Modal Characteristics of POC Specimen	182

Section 1 INTRODUCTION

1.1 BACKGROUND

This report describes work performed at LMSC on the DARPA/ACOSS Phase II program (ACOSS-12). This active control of space structures (ACOSS) research activity, sponsored by the Defense Advanced Research Projects Agency (DARPA), has encompassed three major phases, beginning with basic analytical investigations in Phase I, detailed experimental brassboard development in Phase 1A, and experimental testing and proof-of-concept demonstrations in Phase II. The overall ACOSS program was motivated by mission planning objectives requiring deployment of large flexible structures, usually for surveillance, space defense, or communications applications, which must have stability augmentation or dynamic shape control (including shape error suppression) to meet performance requirements. Achievement of these system objectives is quite difficult and usually requires near diffraction-limited performance for aperture diameters greater than 5 m.

The difficulties in achieving high performance arise both from the need to minimize system mass and fundamental limitations imposed by material properties. High system mass may entail multiple launches and on-orbit assembly, greatly increasing system cost. In addition, structural design and materials limitations may, in many cases, make high performance unreachable with any mass in a passive system. In general, such constraints result in highly flexible spacecraft which exhibit poor dimensional precision. Our current ability to conceptualize space systems, to select structural materials, and to build mechanisms for on-orbit construction and deployment has now far outstripped our demonstrated ability to control the resulting structures. This observation has, in recent years, given impetus to the idea of building control-configured spacecraft using active stability augmentation systems, integrated with the spacecraft structure in the design process, to achieve what passive methods alone cannot accomplish.

Integration of structural and control design is, of course, a well established discipline for high-performance aircraft, but its extension to flexible spacecraft is by no means straightforward. Not only are the control requirements quite different, but spacecraft structural dynamics also give rise to a dense spectrum of nearly undamped, poorly identified modes, some of which must be significantly controlled without destabilizing the closed-loop system. These features of the Large Space Structures (LSS) control problem place particularly strong emphasis on model reduction techniques which can produce good control design models and on control synthesis procedures which limit high controller performance to regions where model fidelity is sufficient to guarantee a robust design. It has now been demonstrated that both design model selection and controller synthesis are closely linked to the specification of the system performance metric, and, indeed, the difficulty of these tasks is extremely sensitive to this performance specification. It is essential that the contribution of various components of the plant dynamics to overall performance be clearly identified at the outset.

The control requirements for large structures may be broadly divided into three categories: (1) attitude control in the presence of structural bending; (2) transient vibration suppression (usually required during maneuvering); and (3) suppression of steady-state vibration propagation due to on-board disturbance sources. Stability augmentation and flight control system configurations are dictated by mission-dependent mixes of these objectives. Three other considerations can also influence these configurations. Vibration isolation, an important ingredient in vibration suppression architectures, is nonetheless an electromechanical design problem and is not, per se, part of the control configured structural design process, i.e., isolator properties may be embedded in the design prior to controls synthesis activities. Similarly, the insertion of passive damping via materials selection has not properly been a subject for research in ACOSS. Small amounts of passive damping are generally desirable for LSS systems. It has been shown [1], however, that high performance is not obtainable via passive techniques and, in some instances, large amounts of structural damping can actually degrade system performance. Finally, jitter suppression systems may also

involve active mirrors or adaptive antenna feed structures which are often required to perform beam steering or high-bandwidth jitter suppression. Control design for these systems is a well established discipline developed in other research activities.

The main purpose of the ACOSS control strategies is to reduce structural vibration amplitudes to acceptable levels. In this context, shape control can be interpreted to mean reduction of dynamic shape error (wave front error) and, thus, only static absolute shape measurement would be required; vibration suppression about a nominal shape requires no dynamic shape measurement or actuators which directly control shape. For some systems designs, dynamic figure control is proposed to implement adaptive optics. For large reflecting surfaces, dynamic absolute shape control then requires both high-bandwidth figure sensing systems and structural stability augmentation. This approach to shape control may be considered excessively complex and is yet to be tried on high-order strawman systems.

The purpose of the DARPA/ACOSS program, through the first three program phases, has been to investigate the feasibility of implementing control-configured spacecraft through development of control synthesis and performance evaluation procedures and by assessment of hardware requirements, through brassboard demonstrations, for flight experiment programs. During the initial program phases, the principal points of concentration were: (1) ensuring system stability (the "spillover" problem) and, (2) the construction of adequate ground based experiments (experiments unaffected by aerodynamics and suspension interaction). After numerous analytical studies on both the (Charles Stark Draper Laboratory) CSDL #2 strawman optical system and various experiment designs, together with hardware verification on seven ground test experiments, the research emphasis has now shifted to achieving high performance with robustness and to developing actuators, sensors, and signal processing to handle constraints imposed by operational systems. These issues are very much brought to light in the Phase II activity discussed in this report.

The controls synthesis approach advocated in this study is basically the two-level technique discussed in detail in the ACOSS Five Final Report [1]. At one level, specific structural mode shapes and modal dampings were significantly modified by plant-dependent estimator/controller forms referred to as high-authority controllers (HAC). At the other level, small amounts of damping were introduced by colocated actuator/sensor pairs using rate-feedback (output feedback) control laws synthesized with very little dependence on knowledge of plant parameters. These low-authority control (LAC) mechanizations provided the basis for reducing spillover instability created by high-authority controls. This methodology was exercised in detail during Phase II.

1.2 OBJECTIVES FOR PHASE II

The principal objectives for this study were organized to extend the results obtained in Phase IA by increasing the depth of some investigations and by implementing more complex controllers on existing brassboards. For these reasons, the research consolidates understanding rather than attempting development of entirely new areas. The analytical objectives include:

- 1) Extension of disturbance rejection techniques to include broadband input power spectra.
- 2) Refinement of model reduction methods.
- 3) Examination of recursive identification methods.
- 4) Identification of appropriate adaptive control strategies.

The experimental objectives were:

- 1) Demonstration of digital multi-mode control for the circular plate brassboard including a general assessment of sampling effects.
- 2) Integration of the microvibration sensing system (constructed during Phase IA) into the circular plate control system.
- 3) Investigation of system identification methods on the plate and truss-wheel structures.

- 4) Demonstration of modal control on the proof-of-concept (POC) structure.

1.3 SCOPE

This report summarizes the Phase II ACOSS activity in terms of principal results, conclusions, and supporting data. Sufficient detail is provided so that interested researchers can replicate the analytical results for CSDL #2. Experimental details are adequate to express the depth of the investigation and to motivate the findings, but not to replicate the experiments. Many references are made to the ACOSS Five Final Report [1], and the technology primer within that report which details much of the controls synthesis and evaluation procedures. This report represents an adjunct to [1].

1.4 REPORT FORMAT

The report begins in Section 2 with an overview of major findings and a review of previous principal results from the first two phases. The technology status is reviewed and recommendations for continuing research are proposed. In Section 3 the main analytical results for disturbance rejection and model reduction exercises for CSDL #2 are given. System identification and adaptive methods are reviewed here as well. Section 4 discusses experimental verification activities including circular plate, truss-wheel, and POC experiments; Section 5 summarizes program conclusions and recommendations. Model reduction theorems are provided in Appendix A.

Section 2

TECHNOLOGY ACHIEVEMENTS

2.1 MAJOR FINDINGS AND RESULTS

The principal findings in ACOSS Phase II reinforced and expanded the analytical and experimental results first obtained in Phase 1A. These findings may be treated as originating from either the analytical or experimental sides of the program, although in many cases this distinction is artificial. Analytical studies on the CSDL #2 model concentrated on disturbance rejection controls using a colored wideband disturbance which also included three discrete frequencies. Several conclusions were reached regarding this general disturbance rejection problem.

1. Using design models valid for about 25% of the available (and excited) modes, broadband noise effects on the LOS can be reduced by about two orders of magnitude. Further reductions will require some form of identification prior to or during control.
2. Narrow-band Disturbance propagation to the LOS performance metric can be reduced to zero in the absence of input frequency estimate error and sensor noise. Sufficient model accuracy near the disturbance frequency is needed to stabilize the plant. Disturbance frequency identification may be required.
3. Design model selection via internal balancing and mode selection using four disturbability and controllability criteria appears to produce excellent reduced-order synthesis models. This technique also allows evaluation of the selected sensor/actuator configuration.
4. Improvements to performance sensitivity and robustness for narrow-band disturbances have been demonstrated for low-order models using indirect adaptive methods. High-order evaluations remain to be demonstrated for LSS.

Experimental activities further confirmed HAC and LAC synthesis procedures but also underscored particular difficulties with hardware implementation. Specific findings included:

For the Plate Experiment

1. Digital modal control of five bending modes (damping augmentation in the 5-10% range) and three rigid body modes was achieved.
2. Adequate three DOF controllability of the rigid body required three Contactless Electromagnetic (CEM) actuators.
3. Identification of control and sensor distribution matrices was required to correct the analytical design model.
4. Low frequency sensitivity and drift problems of the piezoelectric (PZT) accelerometers necessitated use of microphase optical sensing for rigid body/modal control.
5. Adequate filter performance required static observer pre-filters to reject spatially irrelevant modes.

For the Proof-of-Concept (POC) Experiment

1. Multi-mode digital control was confirmed for a three-rigid-body-mode and five- structural-bending-mode model (3-5% range). Centralized actuators, namely Control Moment Gyros (CMGs), were used with central body rate gyros as sensors.
2. Accommodations in the control design process were necessary to account for non-ideal hardware. These corrections were necessary for:
 - a. time delays in control software
 - b. rate gyro sampling delays
 - c. CMG transfer function zeros near bending frequencies
 - d. rate-gyro bandwidth limitations
 - e. CMG washout at low frequencies

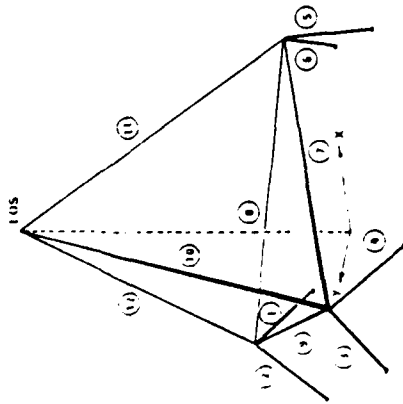
For System Identification

1. Recursive maximum likelihood provided excellent identification of system transfer functions, modal damping, and model parameters as long as spectral filtering was used to eliminate low frequency sensor drift.
2. Maximum likelihood methods provide much more accurate estimates of damping ratios than do Fast Fourier Transform (FFT) methods.
3. Considerably more testing is required to understand the requirements for and the limitations of system identification methods.

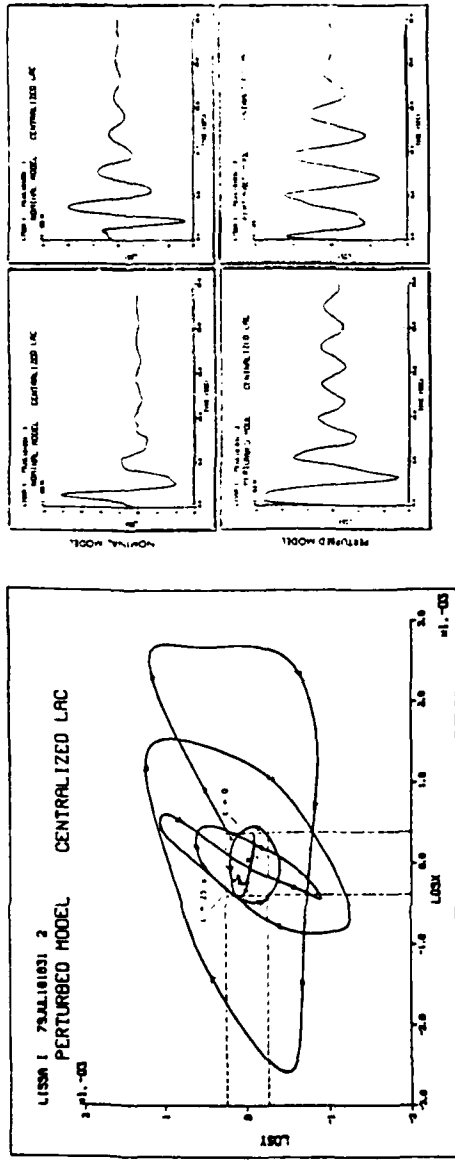
2.2 SUMMARY OF PAST ACHIEVEMENTS DURING PHASES 1 and 1A

For background and to add historical perspective to analytical and experimental activities described in this report, previous results are now quickly summarized. The integrated low and high-authority control policies, described in detail in the technology primer of [1], were applied to the 12 mode CSDL #1 tetrahedral model near the end of Phase 1, a research study on control techniques with no formal experimental requirements. A typical result for the CSDL #1 "Line-of-Sight" (LOS) damping control is shown in Fig. 2-1. The control objective was to increase modal damping in modes 1, 2, 4, and 5 to at least 10% and to reduce vertex transient motion below pre-specified levels within 20 seconds [2]. This was easily accomplished using six colocated actuators and sensors in the legs supporting the structure [2]. Many different control laws (centralized and decentralized) performed adequately. Major conclusions about design methodologies could not be drawn, however, because this example (1) is not representative of actual, complex structures (2) does not require low-order design model selection (3) uses a design model which is too large compared to the evaluation model and (4) requires very modest closed-loop performance. In fact, many control design strategies can be invoked to produce acceptable closed-loop performance for this model.

CSDL-MODEL NO. 1



CLOSED-LOOP LOS MOTION



OPEN-LOOP PERFORMANCE – MOTION NEARLY UNDAMPED (≤ 0.5 PERCENT)

CLOSED-LOOP PERFORMANCE – MODES 1, 2, 4, 5 ≥ 10 PERCENT DAMPING

BASIC TECHNOLOGY VERIFIED

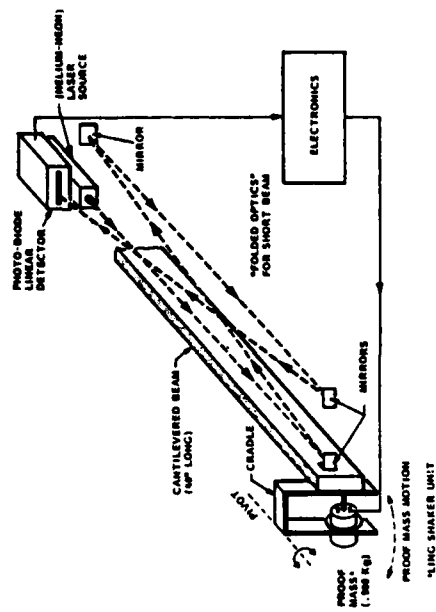
- 8-MODE DESIGN MODEL – 12-MODE EVALUATION MODEL
- TRANSIENT SETTTLING PROBLEM STUDIED
- HAC AND LAC USED TO INCREASE MODAL DAMPING (COLOCATED AND NONCOLOCATED)
- SOFTWARE INTERFACE ESTABLISHED – CONTROL SYNTHESIS AND FINITE-ELEMENT MODEL

Figure 2-1 ACROSS Phase I Analytical Results

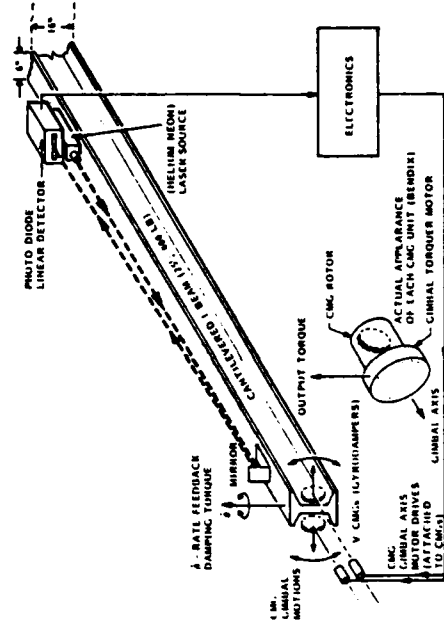
Experimental work in Phase 1 was restricted to low-authority (collocated r feedback) control demonstrations using both a small 40 in. beam with a pr mass actuator and a large 25 ft. beam with a pair of control moment gyros. The basic results are indicated in Fig. 2-2. Because the beam was clamped one end, there was no rigid body mode in either experiment, and high values of modal damping could be obtained in the first bending mode.

Phase 1A focused on more difficult analytical and experimental studies complex enough to test both design methodologies and experiment designs. The CSDL #2 model, shown in Fig. 2-3, was introduced as a more appropriate representation of an actual control design problem with a structure deliberately "softened" to exacerbate the controls/structures interaction. Performance objectives were extended to include narrow-band disturbance rejection, using a vector-valued performance metric, along with the usual stability augmentation. Robustness was examined with a series of perturbation models indicated in the figure. Performance is summarized in Fig. 2-4 with a comparison between open-loop, passive damping, and active control. Artificial insertion of modal damping creates transfer function zero shifting which, for narrow band disturbances, can degrade LOS performance as shown. Active performance using frequency-shaping near the disturbance frequencies, exceeds five orders-of-magnitude, assuming no sensor noise and perfect knowledge of the disturbance frequency. Modest actuator force levels for the 21 actuators used were noted. Numerical problems in the eigenvalue decomposition should be noted here; the actual LOS error should be zero.

Experimental work in this phase concentrated on verification of LAC and L design methods emphasizing problems caused by hardware deficiencies. Fig. 2-5 illustrates the damping prediction and realization results for a thin vertical rod controlled by two orthogonal proof-mass dampers. The control law mechanizations were analog. Extremely good agreement between analytical and experimental results was obtained, due, in part, to the development of the flex-pivoted proof-mass device which uses high-bandwidth electrodynamic motors and local rate feedback to wash out actuator dynamics.

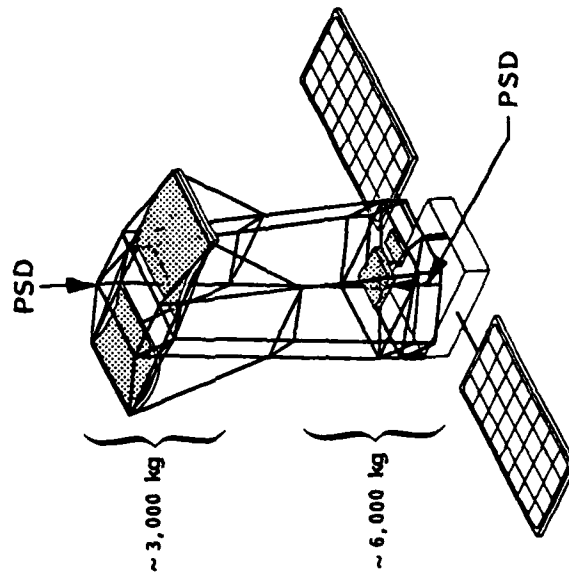


MINIBEAM LAC DEMONSTRATION



MAXIBEAM LAC DEMONSTRATION

- 40-in. BEAM, LASER OPTICS
 - PROTOTYPE PROOF-MASS TESTED
 - LAC CONCEPT - 2-MODE DEMONSTRATION
 - 50 PERCENT DAMPING PRODUCED - MODE 1
 - 20 PERCENT DAMPING PRODUCED - MODE 2
-
- 400-lb, 25-ft BEAM, 1-Hz LASER OPTICS
 - CMC BEAM END ROTATION CONTROL
 - > 20 PERCENT DAMPING - MODES 1 AND 7



CSDL MODEL NO. 2

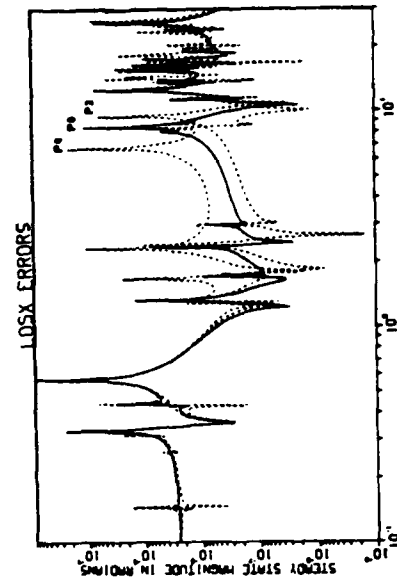
CHARACTERISTICS

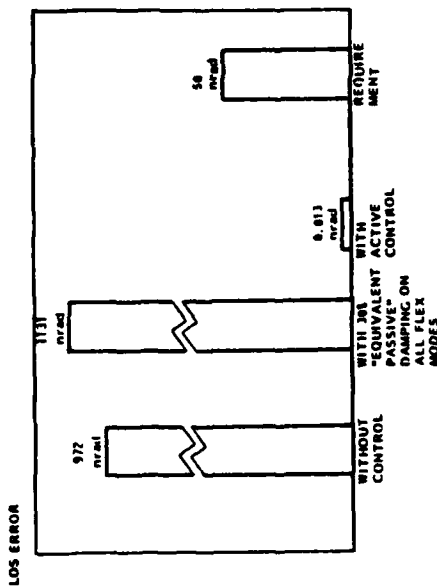
- HEIGHT ~ 28 m, WEIGHT 9,300 kg
- 306 DOF
- 137 STIFFNESS ELEMENTS
- 51 NODES
- 84 NONZERO MASS ELEMENTS

CONTROL IMPLEMENTATION

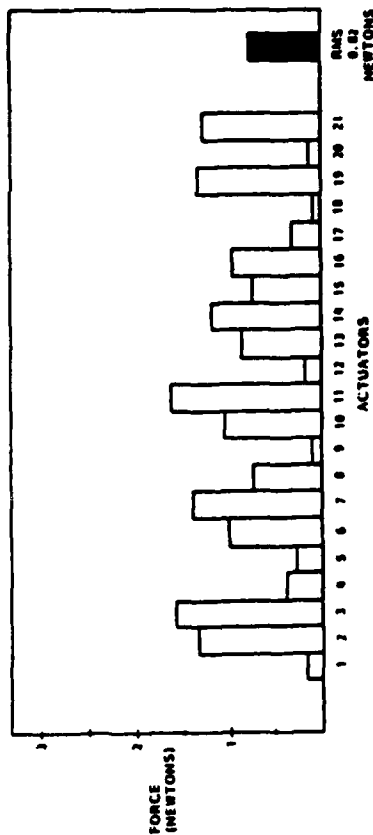
- 3 RIGID-BODY MODES
- 41 FLEXIBLE MODES

DYNAMICS





LOS PERFORMANCE



INPUT DISTURBANCE

- TOP - 10 N AT 10 Hz
- BOTTOM - 20 N AT 5 Hz

CONTROL IMPLEMENTATION

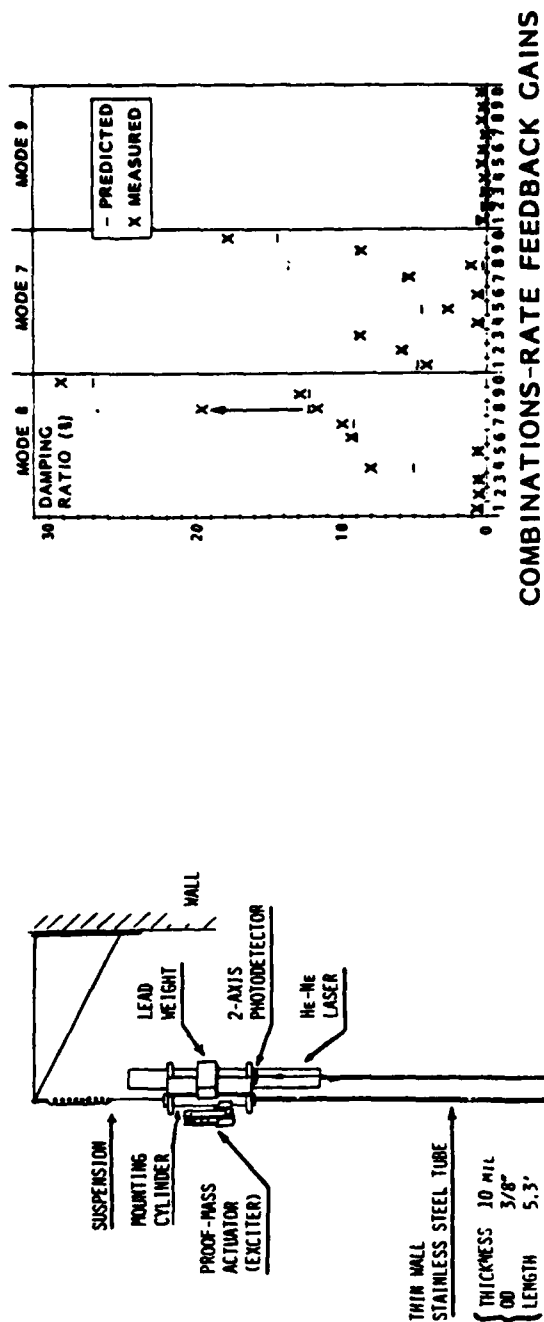
- FREQUENCY SHAPED HAC
- LAC STABILITY AUGMENTATION
- 12-MODE CONTROL DESIGN MODEL
- 44-MODE EVALUATION MODEL
- SENSOR NOISE NOT INCLUDED

PERFORMANCE

- $>10^5$ REDUCTION IN LOS ERROR
- ROBUST OVER P_0, P_2, P_4

Figure 2-4 ACOSS Phase IA Analytical Results - Disturbance
Rejection - CSDL No. 2

SLIM BEAM, LAC EXPERIMENT



RESULTS

- VERIFICATION OF LAC THEORY
- 2-D CROSS-COUPLING EFFECTS CHARACTERIZED
- NONCOLOCATION/NONCONSISTENCY IMPLEMENTATION DEMONSTRATED

SLIM BEAM TEST

Figure 2-5 ACOSS Phase IA Experimental Results

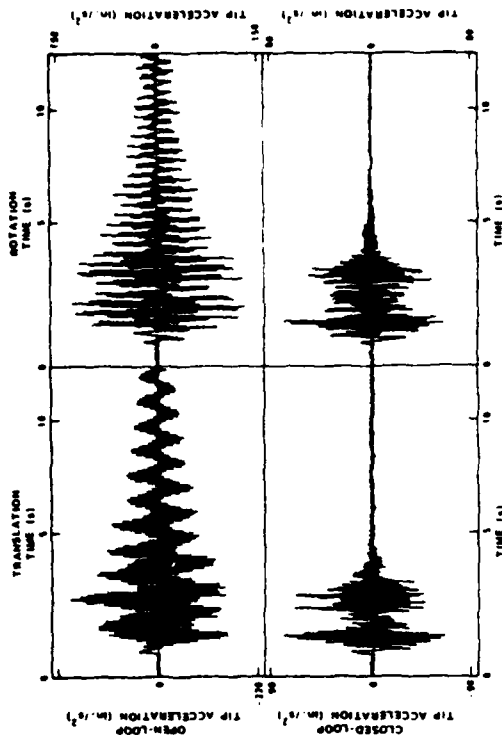
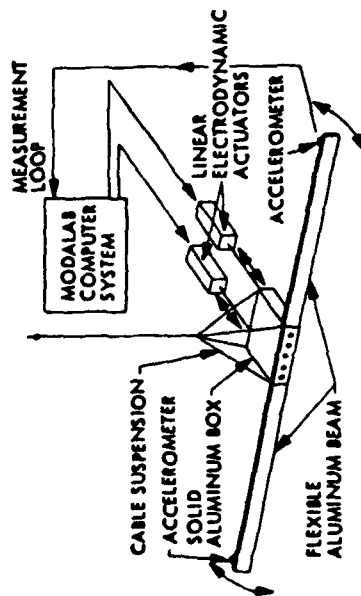
As a precursor to more advanced digital control experiments, two additional brassboard systems were tested in Phase 1A: a dual flexible beam structure called TOYSAT, and a circular plate mirror structure emulator [1]. These are illustrated in Figs. 2-6 and 2-7. Digital control, whose transient settling performance is illustrated in Fig. 2-6, was mechanized via a CSPI MAP 200 array processor. Analog rigid body control was examined for the plate, Fig. 2-7, prior to introducing digital modal control, discussed later in this report. In both of these experiments, array processor architecture limited digital control bandwidth [1].

These experiments served to build experience with sensor and actuator systems and to lay the groundwork for more complete experiments in Phase II. The microphase optical system, developed in Phase 1A [1], was coupled to the plate experiment in Phase II, allowing both attitude control and damping augmentation for five bending modes. Based on the smaller brassboard experience, a 10 meter proof-of-concept structure was built to illustrate modal control via central body actuators. These experiments, as well as system identification work on a complex truss-wheel structure, are addressed in Section 4 of this report.

2.3 RELATIONSHIP TO EXISTING TECHNOLOGY

Technological developments and techniques used in structural testing, helicopter vibration control, and aircraft modal control and flutter suppression are most closely related to the ACOSS technologies. Current activities in closed-loop structural testing require identification before control across a spectrally partitioned range. Most of the methods used are frequency-domain based and produce very low closed-loop bandwidth. Narrow-band system identification in real-time is now being explored for rotor vibration transmission attenuation in helicopter structures. Suppression of bending and flutter mode responses for high-performance aircraft also exemplify many of the techniques used for HAC synthesis. Space structures, however, differ from these applications in several fundamental ways:

TOYSAT (SLEWING) EXPERIMENT



EXPERIMENT

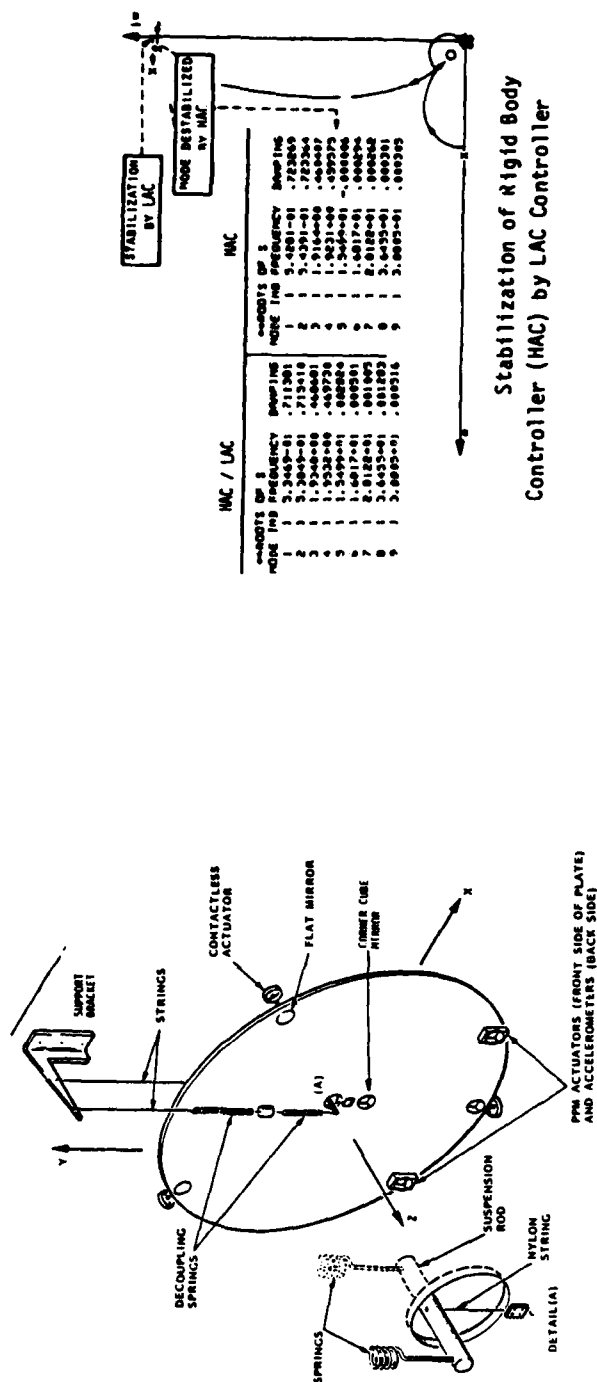
RESULTS

HAC DEMONSTRATED -- FOR TRANSLATION AND ROTATION, RIGID-BODY AND 2 FLEXIBLE MODES

- NONCOLOCATED ACTUATORS AND SENSORS
- DIGITAL MECHANIZATION WITH CSPI MAP-200 ARRAY PROCESSOR
- ELECTROSEIS ACTUATORS TIED TO LABORATORY FRAME

Figure 2-6 ACOSS Phase IA Experimental Results

CIRCULAR PLATE EXPERIMENT – MIRROR-TYPE STRUCTURE



EXPERIMENT

RIGID-BODY STABILIZATION DEMONSTRATION (ANALOG)

- 20 μ rad TOTAL RIGID-BODY POINTING ERROR
- 5 μ rad FLEXIBLE-MODE COMPONENT
- LAC STABILIZATION OF BENDING MODES

Figure 2-7 ACOSS Phase IA Experimental Results

RESULTS

1. Controlled modes and uncontrolled modes may have radically different modal damping.
2. The models are less well identified.
3. Many more modes must be controlled.
4. Frequently, mode shapes must be controlled or modified.

In general, evaluation models for spacecraft are not nearly as well-defined, the control objectives are more complex, and the performance requirements are more difficult to achieve, from both sensing/actuation and algorithmic points of view.

2.4 RECOMMENDATIONS FOR CONTINUING STUDIES

The principal issues which need further resolution in the ACOSS area center on hardware mechanization, identification, and fault-detection, isolation, and accommodation (FDIA). In particular they are:

1. Further investigation of (near) real-time identification on brass-board experiments as a precursor to on-orbit flight experiments.
2. Mechanization of high-speed digital control architectures to eliminate dependence on array processor hardware.
3. Mechanization of FDIA algorithms and robustness evaluations.

Additional exercises in control strategy evaluation will also be meaningful, viz.:

1. Investigation of performance limits using more complex metrics which include system wave-front error.
2. Adaptive disturbance suppression evaluation for high-order design models.

The current lack of available flight hardware for both sensors and actuators will also have to be addressed in programs which emphasize hardware development.

Section 3

ANALYTICAL ACTIVITIES

3.1 OBJECTIVES AND APPROACH

The ACOSS 12 effort encompassed activities which extended the analytical and experimental investigation of ACOSS 5 (Phase 1A). Specifically, the analytical objectives included:

1. Expanded disturbance rejection controller design for CSDL #2 (ACOSS version).
2. Controller robustness methods assessment.
3. System identification methods assessment.
4. Examination of digital controller characteristics.

The test structure used for analytical investigations continues to be the ACOSS version of CSDL #2, described in detail in the ACOSS 5 final report [1]. The disturbance input, for the disturbance rejection studies, is now expanded to include three discrete narrow-band spectra, as well as a colored broad-band noise. The impact of this more general disturbance on control design techniques is evaluated via some specific designs. The issue of improving controller robustness, tied also to both system identification and adaptive methods, is properly the subject for an independent study. Here, some of the pertinent requirements for such a study are described and the natural robustness improvements due to frequency shaping are illustrated. Advanced system identification methods (compared to traditional modal testing techniques) were necessary to achieve desired performance in the circular plate brass-board experiment. These methods are discussed and experimental data are evaluated using recursive maximum likelihood techniques. Digital controller mechanizations place special requirements on controller design. Issues such as pre-filter requirements, word length, and architectures are addressed as part of the analytical objectives.

The experimental objectives for ACOSS 12 were selected to increase understanding of both digital control design and performance assessment for complex structures. The specific objectives were:

1. Implementation of multimode digital control (damping augmentation) for the plate (mirror emulator) brassboard constructed in Phase 1A.
2. Integration of microphase optical measurement into closed-loop controls.
3. Detailed system identification for the truss-wheel structure (constructed in Phase 1A) in preparation for control design activities.
4. Implementation of multi-mode control on the proof-of-concept structure (constructed in Phase II) to demonstrate the control design and evaluation process on a 3-D structure.

The scope of these activities depended to a large degree on successes (and failures) experienced in ACOSS 5. Difficulties with the plate experiment in Phase 1A, largely associated with rigid-body/bending mode coupling, were resolved in Phase II by integrating the microphase optical system, built under ACOSS 5, into the experiment. The groundwork for control design of a structure with very dense modal packing was developed via system identification on the truss-wheel structure. Resources did not permit control of this structure during this phase. The proof-of-concept (POC) experiment represented the first brassboard with the appearance and size of an actual spacecraft. As an emulator for an offset-fed, wraprib reflector, the brassboard provides for modal control using both central body and distributed actuators. For this phase, the approach taken was to control selected bending modes via the central body CMG actuators and (colocated) rate gyro sensors.

3.2 TASKS RELATED TO THE STATEMENT OF WORK

The original Phase II statement of work was substantially modified in the course of the research to achieve maximum results over the study period. The LMSC/ACOSS program for DARPA has traditionally addressed as wide a range of

topics as possible in order to make the technology responsive to systems level problems. This breadth of topics is retained in this phase, although some areas are more thoroughly investigated than others. The two major tasks divide the analytical and experimental work as follows:

Task		
<u>No.</u>	<u>Topic</u>	
Analytical	1.1	Investigation of Disturbance Rejection
	1.2	Controller Robustness Investigation
	1.3	System Identification Methods Assessment
	1.4	Digital Controller Implementation
Experimental	2.1	Plate Brassboard Digital Control
	2.2	Truss-Wheel Brassboard Development
	2.3	POC Digital Control

As the program evolved, this statement of work remained unchanged in form, but the depth and content of the tasks were modified. These modifications are now briefly listed so that the major contributions of the study can be identified. Disturbance rejection control design was more rigorous than originally planned (Task 1.1) and new model reduction criteria were invoked to improve the control synthesis process. The controller robustness investigation (Task 1.2) was limited to a top level survey of (frequency domain) techniques and how adaptive strategies might ultimately be used. This area of study involves a substantial amount of computation and requires integration of parameter sensitivity, system identification, and adaptive techniques, as well as detailed assessment of expected parameter variations in actual structures; it is properly the subject for follow-on activities. System identification, particularly with respect to recursive prediction error methods is addressed in detail in Task 1.3 using actual test data. A detailed assessment of pre-filter requirements and hardware architectures is given under Task 1.4.

Experimental activity, under Task 2, was concentrated principally on the plate and POC brassboard digital control experiments, both of which successfully demonstrated the control technology. Control design for the truss-wheel experiment proved untenable without detailed system identification to refine the analytical model, and remaining resources were directed to this activity.

3.3 CONTROL DESIGN METHODOLOGY SUMMARY: COMMENTS ON ACOSS 5

In [1] a detailed account is given of the theory and methodology applied to a large complex optical structure (CSDL No. 2) to illustrate the procedures developed in the ACOSS program. In summary form, these steps are:

1. Definition of the structural model, the disturbances, and the control objectives. For nontrivial applications, finite-element structural modeling is used, providing a specially formatted data file containing modal frequencies and mode shape values at nodal stations on the structure.
2. Creation of the state-space model to prepare the structure for control systems. This requires a preliminary selection of sensors and actuators first obtained from examining the physics of the problem and then refined by the use of controllability, observability, and various modal cost criteria. This initial model is taken to be the "truth-model" or evaluation model, and is generally of large dimension. All control laws subsequently designed are tested against this model for stability and performance.
3. Reduction of the previous model to a workable size for control synthesis. This reduction process also involves controllability, observability, and modal cost criteria. In general, the first reduction is used for LAC synthesis and a further reduction for HAC synthesis. The model reduction criteria may indicate different actuator/sensor selection or structural redesign which will require that step 2 or steps 1 and 2 be repeated.

4. Control synthesis is carried out for HAC, then the spillover is estimated from evaluation model, and can be used to synthesize the LAC gains. LAC can also be synthesized independently. This latter approach is used exclusively in Phase II.
5. The LAC control law is then incorporated into the HAC state estimator, and the combined HAC/LAC control laws are evaluated for stability (spillover correction) and performance on the evaluation model. For robustness tests, the same controller is evaluated on perturbed evaluation models. It should be noted that this "cook-book" approach works for all systems, but should not be taken as a substitute for engineering judgement. Some systems do not require a separate LAC, and others need only LAC mechanizations. The level of complexity is quite problem dependent.

General Comments on the Results of ACOSS 5

Since the publication of the ACOSS 5 final report [1], several questions have been raised over details in the design methodology. In particular, important questions exist in two areas, namely:

- (1) How does model reduction methodology used in ACOSS 5 relate to that proposed in ACOSS 12, and
- (2) Is frequency shaping relevant to the control designs presented in ACOSS 5 and later in ACOSS 12?

The questions are actually more complex than these simplistic versions, but the discussions below will attempt to address the broader issues.

Model Reduction

In the next section of this report, a detailed development of model reduction using internal balancing theory will be presented. In this theory, scaling of the modal states for lightly damped structural models allows

reduced-order models to more exactly replicate the impulse response of the appropriate evaluation model. Four mode-selection criteria are applied to make the reduced model selection. In ACOSS 5, a precursor to this method was employed which represented basically the same idea without the formal sophistication (and justifiability) of internal balancing. In that report, no attempt was made to balance the states and only two selection criteria were used, namely, (1) controllability to LOS and (2) disturbability to LOS. Since these are the two most important criteria, the only real deficiency in the selection process in ACOSS 5 was lack of state balancing. This might have resulted in a slightly different reduced order model but the differences in this case are not significant to the results and conclusions. As the reader will see in the next section, the rather intuitive ideas set forth in ACOSS 5 have been developed into a more sophisticated theory in ACOSS 12 which makes its applicability more generally acceptable in situations requiring "cookbook" strategies. In this context, the methods employed in the two contracts are not substantially different; the ACOSS 12 work is just more sophisticated and requires little or no heuristic justification.

Comments on Frequency Shaping

Questions have been raised regarding the use of frequency shaped control and estimator design in both ACOSS 5 and ACOSS 12. The major issues raised centered on:

- (1) Theoretical "errors" in the ACOSS 5 technology primer,
- (2) Inapplicability of the idea to disturbance rejection, and
- (3) "Failure" of the technique in broadband noise rejection.

These questions are principally the result of some confusion over the control issues which frequency shaping is designed to address. Before looking at the reasons for using frequency shaping techniques, it is important to resolve the issue of theoretical "correctness". This

issue was raised because the cost functional in [1] (and the underlying reference by N. K. Gupta) should have properly been written as a stochastic cost. This failure to write the stochastic cost correctly is a common "looseness" in notational convention and, as pointed out by Safonov, who committed the same error [3], the conclusions and the synthesized controls remain unaffected. In any event, the theoretical foundations of frequency-shaping are well established by refs. 4 through 10 (in this report). The purpose of the ACOSS 5 technology primer was not to reestablish the theory but rather to explain how this theory can be used to synthesize the controls (in detail). None of the aforementioned references address these details.

Frequency-shaping was introduced as a general tool to limit system gain in regions of poor model fidelity (i.e., spillover reduction). As illustrated in ACOSS 5 and later in this report, it can also be used as a method to synthesize robust controls which reject disturbances whose models are well known. This is accomplished through the so-called internal model principle. The sinusoidal disturbance rejection levels illustrated in ACOSS 5 showed a reduction factor near five orders-of-magnitude. The actual value is much better, for precisely known disturbance frequencies, since the controller is introducing blocking zeros; the correct residual LOS error should have been zero. Numerical problems in the eigensolver used at the time produced these errors which were unfortunately not recognized. Such controllers are fully realizable and, in fact, roll-yaw momentum control systems for earth pointing satellites contain just such mechanizations. Some additional comments on the theory, however, are in order here to add further clarification to the synthesis process for narrow band disturbance rejection controls.

It is well established for scalar systems that in order to track a constant set-point command with zero asymptotic error, despite model error in the plant, an integrator is required in the control loop. The integrator is actually an internal model of the signal to be tracked. The

extension of this notion to the multivariable case and to arbitrary commands and disturbances yields the internal model principle, namely [12]: asymptotic tracking and disturbance rejection in the presence of model error can only be achieved if the controlled system contains a replica of the commands and disturbance signal generators. This same principle can be applied to design fault tolerant estimators which do not exhibit "hang off" due to model error or sensor bias signals. Controllers or estimators which have an internal model are referred to as robust servomechanisms.

There are several well established design methods which result in a controller (or estimator) with an internal model. For example, consider the plant

$$\dot{x} = Ax + Bu + Dw$$

$$y = Cx$$

where x is the state, u is the control, and w is a disturbance. Suppose that w is a sinusoidal disturbance of known frequency α . Thus, w satisfies the differential equation,

$$\dot{w} + \alpha w = 0$$

We seek an LTI control of the form,

$$u = -F(s)y$$

such that $y(t) \rightarrow 0$ as $t \rightarrow \infty$. The design can be obtained by defining an equivalent error system [9],

$$\dot{x}_e = A_e x_e + B_e u$$

$$y_e = C \xi$$

where

$$x_e = \begin{pmatrix} y \\ \dot{y} \\ \xi \end{pmatrix}, \quad A_e = \begin{bmatrix} 0 & I & 0 \\ -\alpha I & 0 & 0 \\ 0 & 0 & A \end{bmatrix}, \quad B_e = \begin{bmatrix} 0 \\ 0 \\ B \end{bmatrix}$$

with ξ and μ defined by

$$\xi := x + \alpha x$$

$$\mu := \dot{u} + \alpha u$$

Using LQG design on the error system gives,

$$\mu = -Kx_e$$

$$\dot{\hat{x}}_e = A_e \hat{x}_e + B_e \mu + L(y - C_e \hat{x}_e)$$

with K and L the optimal controller and filter gains, respectively. If the cost functional is of the form,

$$J = \int_0^{\infty} (q_0 |y|^2 + |\mu|^2) dt$$

and the closed-loop system is stable despite model errors, then the controller above contains robust blocking zeros [9] at the disturbance frequency, i.e., $y(t) \rightarrow 0$ asymptotically.

A control law with the very same robustness property can also be obtained from the frequency shaped cost functional,

$$J = \frac{1}{2\pi} \left(\int_{-\infty}^{\infty} q_0 |\hat{y}|^2 + q_1 \left| \frac{b}{b^2 - \omega^2} \hat{y} \right|^2 + |\hat{u}|^2 \right) d\omega$$

Frequency Shaping

Frequency shaping can also be used in conjunction with detection robustness analysis to design a robust estimator with an internal model of commands and disturbances.

The remaining question relates to rejection of broadband disturbances - those which look white to large spectral portions of the model. Here, ultimate performance of the disturbance rejection controls depends very little on the synthesis procedure used. Frequency-shaping would be used, if necessary, to control spillover in the closed-loop (especially

if the system configuration did not permit mechanization of decentralized LAC systems). Frequency shaping, however, has no applicability to rejection of this type of noise. Rather, the system performance is limited by control design model fidelity and, ultimately, by measurement of the disturbance. If the evaluation model can be used to design the control, any performance can be achieved. Practical modeling and system identification constraints, however, make it highly unlikely that more than a small portion of the actual system dynamics will be known to the controls designer. For these reasons, the reader will notice in this report that frequency shaping is not used to reject broadband noise and that only about 50% of the evaluation model is used in the controls design [13].

3.4 NEW RESULTS ON MODEL REDUCTION METHODOLOGY

3.4.1 Introduction

Flexible spacecraft control design requires a mathematical model of plant dynamics, actuator/sensor locations, and disturbance environment, all defined with respect to performance objectives. This "evaluation model", which must be sufficiently accurate to predict system performance under any candidate control, can contain hundreds of structural modes known with varying degrees of accuracy.

Model reduction for control design is motivated by practical issues: hardware limitations, reduced computation power on-line, and robustness. In principle, an "optimal" control can be generated for a large model using modern control techniques, but this control is at least as complex as the model itself. When the "reduced controller-order" constraint is formally imposed, optimal control methods lose their attractive closed-form solutions. Therefore, a reduced-order "control design" model is selected using the same criteria as for the evaluation model: namely, to represent the system accurately with respect to the performance objectives. In this context, the "best" reduced model is one which produces the optimal reduced-order controller; and model reduction techniques can be viewed as attempts to approximate a parameter optimization solution.

Much of the conceptual clarity of the model reduction problem is lost when finite-element evaluation models are used, due to the characteristic inaccuracy of the high-frequency modes. Although necessary for accurate modeling at lower frequencies, these high-frequency modes give only a qualitative indication of system dynamics. Since the "true" evaluation model cannot be known a priori, the idea of an optimal (or even stable) constant-gain "full-order LQG" control is meaningless.

The typical approach to open-loop structural model reduction is mode selection. One such method is straightforward dominant-frequency selection [14], in which the lowest frequency modes are retained. While this method clearly addresses the high-frequency uncertainty issue, it ignores the fact that actuator and sensor placement, disturbances, and performance requirements also affect modal dominance. A more sophisticated approach is modal-cost analysis [15], in which modal rankings are based upon relative contributions to a stochastic cost functional. The influence of actuator/sensor placement upon modal dominance is not treated, however, and the problem remains that feedback control can couple the disturbance into open-loop "undisturbed" modes.

Recently a general model-reduction approach based upon state selection from a grammian-balanced ("internally-balanced") coordinate representation has been proposed [16,17]. For a given input/output configuration, this approach produces a "balanced approximation" to the large model by defining and retaining the "most controllable/observable" states. Open-loop application of this reduction method to problems involving two sets of inputs (disturbances and actuators) and outputs (regulated variables and sensors) is in general not possible, because a different coordinate basis is required for each input/output pair. However, results have been obtained which show that the modal coordinates for lightly-damped structural models are approximately balanced by a block-modal transformation.

This section gives an overview of the approximate internal balancing approach to flexible spacecraft model reduction. The details of the derivation are provided separately in Appendix A.

3.4.2 Model Reduction Issues

Mode-selection for control design requires evaluation of the relative importance of each mode to the control problem. The specific issues which influence this evaluation are:

- modal fidelity
- controllability
- observability
- disturbance environment
- performance objective

None of these criteria stands alone. For example, it makes little sense to retain the most accurately modeled mode if it is neither controllable nor observable in the measurements. Similarly, a highly controllable mode adds little to the controller performance if it is (strictly) unobservable in the sensors and in the performance. The problem is to find a reduced-order model which addresses each of these design issues such that controls designed for the reduced model perform well on the evaluation model.

3.4.3 Mode-Selection Using Internal Balancing Theory

In general, balanced model reduction is state selection in a special coordinate system. This coordinate system, which exists for any asymptotically stable linear system having one set of inputs and one set of outputs, is one for which the controllability grammian and observability grammian are equal and diagonal. The diagonal elements of the balanced grammian are termed "second-order modes" or "principal-component magnitudes" of the system. The internally balanced coordinate representation has a number of desirable properties with respect to model reduction. It is unique (to within a sign change on the basis vectors) provided the second-order modes are distinct, and the second-order modes are similarity invariants of the system. Most remarkably, any arbitrary subsystem guaranteed to be asymptotically stable (subject to an additional restriction on the basis vectors in the nondistinct case [17]).

Application of balanced reduction to very large models is no easy task. Indeed, "transformation methods" are generally undesirable for large structural models because of computational problems and loss of a physically meaningful state vector. For lightly-damped structural models, however, it has been shown (see Appendix A) that balanced coordinates are a special case of modal coordinates, and thus that no explicit change of basis is necessary, provided the damping is very small and the frequencies are sufficiently distinct. The salient feature of this result is that the second-order mode (principal-component magnitude) for the i 'th structural mode having input coefficient vector b_i , rate output vector c_{1i} , displacement output vector c_{2i} , frequency ω_i , and damping ζ_i , is approximated by the following simple formula:

$$\sigma_i^2 = (4\zeta_i\omega_i)^{-1} \left(\|b_i\| \left(\|c_{1i}\| + \omega_i^{-2} \|c_{2i}\| \right) \right)^{1/2}$$

3.4.4 Mode-Selection Methodology

The approximate modal balancing result enables quantitative modal analysis of the evaluation model with respect to physically meaningful design issues. Four modal rankings are discussed, followed by a suggested mode-selection procedure.

Disturbance to Regulated Variables

This gives a modal ranking in terms of open-loop performance. Large values indicate high disturbance propagation to the output, while small values imply low open-loop performance contribution. If the goal were simply to match open-loop performance, mode selection would be based on these rankings. Observe that the balanced grammian is equal to the balanced steady-state covariance when the model is forced with unit-intensity white noise.

Actuators to Regulated Variables

These rankings show modal controllability of the performance. A small principal-component magnitude indicates that the given actuator configuration has little direct effect upon the contribution of the mode to the performance, regardless of its open-loop performance contribution.

Disturbances to Sensors

These rankings show modal observability of the disturbance in the sensors. A mode having a small relative value may be impossible to estimate on-line. If the corresponding open-loop performance ranking is large, the selection of sensor locations or types is inappropriate.

Actuators to Sensors

These rankings provide a modal analysis of potential controller authority for the given, the actuator and sensor configuration. Ideally these rankings should align with the open-loop performance rankings, so that controller authority "matches" the performance objective. A mode with that ranks highly here should be included in the design model even if its open-loop performance ranking is low, particularly if it is in the controller bandwidth, to prevent spillover problems.

Mode-Selection Procedure

Using the four modal rankings, the mode-selection process is performed as follows:

1. Select the modes having the largest open-loop performance ranking. These modes contribute most to the performance objectives, and assuming reasonable actuator and sensor placements, it should be possible to control each of the modes to some extent.

2. Examine the actuator-to-sensor rankings. Include in the design model any highly controllable/measurable modes not selected in (1), especially if they are close in frequency to selected modes. Omission of these modes can cause spillover, which can destabilize the system.
3. Examine the disturbance-to-sensor and actuator-to-regulated-variable rankings. Unselected modes having large values in either of these rankings indicate actuator/sensor configuration pathologies. A large disturbance-to-sensor ranking indicates an unmodeled mode in the measurements, which will inhibit state estimation. An unmodeled mode with large actuator-to-regulated-variable ranking may be driven unpredictably by the controller to the detriment of performance. In either case, the modes should be included.

3.5 ACOSS MODEL RESULTS FOR DISTURBANCE REJECTION

This section extends the results obtained in [1] for the CSDL #2 model (ACOSS version) to the case of complex disturbance rejection. Both broadband and discrete frequency spectra are handled simultaneously by the controls; the disturbance rejection limitations are explored. Sensitivity to discrete frequency input is also investigated.

3.5.1 Modifications of the Disturbance Input

The CSDL No. 2 model, shown conceptually in Fig. 3-1, represents a wide-angle, three-mirror optical space system, together with a line-of-sight model giving the law of displacement of the image in the focal plane when the structure deforms. The assumption is made that the mirror surfaces are simply displaced and maintain their nominal (rigid) shapes. The mirror shapes are off-axis sections of rotationally symmetric coaxial surfaces. Since the intent is to derive a first-order optical model (by neglecting the influence of light redistribution in the image), the asphericity of each mirror is disregarded. Model details are given in [1]. The total structure is approximately 28 m high, has a mass of about 9,300 kg, and embodies a structural design based on realistic sizes and weights (Fig. 3-1).

In Phase 1A (ACOSS 5), two sine disturbances were used—one at 10 Hz and 10 N amplitude on the top of the truss and one at 5 Hz and 20 N amplitude on the aft body. Since discrete sinusoidal disturbances represent only one class of disturbance, they do not fully test the theory being demonstrated. A more general model for the disturbance, proposed by Riverside Research, is shown

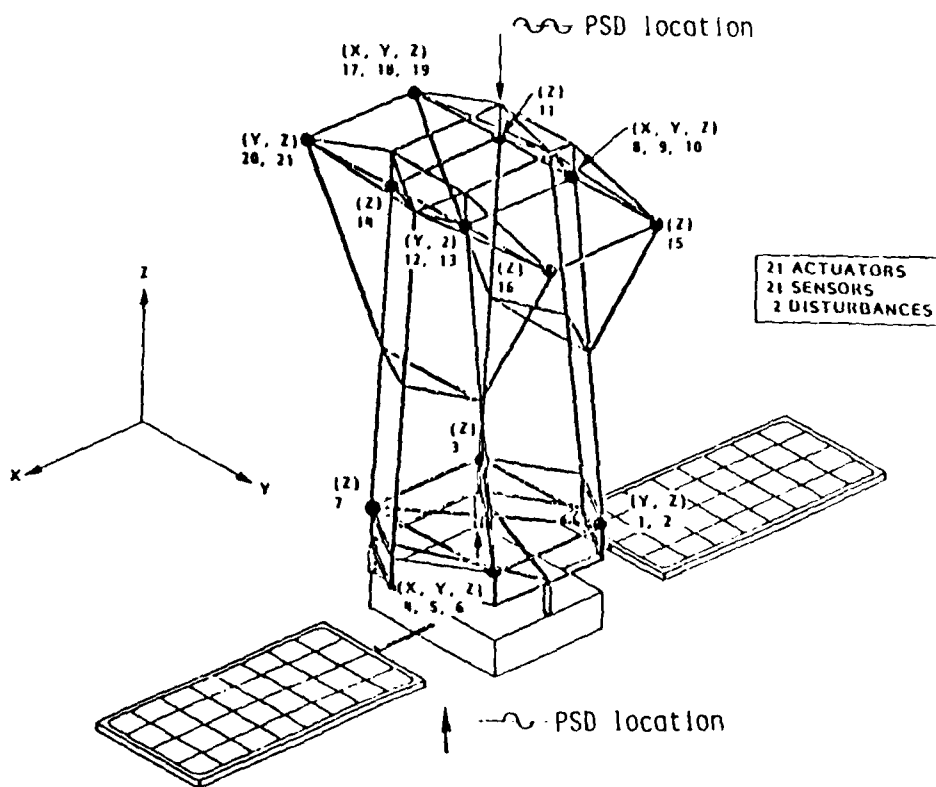


Figure 3-1 CSDL #2 - Disturbances and Actuator/Sensor Locations

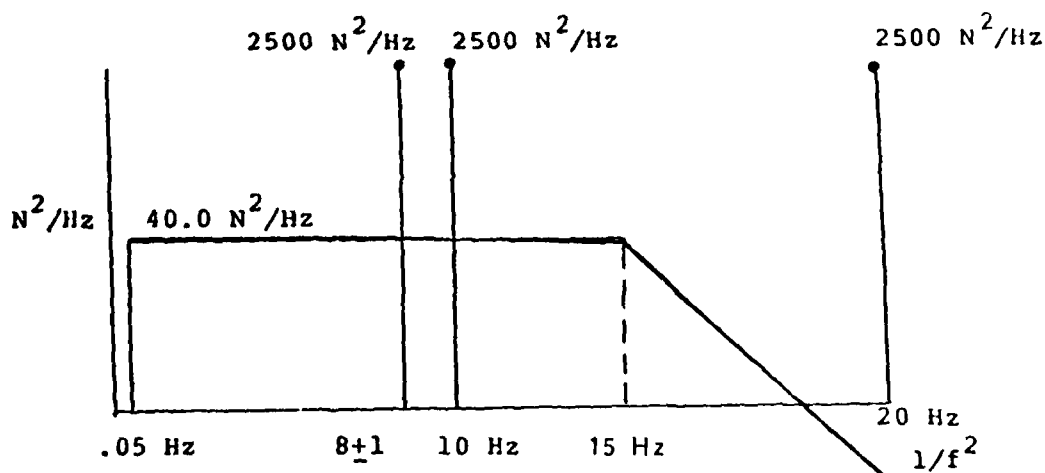


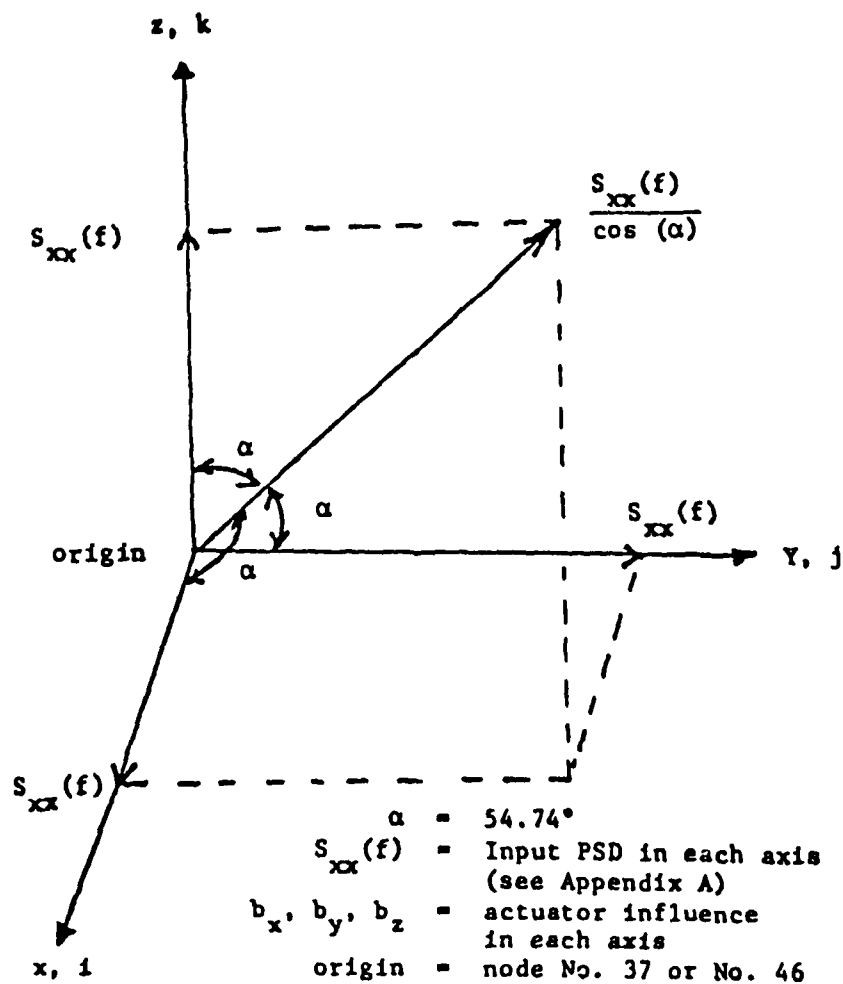
Figure 3-2 Disturbance PSD

in Fig. 3-2. The level of the colored spectrum selected was chosen on the basis of supplying wideband approximately as much disturbance energy to the system as the original two discrete systems supplied if one assumed a damping ratio of 0.002. The 15 Hz rolloff was selected to ensure excitation of most low frequency modes. It will be shown, however, that principal LOS errors are caused by modal excitation below 4 Hz and, thus, this disturbance looks "white" to the system.

The three discrete frequencies are selected to represent motors, coolers, and momentum storage devices. The 10 and 20 Hz frequencies were originally selected to present the problem of control of frequencies having a common integer multiple. The 8 Hz frequency was originally selected to provide a beat frequency against the 10 Hz frequency that was in the structural control bandwidth. Since nonlinear elements are not included in the models, these issues are not relevant at this time. The ± 1 Hz on the 8 Hz frequency was both to ensure that a mode would be directly excited by a sinusoidal source and to investigate sensitivity to input frequency variation.

At both disturbance input nodes, the disturbance geometry has been modified so that one source excites three axes of the CSDL structure as shown in Fig. 3-3. The disturbance model (augmenting state equations) is now given, for the colored spectrum, by the equations in Table I.

A preliminary selection of controls may be made based on the noise components which are most difficult to suppress in the structure. In previous work (Phase 1A Final Report), the effect of sinusoidal type disturbances on the LOS was controlled by forcing the structure to vibrate, so to speak, in the null space of the line-of-sight metric. This required active controls to modify certain eigenvectors (mode shapes) of the open-loop system. This is accomplished by feeding back the LOS performance measurement with a high gain near and at the disturbance frequency. The only damping augmentation employed was that required to stabilize HAC spillover effects in the unmodeled plant dynamics and was not very significant. The new disturbance spectrum poses no new monochromatic rejection problems. Within a narrow band reduced-order



Note: $S_{xx}(f) b_x + S_{xx}(f) b_y + S_{xx}(f) b_z = S_{xx}(f) (b_x + b_y + b_z)$

Figure 3-3 Input PSD Geometrical Relationship
at Node No. 37 and Node No. 46

TABLE I Disturbance Model

DISTURBANCE IS MODELED AS TWO INDEPENDENT COLORED NOISE SOURCES

$$\begin{bmatrix} \dot{v}_1 \\ \dot{v}_2 \end{bmatrix} = \begin{bmatrix} -B & 0 \\ 0 & -B \end{bmatrix} \begin{bmatrix} v_1 \\ v_2 \end{bmatrix} + n(0, \begin{bmatrix} M & 0 \\ 0 & M \end{bmatrix})$$

$$B = 30\pi ; \quad M = 18000\pi^2 \text{ N}^2/\text{sec}$$

$$\text{COVARIANCE: } E\{vv^T\} = \begin{bmatrix} 942.48 & 0 \\ 0 & 942.48 \end{bmatrix} \text{N}^2$$

DISTURBANCE IS APPLIED IN DIRECTION INDICATED

AUGMENTED EVALUATION MODEL:

$$\begin{bmatrix} \dot{x} \\ \dot{v} \end{bmatrix} = \begin{bmatrix} A & D \\ 0 & \equiv \end{bmatrix} \begin{bmatrix} x \\ v \end{bmatrix} + \begin{bmatrix} 0 \\ I \end{bmatrix} \omega + \begin{bmatrix} B \\ 0 \end{bmatrix} u$$

$$z = [M \ 0] \begin{bmatrix} x \\ v \end{bmatrix}$$

model, these disturbances can be suppressed as before, and this will be illustrated later in the section. Coincidence of the disturbance frequency with a structural mode frequency may require some HAC modal frequency shifting, which is easily accomplished since the disturbance frequency can be readily identified. If this is not possible, the system model, as it affects LOS, will have to be identified close to the disturbance frequency. This is generally straightforward and will be illustrated for the 20 Hz disturbance. The broadband disturbance poses more severe problems, because broadband excitation means that:

- damping may only provide small performance improvements
- reduced order models may not adequately describe propagation to LOS
- eigenvector modification (zeros distribution) will produce less dramatic improvement compared to discrete frequency results.

The control design will now be illustrated with some results for broadband noise suppression. Later, these results will be compared for the full disturbance spectrum which contains the discrete frequencies.

3.5.2 Broadband Disturbance Control Design

To investigate the impact of a broadband disturbance input on LOS performance, the closed-loop system design will be initially evaluated without discrete frequency controls. As will be seen later, the broadband response dominates the performance problem anyway so that this control problem is most relevant to performance improvement. Certain assumptions will be made for the broadband control design, which are reasonable in light of past experience, viz.:

1. Frequency-shaping will not be required (see Sec. 3.3).
2. Rigid-body modes can be neglected.
3. A line-of-sight measurement is available.
4. The design model is restricted to modes below 9 Hz.

These assumptions vary in importance. Except for gain stabilization at h frequency, shaping controller response will have little effect on broadband performance, since precise modal distribution is not of particular concern. The broadband disturbance is truncated at zero frequency so that rigid-body modes will not be excited. They will be reintroduced later for the full spectrum controller. The line-of-sight measurement removes the need for algebraic estimates of the LOS and is easily obtained from the focal plane alignment system. Using LOS measurements may be necessary in systems with distributed sensing, and driving a state estimator with them usually increases spillover sensitivity.

Restriction of design model bandwidth is essential to a practical design process. If the entire model were known to the designer, large performance improvements in closed-loop could be achieved. However, this is never the case in real systems, even when system identification methods have been used to identify parts of the model. Thus, acceptable design models must use restricted low-frequency versions of the evaluation model. Otherwise the resulting design becomes sensitive to inaccurate modal representations which are common for the higher modal frequencies. The design model here is limited to 9 Hz which represents one third of the structural vibration spectrum, or approximately one-half of the structural modes in the evaluation model. This partitioning is generous, and smaller design models may be necessary for actual systems. This "fidelity limit" is illustrated in Fig. 3-4 where the clustering of open-loop modes (without rigid body) makes the design model truncation somewhat more appealing. By definition, the control design process has access only to this lower order design model.

Control design can now proceed via selection of a reduced-order design model (which does not violate the fidelity constraints above), LQG synthesis, and performance evaluation. Performance improvements are now completely established by the size of the design model, and not by the controls design approach.

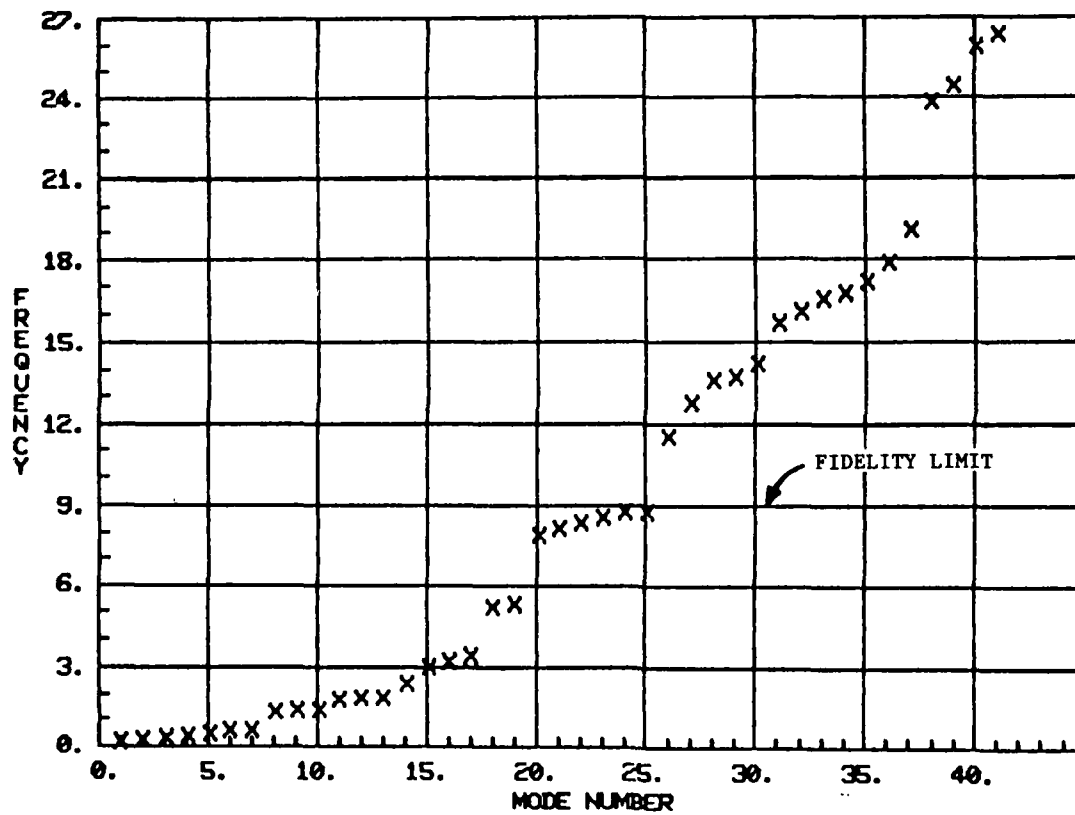


Figure 3-4 Open-Loop Flexible Modes

3.5.3 Model Reduction

The model reduction process follows the development in Section 3.4 using internal balancing. The second-order open-loop modes are shown in Fig. 3-5 where the notation of 3.4 is used. Controllability to LOS and disturbability to LOS are closely matched which indicates appropriate actuator placement on the structure. The LOS breakdown into x and y components in Fig. 3-6 confirms the controllability/disturbability match and illustrates the dominance of the "y" LOS error. Stochastic modal cost (without the scaling due to internal balancing) shown in Fig. 3-7 gives a much more restricted modal selection for pure contribution to LOS error. The modal rankings and selections for the two major balancing criteria are indicated in Table II with four additional modes being selected to include disturbability effects in a reduced model principally determined by controllability issues. Thus, 12 modes are selected as indicated also in Fig. 3-5.

3.5.4 Control Design

An LQG controller-estimator is now designed according to the guidelines in Table III. Weights on control effort and artificial measurement noise (not used in the evaluation model) are used to "tune" the system so that the maximum bandwidth of shifted reduced-order poles does not exceed 15 Hz. The results of this design, using the 12 mode plant, and 2 states for the two independent colored state noises, are shown in the closed-loop spectrum of Fig. 3-8 and Table IV. Mode 8 is not affected by the control design and can probably be eliminated. Evaluation of this design, for stability, in Fig. 3-9, shows no in-band spillover with the first spillover mode at 11.5 Hz. Thus, the 12 mode design model is adequate in this case. The spillover is entirely suppressed by adding the LAC system designed in Phase 1A [1], using those feedback gains for the colocated sensor/actuator system, as shown in Fig. 3-10 with the lower figure providing an expanded scale near the open-loop damping line. A "component cost" evaluation is shown for the closed-loop in Fig. 3-11 using identical scales to compare open and closed loop response. Low-frequency reduction produced by HAC is now closely matched to

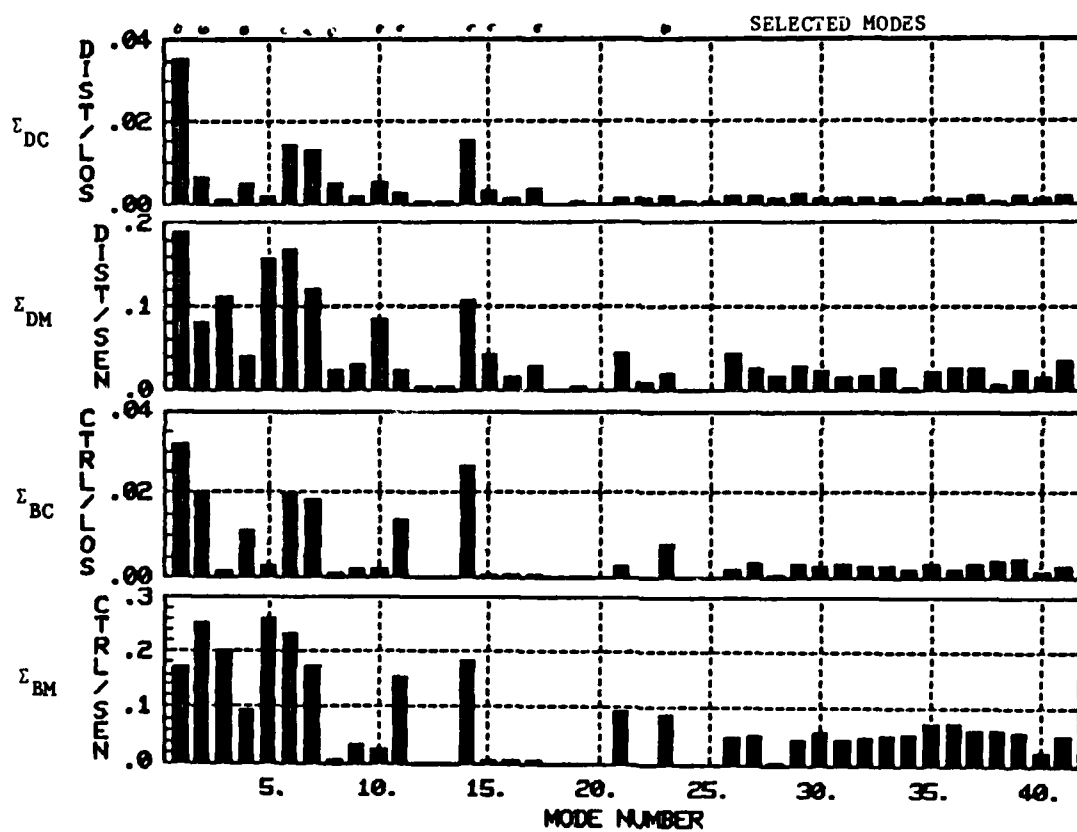


Figure 3-5 Open-Loop Modal Analysis

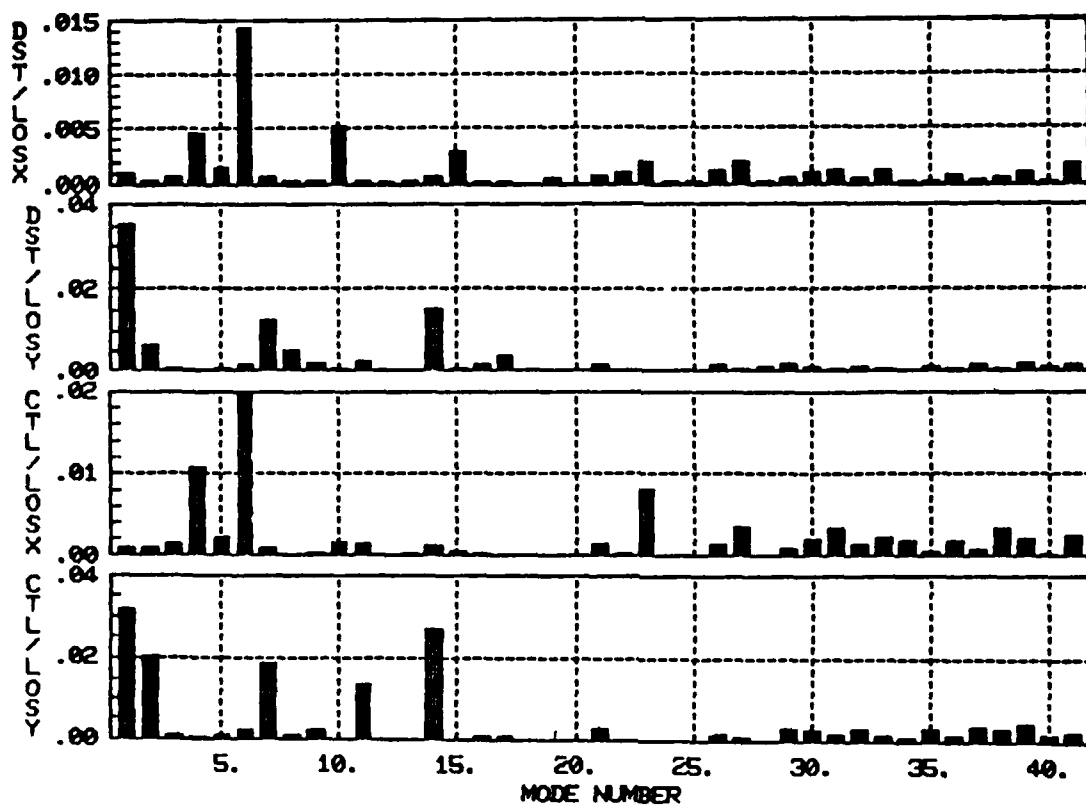


Figure 3-6 Modal Analysis - LOS Breakdown

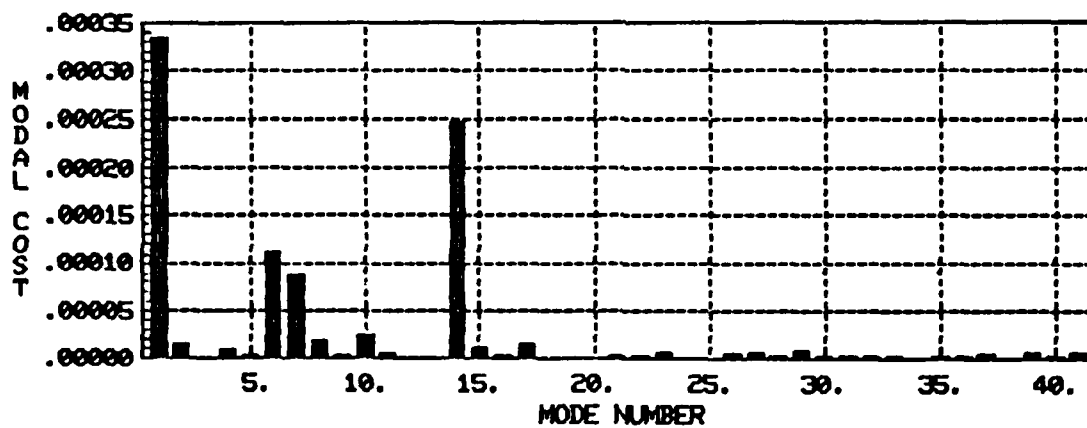


Figure 3-7 Open-Loop Modal-Cost

TABLE II Rankings Used for Mode Selection

<u>CONTROL/LOS</u>		<u>DISTURBANCE/LOS</u>	
MODE #	VALUE	MODE #	VALUE
• 1.0000	0.0318	• 1.0000	0.0351
• 14.0000	0.0266	• 14.0000	0.0151
• 2.0000	0.0201	• 6.0000	0.0143
• 6.0000	0.0197	• 7.0000	0.0128
• 7.0000	0.0185	• 2.0000	0.0065
• 11.0000	0.0137	• 10.0000	0.0053
• 4.0000	0.0108	• 8.0000	0.0047
• 23.0000	0.0081	• 4.0000	0.0045
		• 17.0000	0.0035
39.0000	0.0043	• 15.0000	0.0029
38.0000	0.0038	• 11.0000	0.0023
27.0000	0.0036		
31.0000	0.0033	29.0000	0.0019
37.0000	0.0033	• 23.0000	0.0019
29.0000	0.0030	27.0000	0.0019
35.0000	0.0030	41.0000	0.0018
•		•	
•	• RETAINED MODE	•	
•		•	

TABLE III LQG Design for Wideband Disturbance Rejection

DESIGN MODEL: $\dot{x} = Fx + Gu + w; w \sim n(0, W)$

$z = Mx$ (LOS OUTPUT)

CONTROL WEIGHTS: $J = \lim_{t \rightarrow \infty} \{ z^T z + r \cdot u^T u \}$

- LOS OUTPUT WEIGHT
- r : TUNING PARAMETER

FILTER WEIGHTS:

- USE W FOR STATE-WEIGHT
- v : TUNING PARAMETER ("MEASUREMENT NOISE")

OBJECTIVE: CLOSED-LOOP SPECTRA LESS THAN 15 Hz

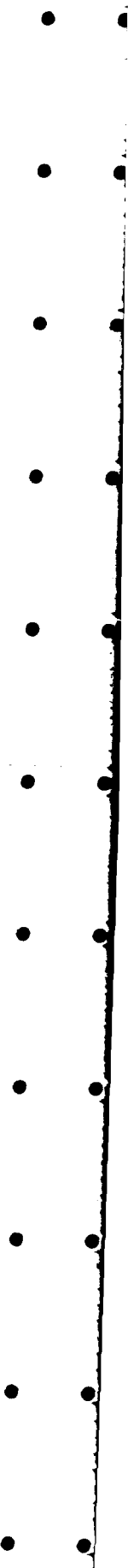


TABLE IV Closed-Loop Filter Spectrum

REAL PART	IMAG. PART	FREQ. (Hz)	DAMPING
-118.2393	0.0000	18.8184	1.0000
-94.2480	0.0000	15.0000	1.0000
-53.5684	75.6030	14.7469	0.5781
-6.1570	54.1999	8.6817	0.1129
-11.8839	21.5176	3.9122	0.4835
-0.0976	21.2406	3.3806	0.0046
-10.4177	3.6472	1.7567	0.9438
-0.4876	11.3564	1.8091	0.0429
-0.0158	10.8706	1.7301	0.0015
-0.0104	7.6804	1.2224	0.0014
-0.0152	4.2003	0.6685	0.0036
-0.2777	2.0738	0.3330	0.1327
-0.2547	2.0783	0.3332	0.1216
-0.0041	1.5772	0.2510	0.0026

TABLE IV Closed-Loop Filter Spectrum (Cont.)

REAL PART	IMAG. PART	FREQ. (Hz)	DAMPING
-56.4339	58.2927	12.9130	0.6956
-51.8276	74.5944	14.4563	0.5706
-0.0213	21.2720	3.3855	0.0010
-0.0261	18.7813	2.9891	0.0014
-0.6279	11.0445	1.7606	0.0568
-4.9308	7.7593	1.4632	0.5363
-0.0990	8.4183	1.3399	0.0118
-0.0081	7.6905	1.2240	0.0010
-0.6473	4.0151	0.6473	0.1592
-0.3902	1.7269	0.2818	0.2204
-0.1997	1.1672	0.1885	0.1687
-0.0163	2.2671	0.3608	0.0072
-94.2478	0.0000	15.0000	1.0000

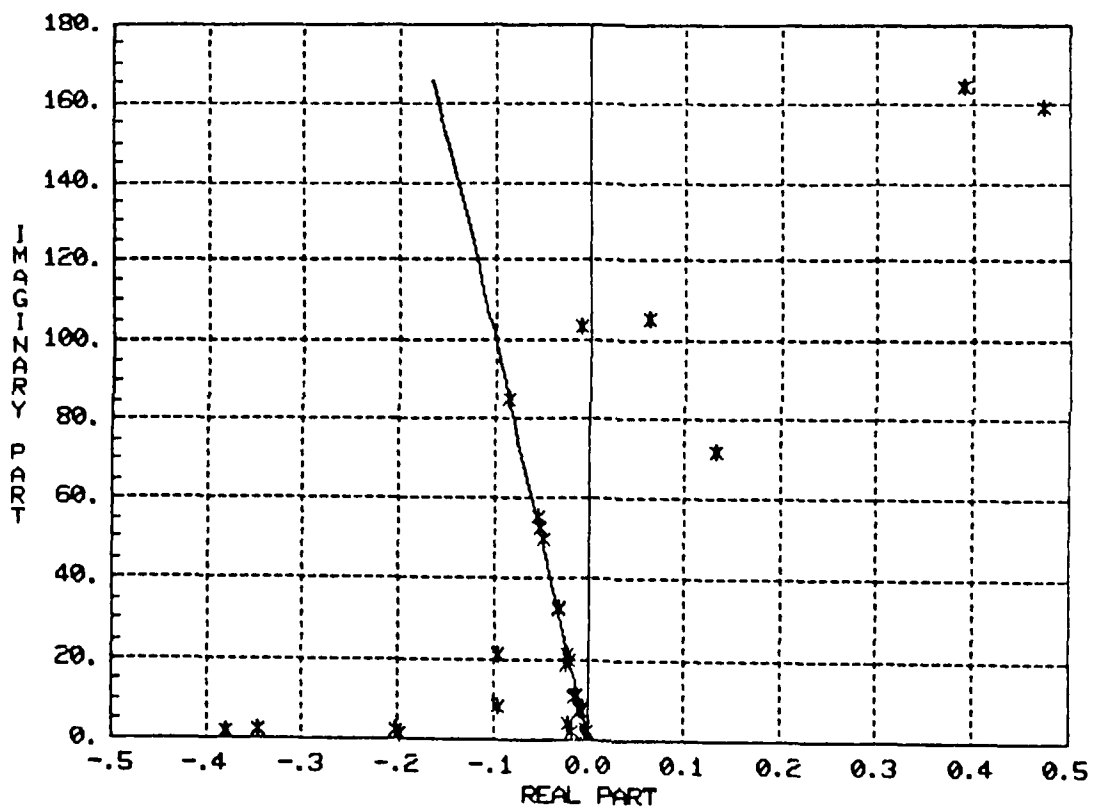


Figure 3-9 Closed-Loop HAC Spectrum - Broadband Disturbance Control

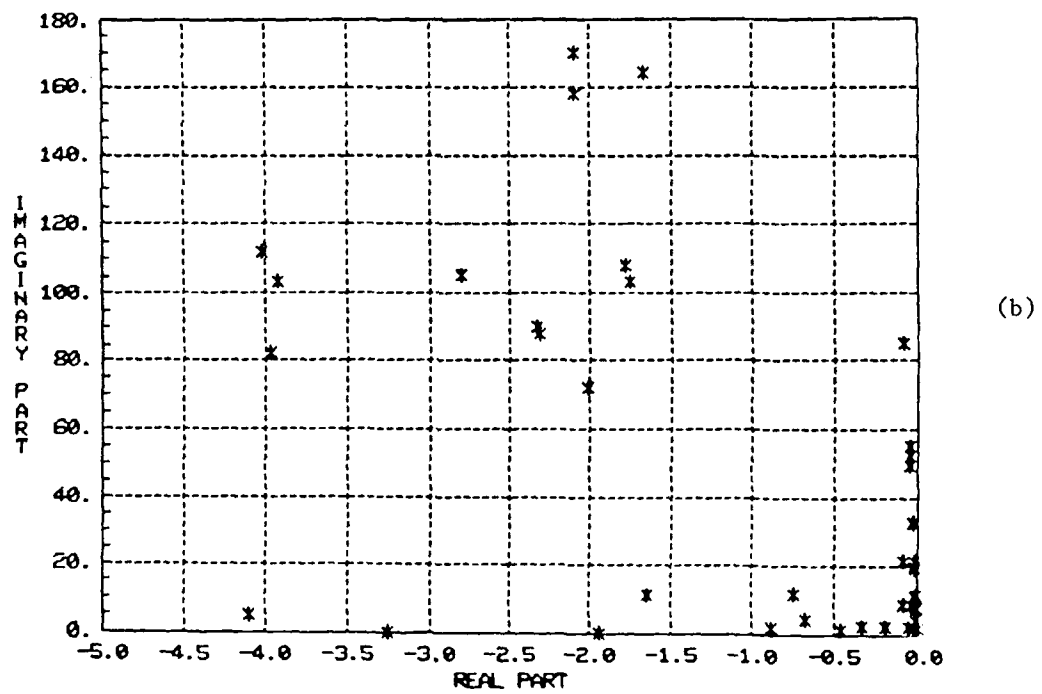
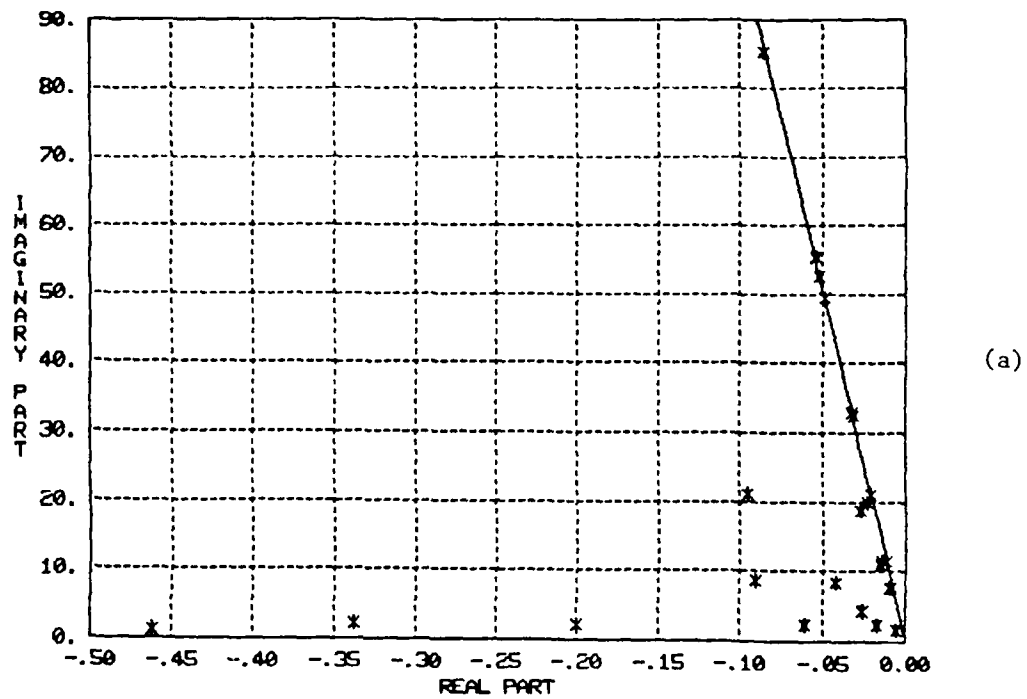


Figure 3-10. Closed-Loop HAC/LAC Spectrum - Wideband Disturbance Control

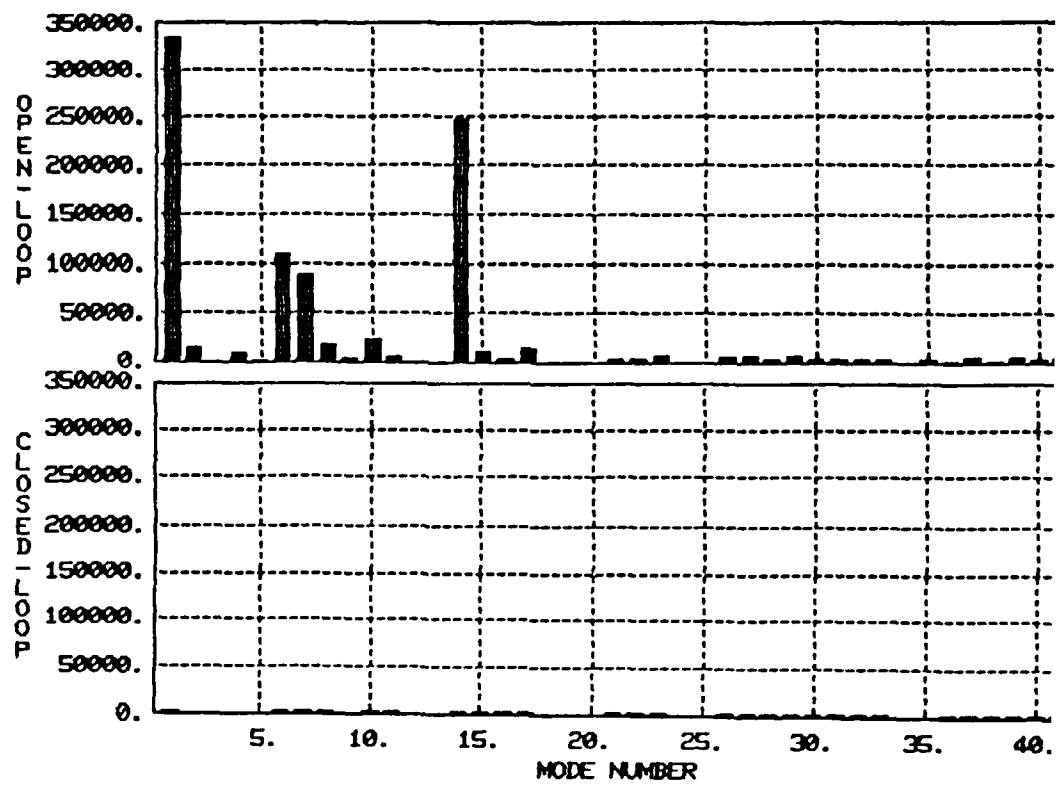


Figure 3-11 "Component-Cost" For Open-Loop Modal Coordinates

high-frequency reduction produced by LAC. Thus, no substantial further improvements in performance can be expected without increasing the size of the design model. This latter approach is not particularly realistic in context of actual system design. The performance is summarized in Table for the nominal model where it is seen that approximately two orders of magnitude LOS error reduction are obtained for a root sum square control effort of 64 N. In light of the disturbance level, this represents a practical maximum limit for control effort and, again, the limits of this design have been reached. This result is not unexpected.

3.5.5 Full-Spectrum Control Design

Now that expectations for performance improvements for the broadband noise are established, the full disturbance spectrum can be realistically treated. The rigid body modes are now reinstated into the model, (this adds 3 to previous mode number), and the control design model selection will be reinvestigated based on the sinusoidal disturbance effects. System evaluation will then be based on the full disturbance input. Treatment of the discrete frequencies can be handled by frequency shaping as before.

In this case, frequency shaping provides a formal mechanism for introducing notch filters into a complex MIMO System. Other techniques may work just as well but require more understanding of system behavior and more experienced engineering designers (see Sec. 3.3).

Selection of the design model is now also predicated on adequate representation of system dynamics near the discrete disturbance frequencies. To explore this more fully, consider the open and closed loop LOS spectral responses of Fig. 3-12 along with the modal analysis of Table VI. Moving from open-loop to closed-loop responses using the broadband disturbance control developed in the previous section, it is evident that such controls effectively broaden the discrete frequency modal excitation. The open-loop analysis indicates, however, that the previously selected reduced-order model is adequate to represent effects at 8 and 10 Hz but is not adequate at 2

TABLE V Stochastic Performance Analysis for Wideband
Disturbance Rejection Control (PO)

	OPEN-LOOP	HAC/LAC	REDUCTION FACTOR
RMS LOS x (n RAD)	114110	3273.0	34.87
RMS LOS y (n RAD)	425390	4636.2	91.75
TOTAL RSS LOS (n RAD)	440430	5675.1	77.61
RSS CONTROL EFFORT (N)	0	63.46	-

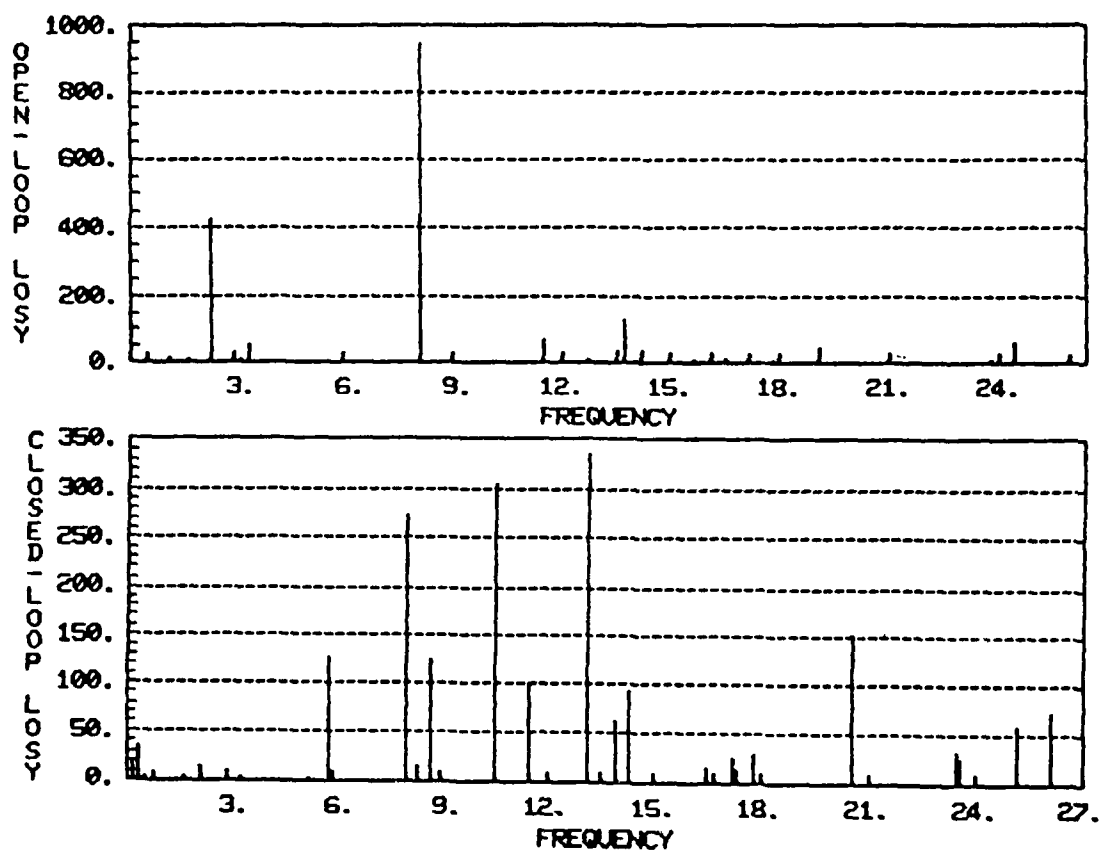


Figure 3-12 Modal Excitation Due to 8 Hz Sine Disturbance

TABLE VI Modal Analysis of Sine Disturbances

- TOTAL LOS CONTRIBUTION IS COMPUTED BY

$$\begin{matrix} \text{LOS } x1 & \text{LOS } x2 \\ \text{LOS } y1 & \text{LOS } y2 \end{matrix} = M(j\omega_k I - F)^{-1} D |w_k|$$

$$\text{LOS } x = |\text{LOS } x1| + |\text{LOS } x2|$$

$$\text{LOS } y = |\text{LOS } y1| + |\text{LOS } y2|$$

$$\text{TOTAL LOS} = \sqrt{\text{LOS } x^2 + \text{LOS } y^2}$$

- MODAL CONTRIBUTIONS ARE COMPUTED USING

$$M_1(j\omega_k I - F_1)^{-1} D_1 |w_k|$$

I.E., THE TRANSFER FUNCTION OF EACH MODAL BLOCK

To ensure modal stabilization, mode 42, the next most controllable mode at ~ 24.5 Hz, is included to describe system behavior near the 20 Hz disturbances. In actual systems, this mode might have to be identified. The effects of the sinusoidal disturbances are summarized in Table VII.

The control and filter designs are now recomputed using the full input disturbance spectrum. The frequency shaping is added via:

Design model: $\dot{x} = Fx + Gu + Dw$

$$y = Mx \quad (\text{scalar})$$

Frequency shaped cost: $J(j\omega) = \int_{-\infty}^{\infty} \left\{ y^*(j\omega) [P^*(j\omega)P(j\omega)] y(j\omega) + ru^*u \right\} d\omega$

$$P(j\omega) = \frac{\Omega^2}{\Omega^2 - \omega^2}$$

A "synthetic" output defined by: $\xi(j\omega) \triangleq \frac{\Omega^2}{\Omega^2 - \omega^2} y(j\omega)$

$$\rightarrow J(j\omega) = \int_{-\infty}^{\infty} \left\{ \xi^* \xi + ru^*u \right\} d\omega$$

In the time domain, $\xi(t)$ is realized by:

$$\begin{bmatrix} \ddot{\xi} \\ \dot{\xi} \\ \xi \end{bmatrix} = \begin{bmatrix} 0 & -\Omega^2 \\ 1 & 0 \end{bmatrix} \begin{bmatrix} \dot{\xi} \\ \xi \end{bmatrix} + \begin{bmatrix} \Omega^2 \\ 0 \end{bmatrix} y$$

The resulting frequency-shaped LQG problem is:

$$\begin{bmatrix} \dot{x} \\ \ddot{\xi} \\ \dot{\xi} \end{bmatrix} = \begin{bmatrix} F & 0 & 0 \\ \Omega^2 M & 0 & -\Omega^2 \\ 0 & 1 & 0 \end{bmatrix} \begin{bmatrix} x \\ \dot{\xi} \\ \xi \end{bmatrix} + \begin{bmatrix} G \\ 0 \\ 0 \end{bmatrix} u + \begin{bmatrix} D \\ 0 \\ 0 \end{bmatrix} w$$

$$\begin{pmatrix} y \\ r \end{pmatrix} = \begin{bmatrix} M & 0 & 0 \\ 0 & 0 & 1 \end{bmatrix} \begin{bmatrix} x \\ \dot{\xi} \\ \xi \end{bmatrix}; \quad J = \int_0^\infty \left\{ \xi^T \xi + ru^T u \right\} dt$$

TABLE VII LOS Effect of Sine Disturbances

		8 Hz	10 Hz	20 Hz
OPEN- LOOP W/RIGID BODY	LOS x	827.6	44.4	252.8
	LOS y	618.5	281.2	754.1
	TOTAL	1033.1	284.7	795.3
OPEN-LOOP WITHOUT RIGID BODY	LOS x	861.7	62.0	248.4
	LOS y	584.3	290.5	759.6
	TOTAL	1041.1	297.0	799.2
CLOSED-LOOP WIDEBAND HAC/LAC	LOS x	269.4	346.6	223.1
	LOS y	382.7	369.9	1086.8
	TOTAL	468.0	506.9	1109.5

Frequency-shaping requires two "synthetic states" for each sinusoidal disturbance and for each of the LOS components.

Some scaling is necessary to ensure that the added mode at 24.5 Hz (mode 42) is not exploited by the broadband noise HAC. Thus,

$$\begin{aligned}\text{Design model} \quad \dot{x} &= Fx + Gu + Dw \\ z &= Mx \quad (\text{Los Output})\end{aligned}$$

Define modified output: $z' = M'x$ in which columns corresponding to mode #42 are scaled down.

Add 12 "synthetic" frequency shaping states

Note here that frequency shaping is being used to increase system gain at the disturbance frequency. Other techniques can be used to achieve the same result.

The control and filter weightings are summarized in Table VIII. The resulting closed-loop control and filter poles are shown in Fig. 3-13 and listed in Table IX. Results for the full evaluation model in closed-loop are illustrated in Fig. 3-14 where all perturbation models (P_0, P_2, P_4) are shown. The lower "blow-up" shows the absence of spillover and the lightly damped frequency shaping mode at 20 Hz. The system performance for the nominal evaluation model (P_0) is given in Table X with the comparisons for the off-nominal evaluation models (P_2, P_4) given in Table XI. The system response (approximate) for the full closed-loop evaluation model is shown in Fig. 3-15 with unmodeled mode, sine suppression, and LAC damping effects labeled. The sensitivity of system disturbance rejection to input discrete frequency error is illustrated, for 8 Hz, in Fig. 3-16. Performance to specification is shown over an approximately 0.3 Hz range. Broader performance ranges are obtainable by trading maximum performance or by identifying the discrete input spectrum, which is relatively easy to do.

TABLE VIII Control and Filter Design

CONTROL WEIGHTS:

$$J = \lim_{t \rightarrow \infty} E \left\{ z^T z + \alpha_8 \left[\epsilon_{8x}^T \epsilon_{8x} + \epsilon_{8y}^T \epsilon_{8y} \right] + \alpha_{10} \left[\epsilon_{10x}^T \epsilon_{10x} + \epsilon_{10y}^T \epsilon_{10y} \right] + \alpha_{20} \left[\epsilon_{20x}^T \epsilon_{20x} + \epsilon_{20y}^T \epsilon_{20y} \right] + r u^T u \right\}$$

$r, \alpha_8, \alpha_{10}, \alpha_{20}$: TUNING PARAMETERS

- FILTER WEIGHTS: $W + \alpha_{RB}$ ON THE RIGID-BODY RATES

V : TUNING PARAMETER

- α_{RB} IS NECESSARY DUE TO A NEARLY UNOBSERVABLE CLOSED-LOOP RIGID BODY MODE.

- WITHOUT α_{RB} , STABILITY IS EXTREMELY SENSITIVE TO LOW-FREQUENCY MODEL PERTURBATIONS.

- WEIGHTS USED: $r = 10^{-14}$ $\alpha_{RB} = 10^{-12}$
 $v = 8 \times 10^{-15}$
 $\alpha_8 = .1$ M' COLUMNS SCALED BY .1
 $\alpha_{10} = .0001$
 $\alpha_{20} = .000001$

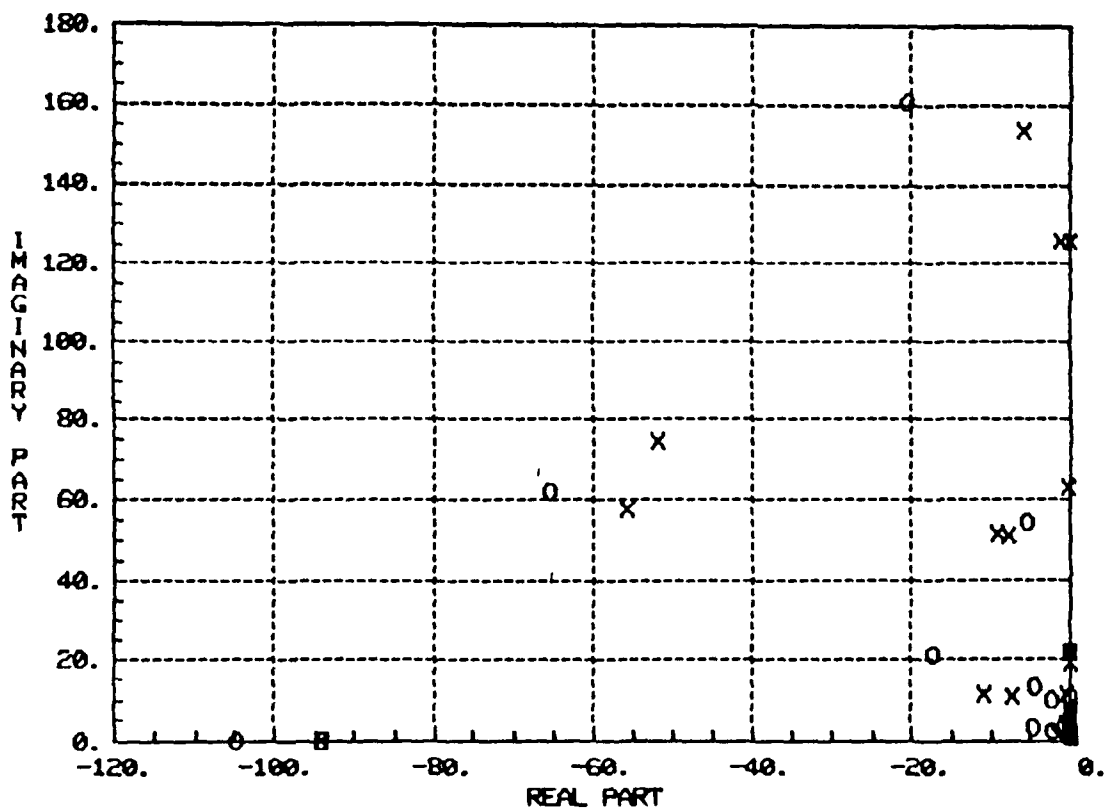


Figure 3-13 Closed-Loop Design Spectrum: Wideband + Frequency-Shaping

TABLE IX Filter Design Spectrum

REAL PART	IMAG. PART	FREQ. (Hz)	DAMPING	REAL PART	IMAG. PART	FREQ. (Hz)	DAMPING
-5.9664	153.5572	24.4578	0.0388	-11.0419	-11.0367	2.4847	0.7073
-52.0657	74.5405	14.4710	0.5726	-7.4706	-10.7544	2.0841	0.5705
-1.3273	125.61-7	19.9938	0.0106	-0.6083	-11.0503	1.7614	0.0550
-0.0330	125.6637	20.0000	0.0003	-0.0475	-8.4215	1.3404	0.0056
-55.9274	57.8213	12.8030	0.6952	-0.0079	-7.6902	1.2239	0.0010
-9.3751	51.2054	8.2851	0.1801	-0.5121	-3.9722	0.6374	0.1279
-7.8602	50.8652	8.1915	0.1527	-0.5549	-2.9767	0.4819	0.1832
-0.2698	62.8311	10.0000	0.0043	-1.7634	-1.0473	0.3264	0.8598
-0.3108	62.8300	9.9998	0.0049	-0.0714	-2.0750	0.3304	0.0344
-0.0213	21.2719	3.3855	0.0010	-0.0789	-1.6944	0.2700	0.0465
-0.0263	18.7775	2.9885	0.0014	-0.0321	-0.9692	0.1543	0.0331
-11.0419	11.0367	2.4847	0.7073	-94.2478	0.0000	15.0000	1.0000
-20.7081	160.6448	25.7790	0.1278	-0.0355	-10.8677	1.7297	0.0033
-104.8759	0.0000	16.6915	1.0000	-4.9229	-3.2617	0.9399	0.8336
-94.3965	0.0000	15.0237	1.0000	-0.0288	7.5805	1.2065	0.0038
-65.6420	62.0226	14.3731	0.7269	-0.0288	-7.5805	1.2065	0.0038
-5.5291	54.0519	8.6475	0.1018	-2.3648	-2.3611	0.5318	0.7077
-17.3067	20.6065	4.2829	0.6431	-0.0278	-3.8055	0.6057	0.0073
-0.1640	21.4110	3.4078	0.0077	-1.1951	-2.6157	0.4577	0.4156
-4.5915	13.0661	2.2042	0.3315	-0.1118	-0.9806	0.1571	0.1133
-2.4106	9.6201	1.5784	0.2431	-0.0121	-2.0719	0.3298	0.0058
-0.0355	10.8677	1.7297	0.0033	-0.0136	-1.6637	0.2648	0.0082

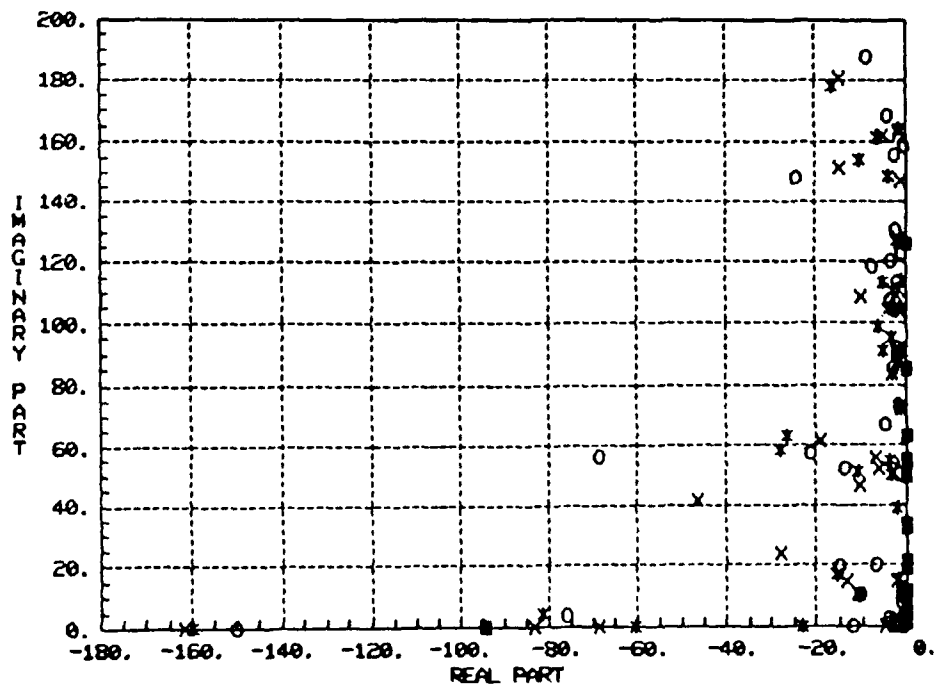
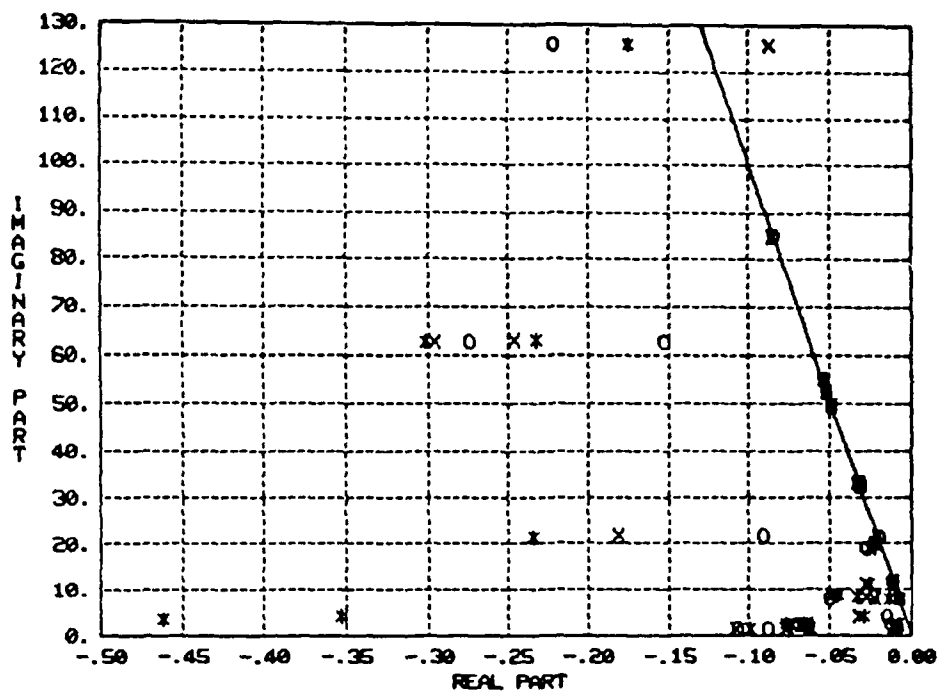


Figure 3-14. Closed-Loop Spectra for Frequency-Shaped HAC/LAC
(X:P0,O:P2,*:P4)

TABLE X Wideband Plus Sine Disturbance Rejection:
Performance Summary (PO)

		WIDEBAND	8 HZ	10 HZ	20 HZ
RSS OPEN LOOP	LOS x	-	827.6	44.4	252.8
	LOS y	-	618.5	281.2	754.1
	TOTAL (n RAD)	-	1033.1	284.7	795.3
RSS CLOSED LOOP	LOS x	3217.3	0 *	0 *	0 *
	LOS y	4132.8	0	0	0
	TOTAL (n RAD)	5237.4	0	0	0
RSS CONTROL EFFORT N		55.23	4.20	2.52	25.32

* VALUES < 10^{-10} n RAD

TABLE XI Wideband Plus Some Disturbance Rejection:
Closed-Loop Performance Comparison

		WIDEBAND	8 HZ	10 HZ	20 HZ
P0	LOS x	3217.3			
	LOS y	4132.8	0 *	0 *	0 *
	TOTAL	5237.4			
	(n RAD)				
	CONTROL EFFORT (N)	55.23	4.20	2.52	25.32
P2	LOS x	3052.9			
	LOS y	3520.3	0	0	0
	TOTAL	4659.7			
	(n RAD)				
	CONTROL EFFORT (N)	53.67	3.27	5.18	5.26
P4	LOS x	4352.1			
	LOS y	4267.8	0	0	0
	TOTAL	6095.5			
	(n RAD)				
	CONTROL EFFORT (N)	58.79	7.60	2.38	6.66

* VALUES < 10^{-10} n RAD

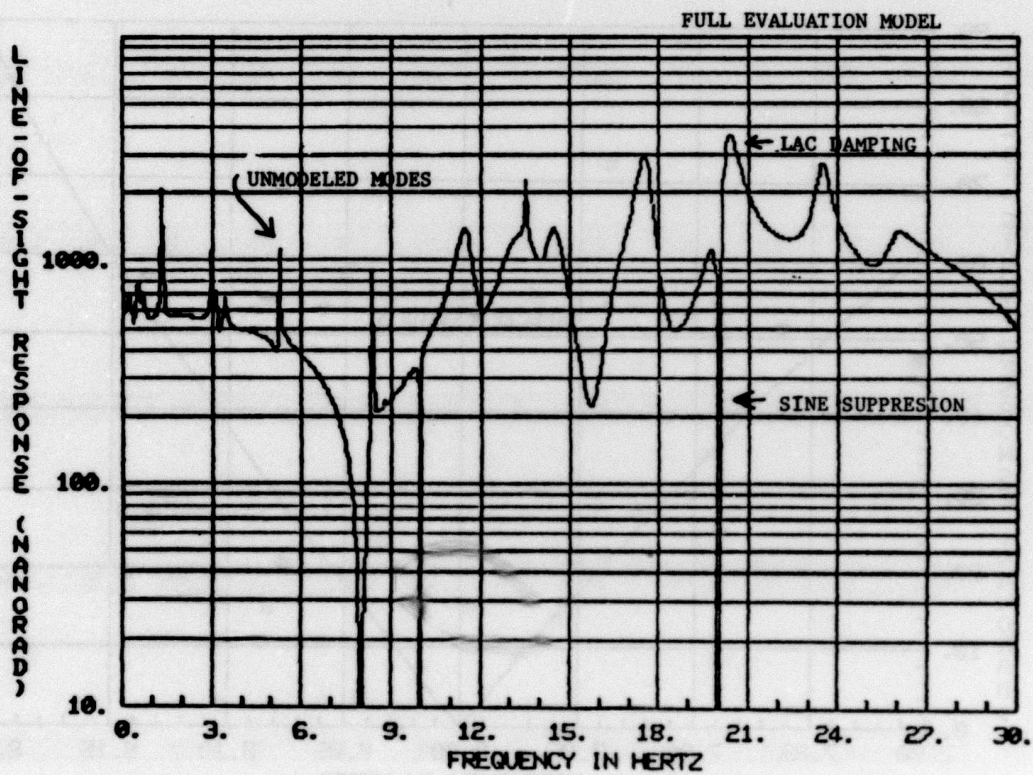


Figure 3-15 Closed-Loop HAC/LAC Frequency Response

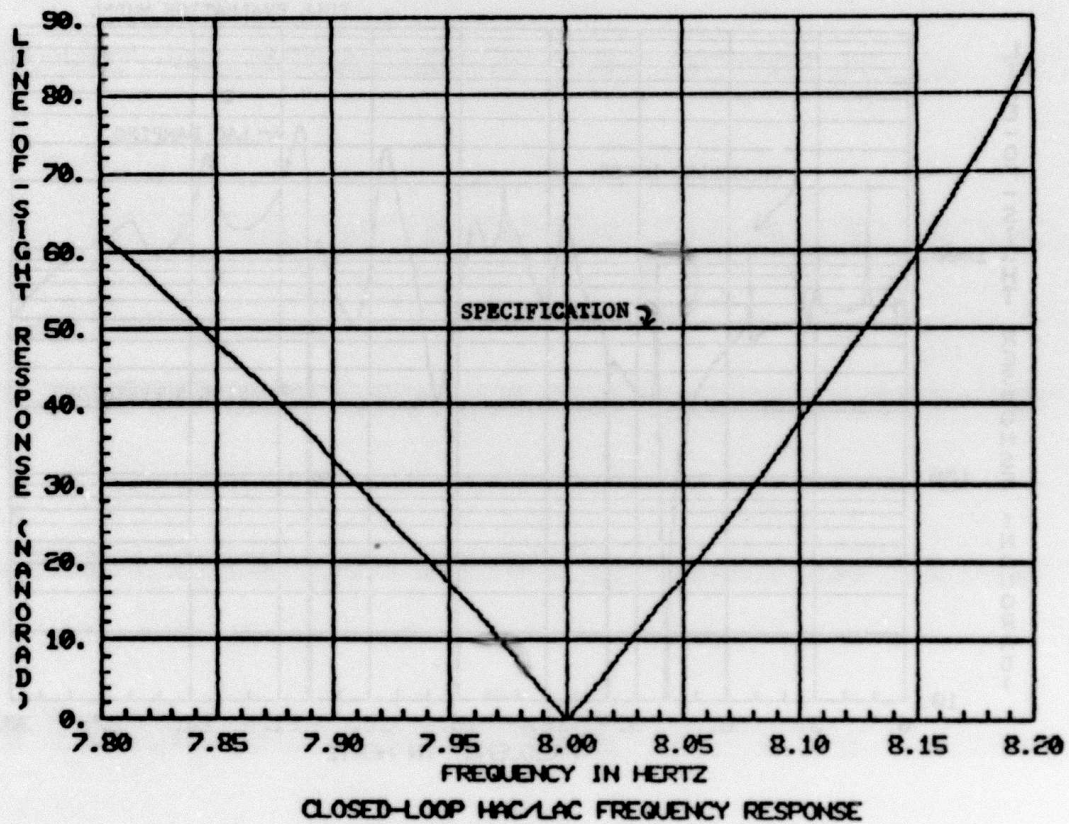


Figure 3-16 Sensitivity to Variations in the 8 Hz Sine Disturbance

3.5.6 Principal Conclusions

Certain general observations may be drawn from this section's results. For broadband disturbance rejection it appears that without substantial isolation at the source, this disturbance rapidly dominates the rejection problem. Without extensive model identification (or perhaps feedforward adaptive techniques) two orders-of-magnitude reduction is near the practical reduction factor limit and the RSS control effort is then commensurate with the disturbance level. Furthermore, proper design of such controls must consider rigid-body mode stability with respect to low-frequency modeling error.

For the discrete frequency disturbance rejection, the control design model must have sufficient accuracy near all discrete disturbance frequencies so that the plant can be stabilized. Once this is accomplished, performance depends only on how well the input frequencies can be tracked. Relatively low RSS control effort is required to achieve almost total suppression. More realistically, sensor noise and actuator nonlinearities must be included to more properly evaluate this approach.

3.6 ROBUSTNESS ISSUES AND TECHNIQUES

The principal objectives may be described as follows:

Develop Synthesis/Analysis techniques to improve/define system robustness properties with respect to:

I. Stability

- Excessive perturbation of unmodeled-pole locations (spillover)
- Parameter sensitivity of controlled/modeled poles
- Gain/phase/frequency margins

II. Performance

- Performance metric sensitivity to:
 - disturbance parameters (modeled and unmodeled)
 - identified modes
 - unidentified modes
- Performance/robustness trade-off

In general, the second class of issues is more important than the first, and the general objective is to understand the limitations imposed by model/disturbance uncertainty on closed-loop performance.

While system stability is important, performance sensitivity to parameter uncertainty for high performance missions is a much more significant issue. In particular, what must be determined is how much performance is lost to ensure stability and acceptable performance sensitivity. Some systems/missions may require identification or adaptive strategies to reduce the risk of losing the mission. At the core of these problems is the difficulty of selecting analysis and synthesis tools to determine robustness properties. Toward this end, analysis tools like generalized Nyquist criteria and singular value decomposition of the return difference matrix can be used to evaluate reduced-order designs. These techniques are known to produce only conservative evaluations of system sensitivity but as yet have not been tested on space structure system examples.

3.6.1 Some Techniques

The most fundamentally important issue is the designer's access to synthesis tools which allow him to synthesize robust controls. Many techniques have been proposed, but only two will be advocated for now, i.e.:

- frequency shaping
- adaptive methods

Direct sensitivity minimization via the usual gradient searches is complex, computationally expensive and usually produces only small improvements. Fixed gain and adaptive controls can be tailored using frequency shaping techniques so that high loop gains are present only in regions of high model fidelity (either identified or known a priori).

Possible definitions of robustness must include specification of performance and parameter variations, viz;

- Performance Criteria

- Stability
- Zero Asymptotic Error
- $\text{MIN MAX } \{J_{\text{Control}}\}$
plant
variations
- $E \{J_{\text{Control}}\}$
plant
variations

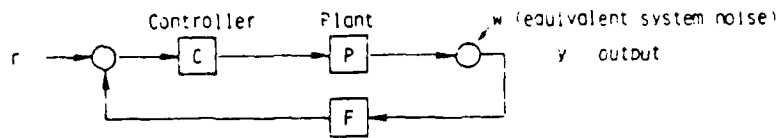
- Specification of Variations

- Parameter variations in design model (too restrictive)
- Frequency-domain specifications (easy to use but pessimistic)
- Function space specifications (too analytical, usable with frequency domain specifications.)
- Probability distributions (computationally expensive)

Monte Carlo type solutions and probability distributions will be avoided for the present, since these techniques are computationally expensive and reduce physical understanding of the problem.

Analysis tools such as the singular value decomposition of the return difference matrix, illustrated in Fig. 3-17, can provide stability boundary (conservative) analysis for given system designs. What are needed, however, are synthesis tools which allow robustness problems to be corrected.

- Stability Robustness:



$$(P.C.F.)_{\text{perturbed}} = (1 + \Delta(PCF)) PCF$$

↑
multiplicative form of uncertainty

$$\sigma_{\min}(\Delta(PCF)) < \sigma_{\min}(1 + (PCF)^{-1}), \forall \omega$$

then the perturbed system is stable, when unperturbed system is stable

- Stability does not guarantee performance improvement

Figure 3-17 Singular Values of Return Difference Matrix

TABLE XII Robustness Improvements Via Frequency Shaping

- Frequency weighted penalties can be imposed for:

- state and measurement noise estimates
- states and controls (control problem)
- likelihood function (identification)
- fault detection (likelihood ratio)

- Loop gain can be controlled in regions of uncertainty

- Factor A & B in $J = \int_{-\infty}^{\infty} [x^*(j\omega)A(j\omega)x(j\omega) + u^*(j\omega)B(j\omega)u(j\omega)]d\omega$

to net augmented time domain controller

- Refer to 2-mode example in ref. 1.

Frequency shaping is one such synthesis tool which allows the designer to avoid exploiting modeling deficiencies in certain frequency regions. Characteristics are listed in Table XII. For the two-mode example developed earlier and explained in the technology primer of [1], the gain reduction achieved with frequency shaping in the region of the unmodeled mode at 5 rad/sec is substantial and is illustrated in Table XIII and Fig. 3-18.

The highest levels of robustness will be attainable with adaptive mechanizations. To illustrate this, disturbance rejection (of a sinusoid) is now shown for a low-order system example (helicopter dynamics in this case). This technique will be used in subsequent studies on the CSDL broadband vibration problem. The technique exploits the characteristics of self-tuning regulators. The objective of the time-domain self-tuning regulator is to develop a time-domain feedback control design approach in which the model, near the vibration frequency, can be continuously identified. Even though the time-domain frequency-shaped formulation is robust with respect to changes in model form, the associated state variable model is difficult to identify in real-time, should this become necessary. The proposed approach can be shown to be convergent for any noise level, because it does not suffer from a leakage problem associated with Fourier transformed data used in the multicyclic approach.

TABLE XIII Comparison of Closed-Loop Modal Shift (2-Mode Example)

	Basic LQG:	Frequency-Shaped
Unmodeled mode	$0.0154 \pm j 4.9084$	$-0.0262 \pm j 5.0002$
Filter poles	$-0.4049 \pm j 0.8627$	$-0.4232 \pm j 0.8952$
Controlled poles	$-0.6466 \pm j 0.8512$	$-0.7018 \pm j 0.5139$
Frequency shaping	-	$-0.3239 \pm j 1.0957$

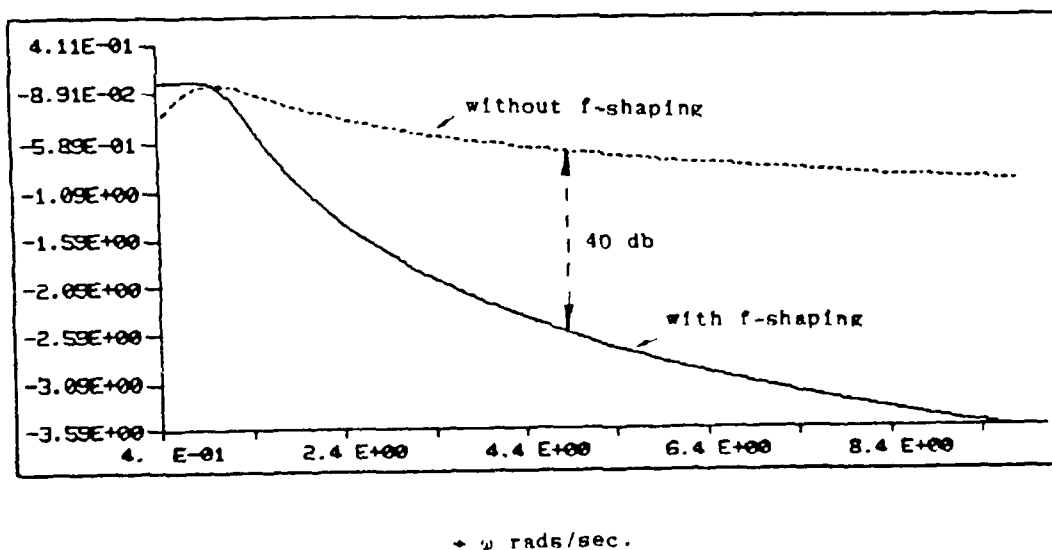


Figure 3-18 $\text{Log}_{10} (L(1+L)^{-1})$ State Feedback Only (2-Mode Example)

Preliminary research conducted to date indicates that this approach can combine the best features of the multicyclic frequency-domain and frequency-shaped time-domain methodologies. The identification part of the approach continuously updates a time-domain model, much like the multicyclic approach. The only difference is that the proposed approach can update the model at each measurement point. The control input is also computed at each point, leading to fast response for changes in dynamics or vibration level. The time-domain self-tuning regulator also has guaranteed convergence characteristics irrespective of the measurement noise and process noise levels, if the system dynamics do not change too rapidly.

The self-tuning regulator concept can be applied to the vibration control problem in the time-domain because of a recent development in which a frequency-shaped error criterion can be minimized instead of the mean-square error. This development is critical because the standard self-tuning regulator as proposed by Astrom cannot be used successfully to control narrow-band vibration using a time-domain formulation, due to the need to focus on the response at the vibration frequency.

The results for the self-tuning regulator are illustrated in Tables XIV and XV and Fig. 3-19. Identification and control adaptation are complete (steady state) in about 1 sec.

3.6.2 Robustness Investigation Program

Some of the tasks needed to enhance robustness evaluation techniques are listed below as subjects for future investigations.

1. Refine parameter sensitivity (model error) definition and synthesis methods.
2. Perform parameter sensitivity study on CSDL strawman model:
 - a. Evaluate singular value analysis for practical parameter variations.
 - b. Select performance variation criteria and evaluate singular value decomposition/robustness properties.
 - c. Evaluate limits of adaptive disturbance accommodation.
 - d. Evaluate robustness/performance trade-off.
3. Assess adaptive control strategies against parameter variations studies in Task 2.
 - a. Model structure changes.
 - b. Lattice form mechanization.

TABLE XIV 3-Mode Example - Model (Reduced)

$$\begin{aligned}\dot{x} &= Fx + Gu \\ y &= Hx\end{aligned}$$

with $x^T = [w \ \xi \ \dot{\xi}]$
 where w is the vertical speed in ft/sec.
 ξ is a structural mode close to the vibration frequency
 u is the collective pitch control in degrees

$$F = \begin{bmatrix} -.5034 & -8.69 \times 10^3 & -67.4 \\ 0 & 0 & 1 \\ .7116 & -5.1372 \times 10^3 & -6.8 \end{bmatrix} \quad G = \begin{bmatrix} -16.92 \\ 0 \\ 13.2 \end{bmatrix}$$

$$H = \begin{bmatrix} 1 & 0 & 0 \end{bmatrix}$$

Sample rate of 180 Hz gives

$$\frac{1}{u} = \frac{-.1294z^2 + .1863z - .0903}{z^3 - 2.8045z^2 + 2.7661z - .9601}$$

TABLE XV Propagation of Noise & Vibration

$$\begin{aligned}y &= \frac{-.1294z^2 + .1863z - .0903}{z^3 - 2.8045z^2 + 2.7661z - .9601}u \\ &+ \frac{z^3 - .12z^2}{z^3 - 2.8045z^2 + 2.7661z - .9601}v + \delta_{vib}\end{aligned}$$

v is white noise
 δ_{vib} is sinusoidal (18 Hz)
 unmodeled pole-pair at 27 Hz

the frequency-shaping filter was chosen to be

$$\frac{r(z)}{d(z)} = \frac{z^2 - 1.6018z + .9801}{z^2 - 1.6180z + 1}$$

Sensor noise level selected to produce 50% of steady-state error

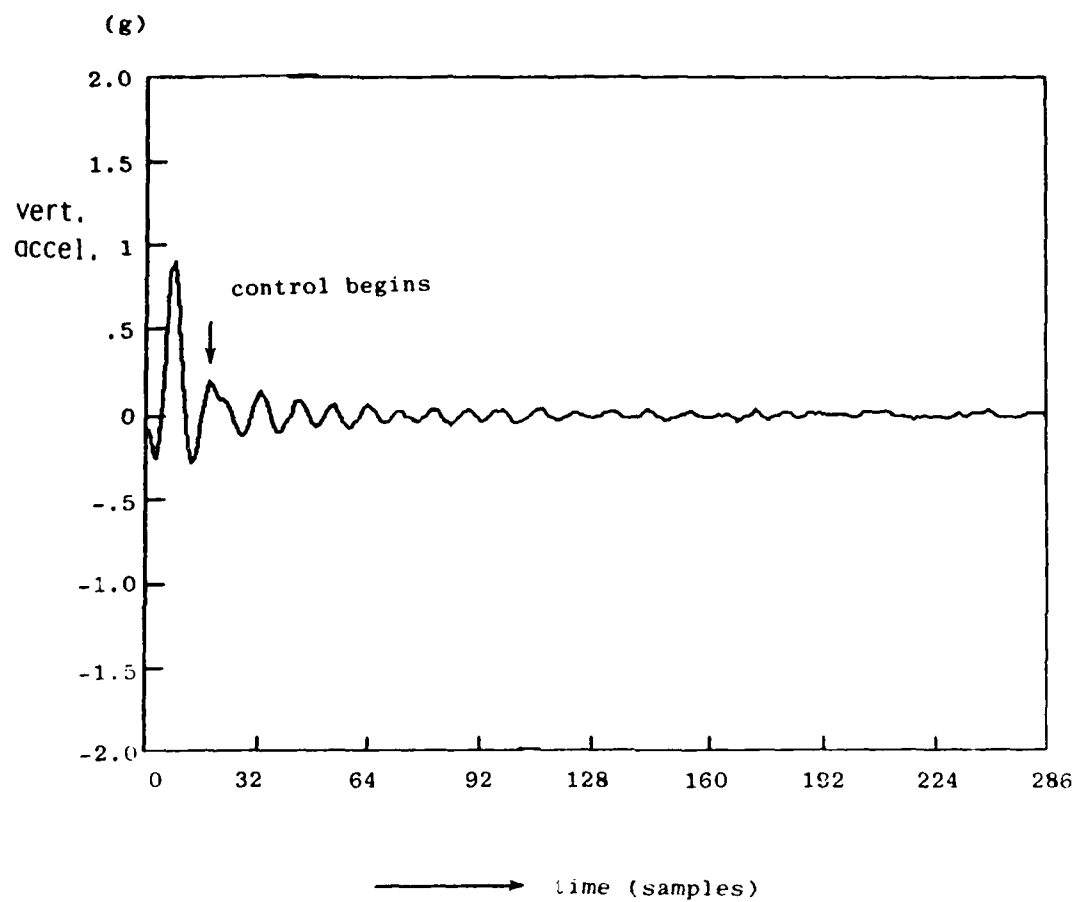


Figure 3-19 Adaptive Control with Unmodeled Pole Pair

3.7 DIGITAL CONTROLLER CHARACTERISTICS AND IMPLEMENTATION

Difficulties experienced in ACOSS Phase IA with digital implementation are addressed in this task. In particular, achieving high sample rates has been difficult for multivariable controllers. New architectures, discussed near the end of this section, will remove sampling rate constraints, but in so doing, raise the issue of filter stability vs. wordlength. These issues are discussed first. The basic tasks are listed below.

Task Objectives for Implementation Issues

- Wordlength and algorithm selection for
 - Minimum pole shift (robustness)
 - Mechanization stability
- Sample rate selection
 - Constraints imposed by stability
 - Constraints imposed by architectures
 - Architecture assessment/memory requirements
- Requirement for anti-aliasing filters
- Additional investigations (to be addressed in subsequent studies)
 - Quantization effects and controller roughness
 - Throughput capacity and efficiency
 - Flexibility, fault-tolerance
 - Emulation on large spacecraft model

3.7.1 Multivariable Control Mechanizations

Multivariable control methods have been highly successful for designing complex control systems for multi-input/multi-output systems. To apply multivariable control methods to spacecraft control, the state, controller and estimator equations of Table XVI are generally used. Multivariable control design is based on the quadratic cost functional shown in the table which produces the closed-loop feedback control law. When the state x is not measured (usually the case for HAC systems), x must be estimated from sensor

TABLE XVI Selection of Control Algorithm Form

MULTIVARIABLE CONTROLLED EQUATIONS	
State and Measurement Equations:	$\dot{x} = Fx + Gu + w$ $y = Hx + v$
Control Design:	$J = \int_0^T [x^T A x + u^T B u] dt$ penalty functional $u = Cx$ control structure $SF + F^T S + A - SGB^{-1}G^T S = 0$ steady-state control gains $C = -B^{-1}G^T S$
Filter Design:	$J = \int_0^T [w^T Q w + v^T R v] dt$ noise covariances (weightings) $\dot{\hat{x}} = F\hat{x} + Gu + Kv$ filter structure $v = y - H\hat{x}$ $FP + PF^T + Q - PH^T R^{-1}HP = 0$ steady-state filter gains $K = PH^T R^{-1}$

TABLE XVII Steady-State LQC Controller Form

Kalman Filter:	$\hat{x}_{k+1} = \phi \hat{x}_k + \Gamma u_k + K(v_k - H \hat{x}_k)$
Control Law:	$u_k = -C \hat{x}_k$
where ϕ and Γ are discrete versions of F and G .	
• Implementation Equation	
$\begin{pmatrix} \hat{x}_{k+1} \\ u_k \end{pmatrix} = \underbrace{\begin{bmatrix} F_{11} & F_{12} \\ F_{21} & F_{22} \end{bmatrix}}_{\text{control design matrix}} \begin{pmatrix} \hat{x}_k \\ v_k \end{pmatrix}$	
where $F_{11} = \phi - KH - \Gamma C$, $F_{22} = K$, $F_{21} = -C$ and $F_{22} = 0$	

outputs using a Kalman filter. In the steady state (the usual case for stability augmentation), the control and filter gains (C and K) are constant and can be computed off-line and can then be used to compute u and \hat{x} in real time. The real-time calculations required to implement a steady-state multivariable controller are given in Table XVII. This real-time implementation can be performed by analog or digital circuits. However, the digital implementation is often more flexible since it can be easily modified.

If one examines the steady-state controller equations it becomes clear that only matrix-vector multiplication is required for implementation. The matrix elements, which are constant in the steady-state designs, can be stored in memory for each vehicle configuration. These observations form the basis for the architecture described later.

3.7.2 Stability Analysis

Because of modeling uncertainties, it is important to examine the margin of stability associated with the computations. The magnitude of the pole shift is dependent on a number of factors, such as modeling uncertainties and finite wordlength considerations. From an analysis viewpoint, it is convenient to lump these considerations into the perturbation of F_{11} and analyze the stability of the eigenvalues of $F_{11} + \Delta F_{11}$.

If F_{11} is perturbed to $F_{11} + \Delta F_{11}$, then the corresponding change in the eigenvalues of F_{11} can be estimated from the following:

For the discrete controller

$$\hat{x}_{k+1} = F_{11} \hat{x}_k + F_{12} y_k$$

$$u_k = F_{21} \hat{x}_k$$

If $F_{11} \leftarrow F_{11} + \Delta F_{11}$, then the change in the eigenvalues of F_{11} are given by Jacobi's formula:

$$\Delta \lambda_i = v_i^T \Delta F_{11} u_i \quad i = 1, 2, \dots, n$$

where U and V are respectively the right and left eigenvectors, of F_{11} , and $v_i^T u_i = 1$.

For stability in the z -plane,

$$|\lambda_i + \Delta \lambda_i| \leq |\lambda_i| + |v_i^T \Delta F_{11} u_i| \leq 1$$

$$|v_i^T \Delta F_{11} u_i| \leq 1 - |\lambda_i|$$

Stability Margin

The perturbation in F_{11} can be represented as

$$F_{11} \leftarrow F_{11} + \Delta F_{11} \text{ where } \|\Delta F_{11}\|_{\infty} \leq \frac{m}{2} 2^{-b}$$

b is the number of bits, and n is the system order.

The stable control computations require

$$b = \left\lceil (1 + \log_2 ((1 - \lambda_{\max})/n)) \right\rceil \geq 0$$

where $\lambda_{\max} = \max_{1 \leq i \leq n} |\lambda_i|$.

This formula represents an effective numerical test for rapidly determining the minimum number of bits required to implement a given digital control law. The magnitude of the maximum eigenvalue of F_{11} is the parameter which defines the margin of stability $= 1 - \lambda_{\max} = \Delta \lambda$. The equation was evaluated for different values of λ_{\max} and n . The results are shown in Fig. 3-20. Note that the number of bits required for stability increases substantially as $\lambda_{\max} \rightarrow 1$ and as n increases. Because λ_{\max} is directly related to the sampling rate $(1/\Delta T)$, Fig. 3-20 indicates, therefore, that at

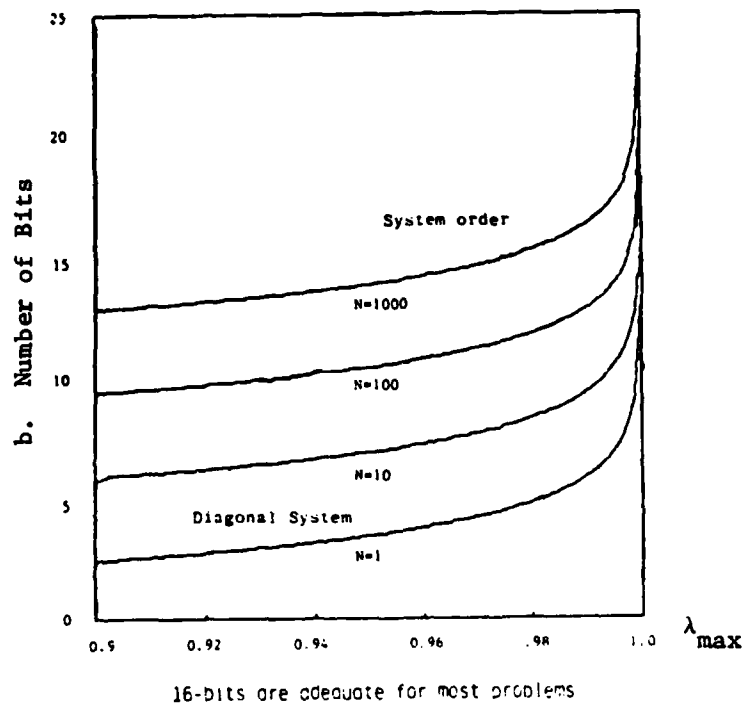
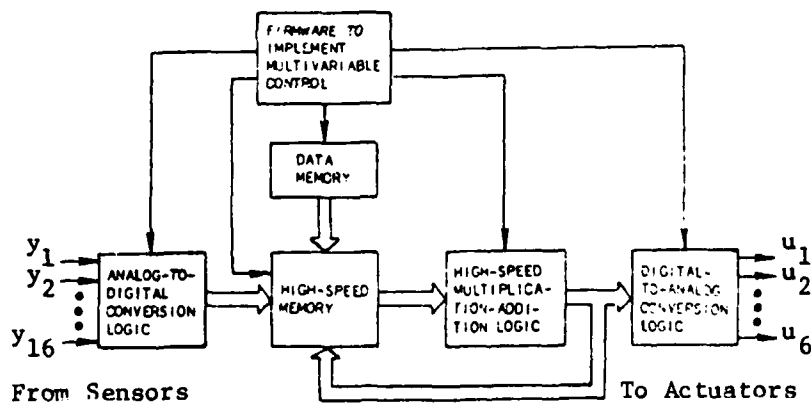


Figure 3-20 Minimum Number of Bits for Stable Control Computations



Architecture has been optimized for control/
filtering computations.

Figure 3-21 An Architecture for High-Speed Control

high sampling rates, a large number of bits are needed to keep the computations stable. Since the improvement in stability is marginal beyond 16 bits, a 16-bit arithmetic processor is frequently sufficient.

3.7.3 Architecture of the Controller

Based on the form of the steady-state estimator-controller equations, the architecture of the digital mechanization can be centered around a high-speed matrix-vector multiplier (see Fig. 3-21). The control design matrix elements are stored in data memory and then downloaded into a high-speed RAM. The analog measurement data are converted to digital form by a highspeed, 12-bit, A/D converter. The results are stored in a high-speed RAM along with the state estimates. The control law is then evaluated by multiplying the control-design matrix by the state estimates and measured data in RAM. A high-speed, 16-bit hardware multiplier/adder performs the matrix multiplications and additions required. All addresses for the RAMs and hardware multiplier/adders are generated by the firmware. The digital controls are then sent to a 12 bit D/A converter. The D/A converts the digital controls to analog signals which are stored in sample-and-hold circuitry. Once the controls have been updated, the controls are simultaneously sent to the actuators.

3.7.4 Requirements for Anti-Aliasing Filters

Digital controllers may require analog filters to eliminate unstable interaction between the controller and the unmodeled bending modes that sampling aliases into the controller frequency band. Also, such filters help reduce the noise aliased into control band and the excitation of unmodeled resonances by harmonics in the reconstructed analog control signals.

A simple example can demonstrate how an analog filter improves a rigid body controller's stability when sampling folds a single unmodeled bending mode whose damping ratio is 0.01. Both a classical and an optimal attitude controller were designed neglecting the effect of the bending response.

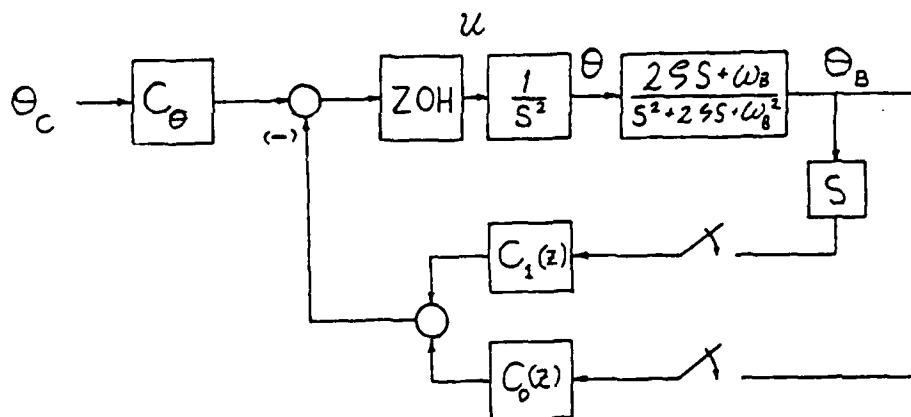
These were exact discrete designs to eliminate the possibility of errors from discretizing a continuous control design. Figure 3-22 shows the block diagram of the total system.

Fig. 3-23 charts the maximum possible controller bandwidth relative to the Nyquist frequency versus the bending-frequency to Nyquist-frequency ratio. Regions (1) through (5) all fold into region (0) like a fan. Line "a" indicates the bandwidth obtainable if no bending pole (i.e., pole corresponding to the bending mode) were present. The striped portions of the curves indicate that the attitude controller is unstable for higher bandwidths; unstriped portions indicate the highest obtainable bandwidth when the controller remained stable.

A cycle of z-plane bending pole movement from B to A and back is common to regions (0) and (1), (2) and (3), and (4) and (5). The bandwidth-limit curve exhibits a W shape in each case. At the arms of the W the pole is at B in the z-plane and the maximum bandwidth compares with the ideal limit 'a' because the large open-loop rigid body response near zero frequency dominates the folded bending response. At the center of the W the bending pole is at A, and the maximum bandwidth is again high because an open-loop phase shift of -360° at the bending resonance turns the resonant peak away from the point $(-1, 0)$ that determines stability in a Nyquist plot.

In summary, Fig. 3-23 indicates that in this example an optimal controller bandwidth below 1/7th the bending frequency or 1/10th the Nyquist frequency will ensure stability. In contrast, a bandwidth less than 40 percent of the Nyquist frequency is safe for a classical design.

To improve the stability of the optimal design, the commanded torque (see Fig. 3-24) signal is passed through a first-order filter. Compensating the filter's phase lag in the control design allows a low filter break frequency, which maximizes the filter's attenuation of the unwanted bending response. Figure 3-25 shows that adding the filter increases the maximum controller bandwidth unless the bending pole is at the favorable z-plane locations A or B.



LEAD COMPENSATION: $C_1(z) = 0$; $C_0(z) = K \frac{z+A}{z+B}$

OPTIMAL DESIGN: $C_1(z)$ MINIMIZES $\int_0^\infty (\lambda e^2 + B u^2) dt$

Figure 3-22 Plant & Control Loop Schematic

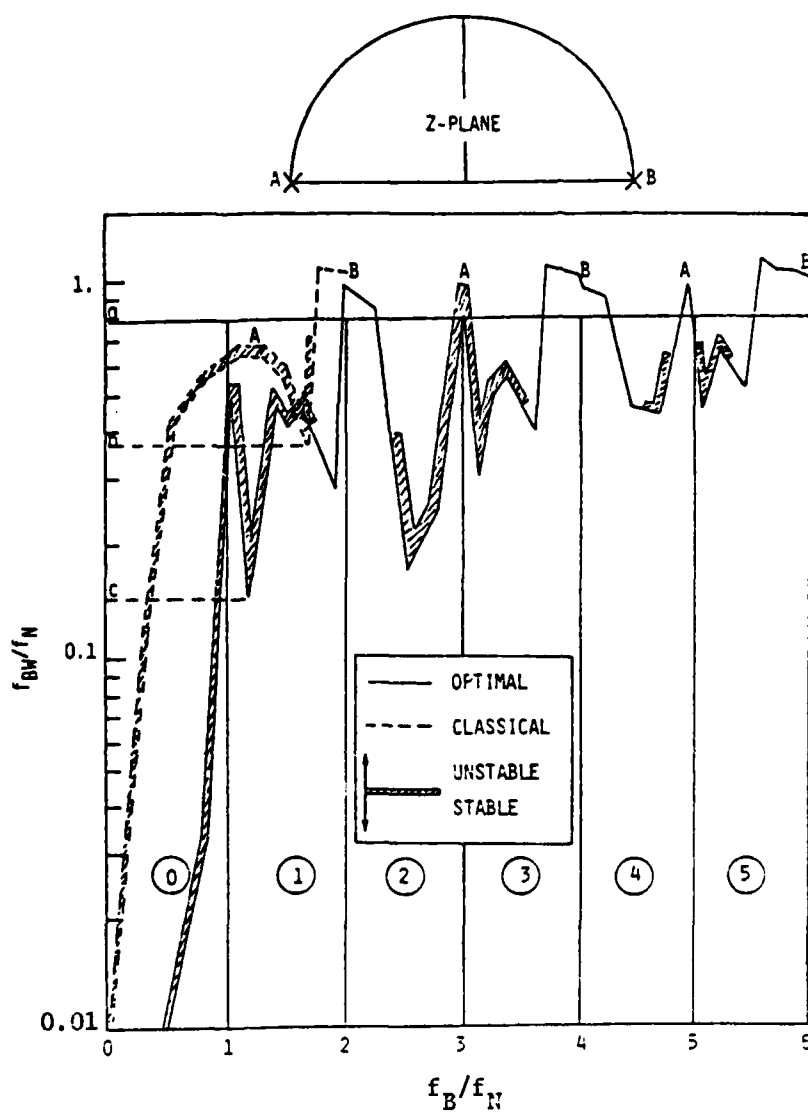
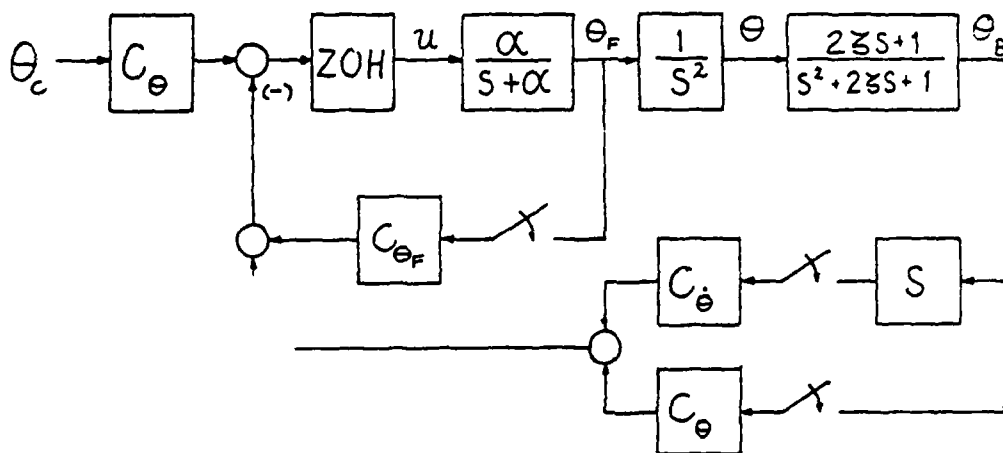


Figure 3-23 Maximum Bandwidth vs Bending Frequency



OPTIMAL DESIGN WITH PREFILTER: $C_\theta, C_{\dot{\theta}}, C_{\theta_F}$ MINIMIZE $\int_0^\infty (A\theta^2 + B u^2) dt$

Figure 3-24 Optimal Design with Prefilter

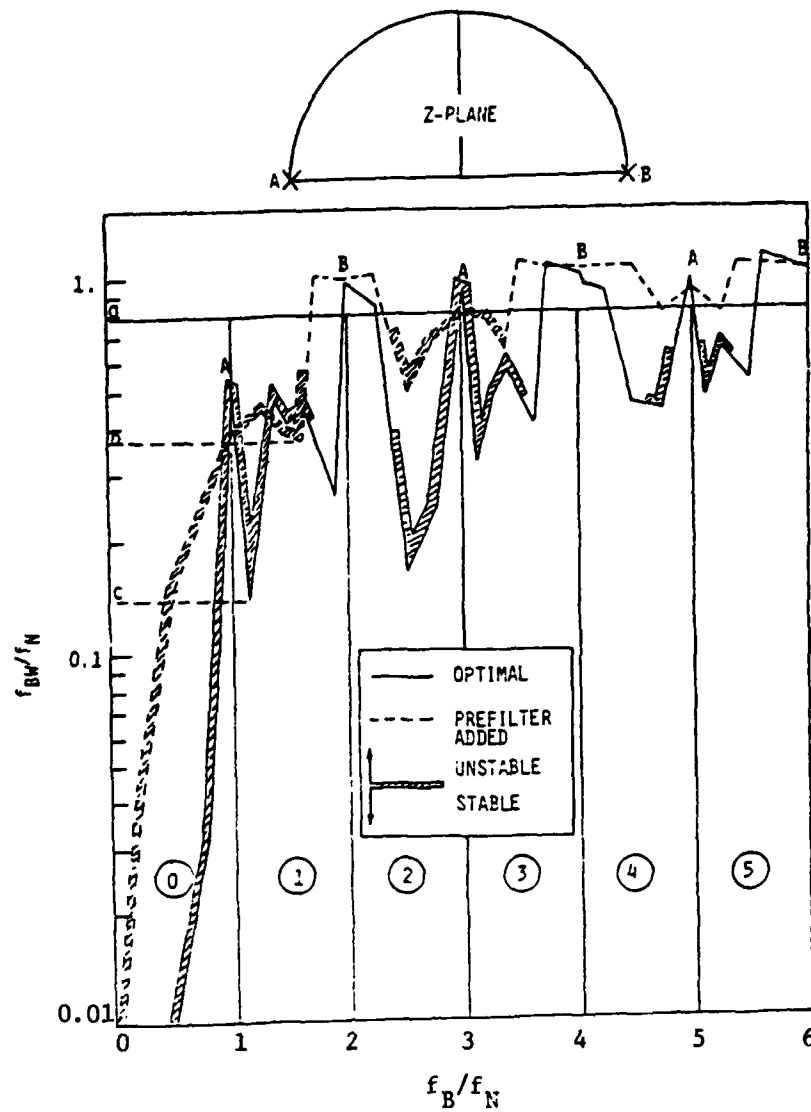


Figure 3-25 Maximum Bandwidth vs Bending Frequency
For Optimal Controller with Filter

In particular, the lowest bandwidth limit in the folding region (1) increases from "c" to "b". The filter is most effective at high frequencies; thus it reduces the unstable region in (3) and eliminates the unstable regions in (4) and (5).

In short, with a filter the maximum optimal controller bandwidth to ensure stability increases from 13.5 to 36 percent of the Nyquist frequency, and the maximum Nyquist frequency for unconditional stability increases from 18 to 29 percent of the unmodeled bending frequency. Judging from frequency response such as shown in Fig. 3-26, a Nyquist frequency below 25 percent of the bending frequency or a controller bandwidth below 33 percent of the Nyquist frequency will insure good response. Without a filter the corresponding values are 14 and 10 percent.

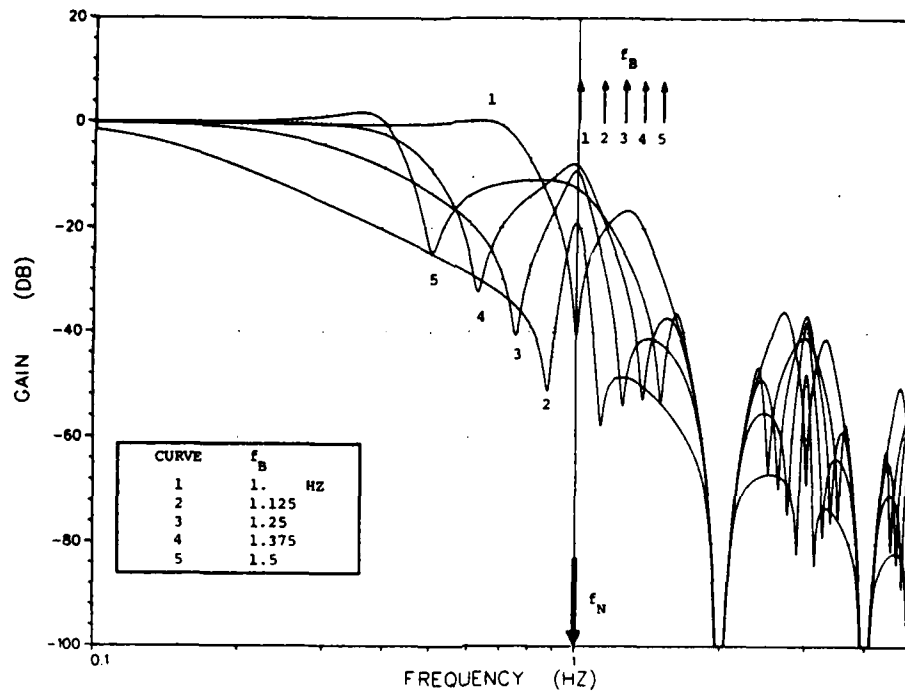
3.8 IDENTIFICATION OF CONTROL DESIGN MODELS

Feedback control design for large space structures requires accurate models of multi-body systems with joints, flexibilities and nonlinear kinematic deflections. Providing such models without dynamic test data may be difficult or impossible. In this section the necessary system identification techniques to obtain complete models from test data are discussed. The algorithms described here are also suitable for (i) validating analytical modeling methods, (ii) real-time monitoring of closed-loop behavior, and (iii) model reduction. The techniques are applied to open-loop and closed-loop data from the plate brassboard experiment described in detail in Section 4. Classical methods were unable to adequately estimate the natural frequencies and damping ratios from this multi-mode data for the closed-loop system.

3.8.1 Identification Requirements

The design of control laws for large space structures requires mathematical models describing the dynamic behavior of structures. The models can be derived from analytical equations or finite-element analysis and other

ATTITUDE RESPONSE W NO PREFILTER



ATTITUDE RESPONSE W PREFILTER

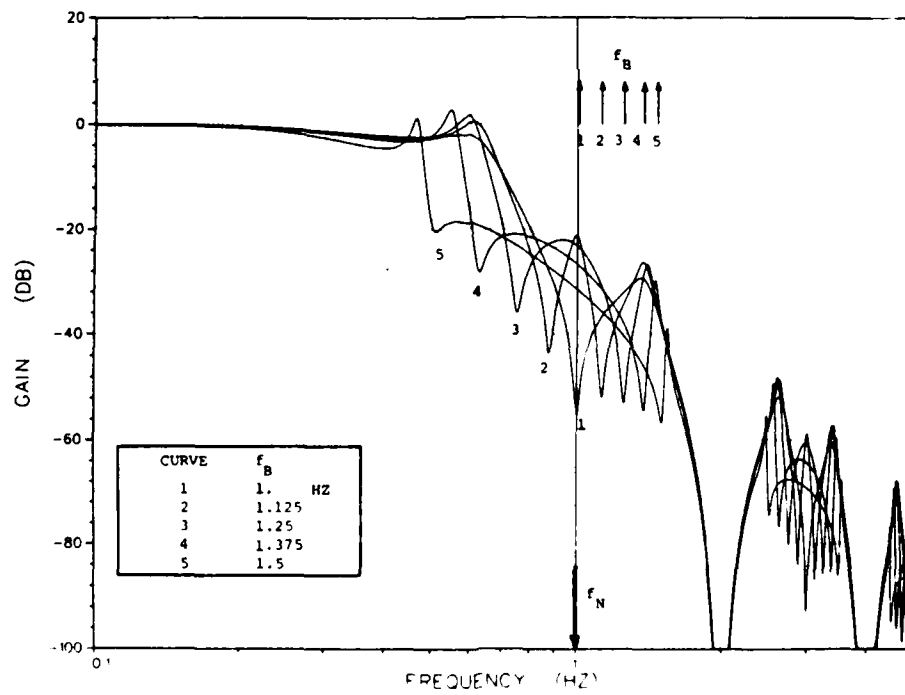


Figure 3-26 Closed-Loop Frequency Responses

numerical procedures. Models derived from physical descriptions of structures are usually inaccurate particularly beyond the first few modes. Tests performed on real structures can provide the basis for the development of accurate models for control law design.

The experimental data must be processed using system identification procedures. For control design, only the input/output behavior needs to be known. In addition, most control design procedures are based on linear or linearized models, thus linear descriptions in the neighborhood of an operating point are sufficient [1]. The techniques specifically described here address the problem of identifying linear multivariable descriptions of input/output behavior. Similar approaches are applicable when complete models are needed to validate analytical modeling methods, real time monitoring, etc.

The system identification technology has been applied previously to various systems including aircraft, missiles, chemical plants, and nuclear reactors. The previous approaches cannot be used directly with large space structures for the following reasons:

- Linear finite dimensional models are at best approximations of distributed parameter structures. Thus, the system identification must be performed in the presence of substantial modeling errors.
- Structures can have a large number of active modes. Previous techniques must be extended for high order models.
- Since modes are poorly damped, the signal is concentrated in certain frequency regions.
- There are modes in actuator/sensor roll-off regions. Thus, it is necessary to model the interactions between actuator/sensor roll-off and structural modes.

- Classical techniques are oriented towards estimating the natural frequencies and damping ratios. Control design requires complete models including system zeros and mode shapes.

In summary, the techniques must be extended to high order systems with unknown model form and must be robust in the presence of model truncation errors.

Sections 3.8.2 and 3.8.3 describe model forms and identification techniques suitable for application to large space structures. The need for robustness and the approaches to extend the techniques to maximize robustness are given in Section 3.8.4. Section 3.8.5 shows the application of the proposed techniques to open-loop as well as closed-loop data from a laboratory experiment with the plate. Finally, the conclusions are given in Section 3.8.6.

3.8.2 Model Forms

The model of a space structure selected for the purpose of identification depends on whether the structure exhibits a linear or nonlinear dynamic behavior. Nonlinearities may arise due to variations in damping at small deflection, other nonlinear structural characteristics, or large variations in the geometry (kinematics). With general nonlinear dynamics, the state equations appear to be the most appropriate representations

$$\dot{x} = f(x,u) \quad (1)$$

$$y = h(x,u) \quad (2)$$

where u is the vector of external inputs, y is the measurement vector and x is the state vector. The order of the state vector depends on the number of modes and the nature of actuator/sensor dynamics.

For linear dynamics, one of the following model forms may be used

- (i) sampled-data on continuous transfer function forms
- (ii) sampled-data on continuous state variables.

This discussion will concentrate on the linear models. These models can be appropriately extended for certain nonlinearities.

3.8.2.1 Transfer Function Models. The $q \times 1$ input u to $p \times 1$ output y transfer function is

$$y(s) = T(s)u(s) \quad (3)$$

where $T(s)$ is a $p \times q$ matrix in the Laplace variable s . The transfer function can be written as a ratio of matrix polynomials.

$$T(s) = \frac{N(s)}{D(s)} \quad (4)$$

$$= \sum_{i=1}^n \frac{R_i}{(s + \lambda_i)} \quad (5)$$

$N(s)$ is a matrix polynomial and $D(s)$ is a scalar polynomial in s . R_i 's are $p \times q$ matrices of residues, and λ_i 's are poles, which relate to large space structure modal frequencies and damping ratios.

For scalar input and output, the transfer function is also written as

$$T(s) = K \frac{\prod_{i=1}^m (s + z_i)}{\prod_{i=1}^n (s + \lambda_i)}, \quad (6)$$

where z_i are the zeros and K is the gain. For Eq. (2) the input and output follow the relations

$$y^{(n)} + \sum_{i=1}^n \alpha_i y^{(n-1)} = \sum_{i=0}^m B_i u^{(m-1)}, \quad (7)$$

where $y^{(j)}$ is the j th derivative of y . This form is also called the autoregressive moving average form.

Discrete transfer functions can be written in a manner similar to the continuous transfer functions, except that a z -transform is used in place of the s -transform. Thus

$$y(z) = T(z) u(z) \quad (8)$$

where

$$z y_k = y_{k+1} \quad (9)$$

This model can be written in any of the forms corresponding to Equations (5) to (7).

The discrete representation maps the imaginary axis into the unit circle. In large space structures most poles are close to the unit circle, therefore, the poles of the discrete formulation are close to the unit circle. Considerable attention must be given to numerical procedures to ensure that the round-off errors do not lead to unacceptable estimates of natural frequencies and damping ratios when a discrete representation is used in the identification of structural parameters.

3.8.2.2 State Variable Models. Defining the state vector as x , one can write a state variable model, as

$$\begin{aligned} \dot{x} &= Fx + Gu + \Gamma w \\ y &= Hx + v \end{aligned} \quad (10)$$

Where w is the process noise vector and v is the measurement noise vector. The F , G and H matrices can take various forms depending on the particular selection of the state vector. In many off-line applications, the state vector is selected to represent a set of physical quantities (e.g., body rates, deflection at a certain point on the structure). Such representations give rise to physical parameters, such as mass, stiffness and damping matrices.

Thus, there are two classes of representations which are useful for system identification:

- (1) a state variable representation based on physical variables, and
- (2) a representation based on any of the canonical forms which would aid system identification.

The canonical forms are applicable when a model is desired only for the purpose of control design because a state variable model $[F, G, H]$ has the same input-output behavior as a $[TFT^{-1}, TG, HT^{-1}]$ model if T is non-singular [2]. In particular, the following representation appears useful

$$F = \begin{bmatrix} B_1 & & & \\ \hline & B_2 & & \\ \hline & & \ddots & \\ \hline & & & B_n \end{bmatrix}, \quad G = \begin{bmatrix} 0 \\ 1 \\ \hline 0 \\ 1 \\ \hline \vdots \\ 0 \\ 1 \end{bmatrix}, \quad (11)$$

$$B_i = \begin{bmatrix} 0 & 1 \\ -\omega_i^2 & -2\xi_i\omega_i \end{bmatrix}, \quad (12)$$

Where ω_i and ξ_i are the natural frequencies and damping ratios of the modes and H is a general matrix with potentially all non-zero elements. With multi-input systems, the remaining part of matrix G is general and unknown. Γ is a general matrix.

For naturally excited structural vibrations, $G = 0$. Then for the purpose of identification, the following Kalman filter representation is desirable

$$\dot{\hat{x}} = F\hat{x} + K(y - H\hat{x}) \quad (13)$$

$$y = H\hat{x} + v \quad \text{and} \quad (14)$$

K now plays the role of G . A combination of natural excitation and known excitation can also be used for system identification.

Note that the representation of Eq. (10) and (11) provides direct estimates of natural frequencies, damping ratios and modal shapes.

Similar representations are also available in discrete form

$$x_{k+1} = \phi x_k + Gu_k + \Gamma w_k \quad (15)$$

$$y_k = Hx_k + v_k$$

The discrete model is particularly useful when the data are sampled uniformly because all system description matrices are then constant. The system identification can then be performed without any solution of differential equations.

3.8.3 Identification Algorithms

Many techniques have been used to identify structural parameters over the last several years. Applicable system identification techniques are conveniently divided into classical and modern techniques as follows [19].

Classical

1. Instrumental variables
2. Extended Kalman filters
3. Maximum likelihood
4. Recursive prediction error (includes recursive maximum likelihood and recursive instrumental variables)

Most of the modern techniques have not been applied to the identification of structural parameters. For large space structures control design problems, modern techniques are preferred because of the following:

1. Modern approaches are based on statistical principles, robust numerical algorithms, and optimization procedures. Classical techniques are mostly ad hoc and were mostly developed in the precomputer era.
2. Each of the modern identification approaches considered here provides a complete description of the observed system behavior. Estimation of mode shapes does not require a different procedure than the estimation of the frequencies.
3. Estimation errors can be obtained in parallel with the estimates themselves when modern estimation methods are used.

The following techniques are discussed in more detail.

1. Least squares,
2. Extended Kalman filter,
3. Recursive prediction error methods,
4. Maximum likelihood and its simplified forms.

All of these techniques can be implemented in the time domain or the frequency domain as discussed later.

3.8.3.1 Least Squares. The measured transfer function $T_m(j\omega)$ is fitted to the parameterized transfer function based on Eqs. (3)-(7). The cost functional is

$$\int_{-\infty}^{\infty} [T(j\omega) - T_m(j\omega)]^* W(j\omega) [T(j\omega) - T_m(j\omega)] d\omega. \quad (16)$$

where $W(j\omega)$ is a positive-definite Hermitian weighting matrix. A nonlinear optimization numerical procedure is required to determine the parameters of the transfer function. The parameters could be the natural frequencies and damping ratios. The measured transfer function, $T_m(j\omega)$, is obtained by dividing the input-output cross-spectrum and the input spectrum.

The approach can give large errors because of the nonconsistency of the Fourier transform estimates.

3.8.3.2 Extended Kalman Filter. The extended Kalman filter (EKF) uses a state-variable formulation with parameters modeled as random functions

$$\dot{x} = F(\theta)x + G(\theta)u + w, \quad (17)$$

$$y = H(\theta)x + v, \quad (18)$$

$$\dot{\theta} = E\theta + \eta, \quad (19)$$

θ is the vector of unknown parameters w , v and η are noise sources. A nonlinear system Kalman filter may be developed for state equations (17) and (19) with measurements given by Eq. (18).

3.8.3.3 Recursive Prediction Error Methods. Recursive prediction error methods are based on minimizing the covariance of one-step-ahead prediction error. If v_k is the innovation, or one-step-ahead prediction error, parameter estimate $\hat{\theta}$ is obtained by minimizing

$$J = \frac{1}{2} \sum_{k=1}^N v_k^2 \quad (20)$$

The minimization, in general, requires solution of a nonlinear optimization problem. The solution is approximated in a recursive form as follows:

$$\hat{\theta}_{k+1} = \hat{\theta}_k + C_k v_{k+1} \quad (21)$$

where θ_k is the vector of parameters (e.g., natural frequencies, damping ratios and zeros of the system). C_k is the gain and is updated using a recursive equation. The manner in which C_k is determined depends on one of several possible recursive prediction error formulations. The v_{k+1} can be computed for the model based on the estimated parameters $\hat{\theta}_k$ and the model equations.

A detailed discussion of recursive prediction error methods is given by Ljung [20].

3.8.3.4 Maximum Likelihood Method. The maximum likelihood approach selects parameters to maximize the conditional likelihood of the parameters given the measurements. For discrete state equations of the form

$$x_{k+1} = \phi x_k + G u_k + w_k \quad (22)$$

$$y_k = H x_k + v_k \quad (23)$$

the likelihood of θ given y_k , $k=1, \dots, N$, is maximized. Statistically it can be shown that

$$\psi(\theta | Y_N) = p(Y_N | \theta), \quad Y_N \triangleq y_1, y_2, \dots, y_N \quad (24)$$

It has been shown that it is typically easier to minimize the negative log-likelihood function. The negative log-likelihood function, J , is written in terms of the innovations as

$$J = \frac{1}{2} \sum_{k=1}^N \left[v_k^T B_k^{-1} v_k + \ln |B_k| \right] \quad (25)$$

where v_k are the innovations and B_k are the innovations covariances. Both of these are outputs of the Kalman filter

$$\hat{x}_{k+1} = \phi \hat{x}_k + G u_k + F K_k v_k \quad (26)$$

$$v_k = y_k - H \hat{x}_k \quad (27)$$

\hat{x}_k is the best estimate of x_k given the measurements up to time $k-1$ and K_k is the Kalman filter gain.

The optimization of the likelihood functions requires solution of a nonlinear programming problem. Techniques to implement such optimization methods have been discussed in reference [21].

3.8.4 Robust Identification

Techniques discussed in the previous section must be significantly extended because of the characteristics of the large space structures and the requirements placed by the need to design robust control laws. Four problems must be addressed directly.

- (i) Lumped-mass models of large space structures approximate a small subset of the infinite modes defining the dynamic behavior of a structure. The identification method must treat large modeling errors, which appear as nonwhite and non-Gaussian state and measurement noise.
- (ii) Several modes can be active simultaneously. In addition, modal separation can be small. Thus, techniques used with single modes are generally inapplicable to large space structures identification.
- (iii) The model order must be specified based on sensor/disturbance bandwidth, or identified from data.
- (iv) If the maximum likelihood method is used, the nonlinear programming method for the optimization of the likelihood function should guarantee convergence.

These problems can be solved by extending the techniques to incorporate the following capabilities:

- (i) Estimation in the presence of nonwhite noise,
- (ii) Estimation with non-Gaussian noise,
- (iii) Model order determination, and
- (iv) Procedures to obtain good starting values to ensure convergence.

Approaches to provide robustness with respect to each of the above is discussed in the following.

3.8.4.1 Nonwhite Noise. As mentioned previously, nonwhiteness arises because large space structures are distributed parameter systems and the identified model is of finite order. The difference between a finite order model and an infinite order system leads to large errors in the high frequency regions. In fact, the high frequency noise can be very nonwhite, and characterized by sharp peaks at modal frequencies.

The problem associated with nonwhite noise made previous applications of the maximum likelihood technique difficult in connection with large space structures. Frequency shaping concepts are being proposed to solve the problem [22]. The basic extension of the maximum likelihood approach involves extending the negative log likelihood function in the frequency domain. Equation (26) in steady state can be written as

$$J = \int_{-\infty}^{\infty} (v^* B^{-1} v + \ln|B|) d\omega \quad (28)$$

where v^* represents the complex conjugate of v in the frequency domain. To make the maximum likelihood method robust with respect to nonwhiteness, B^{-1} is made larger in those frequency regions where the noise is small than in those areas where the noise is large. Similar robust approaches can be used with other algorithms.

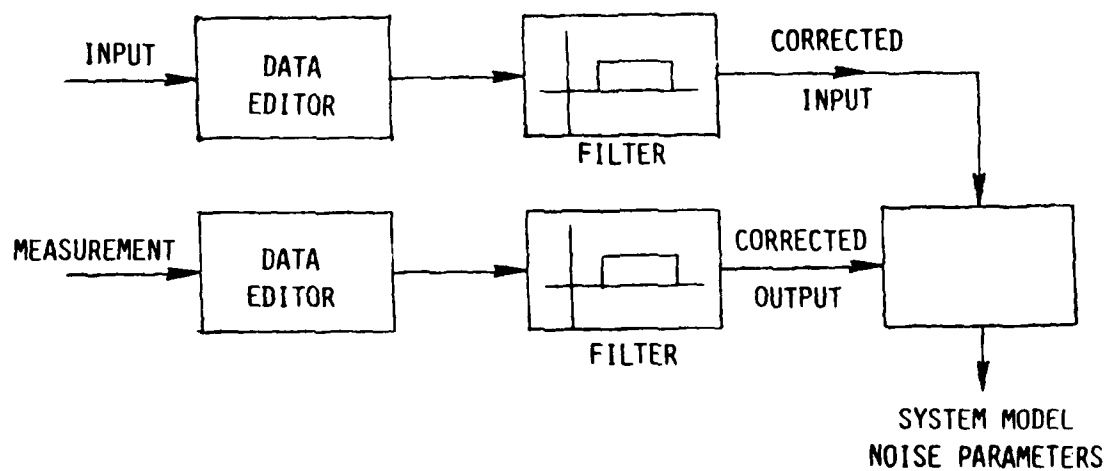
The robust approach can be implemented directly if the output error formulation of the maximum likelihood approach is used. With reference to the system equations (22) and (23), the modification involves using a filtered version of the inputs and the outputs

$$\begin{aligned} x'_{k+1} &= x'_k + G u'_k + w_k \\ y'_k &= H x'_k + v_k \end{aligned} \quad (29)$$

where

$$\begin{aligned} u_c &= \Sigma(s) u, \\ y_c &= \Sigma(s) y. \end{aligned} \quad (30)$$

and $\Sigma^*(s)E(s)$ is the frequency dependent part of B^{-1} . Here we have assumed that $\Sigma(s)$ is a scalar. A robust maximum likelihood implementation is shown in Figure 3-27.



Filters for the input and the output must be the same.

Figure 3-27 Robust Maximum Likelihood Implementation

Note that the frequency-shaping methods may also be used to divide the overall problem into a number of smaller problems. This, perhaps, is one of the most effective tools for model reduction in real-time large space structure estimation.

3.8.4.2 Non-Gaussian Noise. Robustness with respect to Non-Gaussianness is very important because a few bad data points can significantly degrade parameter estimation accuracy. In some cases convergence characteristics would also be affected. The problems of estimation with non-Gaussian noise may be attacked as follows:

1. Use a criterion function that grows more slowly with v than the quadratic one. Then large prediction errors will exert less influence on the parameter estimates and the algorithm thus becomes more robust.
2. Test recursively if the data contain outliers. This can be done by comparing the prediction errors with a specified limit. Large prediction errors mean that an outlier or a measurement error is probable. The bad measurement can then be replaced with the predicted value.

The second approach is preferable when the outliers are large in size but only few in number.

Most identification techniques we have discussed in the previous section are based on minimizing a quadratic penalty functional of the type

$$J = \frac{1}{2} \sum_{k=1}^N v_k^2 \quad (31)$$

The robust procedures modify this cost functional to include a weighting function g which is monotonically decreasing

$$J = \frac{1}{2} \sum_{k=1}^N \frac{g(v_k^2)}{B_k} v_k^2 \quad (32)$$

where B_k is the covariance of v_k . These identification procedures can be incorporated in the numerical implementations in a straightforward manner.

3.8.4.3 Selection of Model Order. Two approaches have been used to specify model order in large space structure identification:

- (i) Start with a model which is known to be of higher order than necessary. The extraneous poles will nearly cancel the extraneous zeros in the identified model.
- (ii) Use a statistical test to select model order. For example, Akaike Information Criterion (AIC may be used [23]).

The first approach appears to work very well in large space structure applications. The second appears to give rise to difficulties, because all known tests are based on the assumption of Gaussian and white noise.

3.8.4.4 Numerical Techniques, Program Architecture and Input/Output Considerations. In large space structure parameter identification, the need for good numerical techniques cannot be overemphasized. The numerical implementation must be robust and should not require excessive computation time or on-line memory. In addition, the numerical techniques must be consistent with the desired software architecture and input/output requirements. Convergence characteristics must be excellent because large space structures may contain modes which are very close to each other and appear as simple modes.

3.8.4.4.1 Numerical Techniques. Computational accuracy is of paramount concern because large space structures would have small damping ratios. A small round-off error could cause a large deviation in the estimate of the damping ratio. Square-root and U-D factorization forms for the propagation of the information and the covariance matrices and the parameter estimates are now standard [24]. U-D factorization is used in all state-of-the-art system identification software.

There are several approaches to improving the identification software:

1. The numerical technique must be capable of quickly detecting wild-points and removing them before they affect parameter estimates. Robust identification methods are discussed in the previous section.
2. In periods of low activity, due to the absence of inputs, the numerical procedure should adjust the data used during estimation in such a way that estimation accuracy is not seriously degraded.
3. The information matrix should not be allowed to become too large, or else new data points will be disregarded.
4. The covariance matrix must be propagated in a nondimensional form. Techniques for nondimensional propagation are shown in [21].
5. If modes over a very large frequency region are to be tracked, numerical accuracy can be enhanced by dividing the overall region into a number of smaller regions.

3.8.4.4.2 Convergence Properties. The convergence properties of most of the algorithms presented previously depend on the selected parameterizations, as well as the starting values. Polynomial representations of continuous or discrete form usually give the best convergence properties. They serve well as starting values. One of the most accurate forms is realized with the F matrix written as 2×2 blocks with frequencies and damping ratios as explicit parameters.

The procedure used have starts with a polynomial model and recursive prediction error techniques. Once adequate convergence is obtained, the polynomials are factored and an equivalent state variable representation is developed to which the maximum-likelihood approach is then applied.

3.8.5 Results from Experimental Data. This section shows results from a laboratory experiment* in which a flat circular plate is used to study active control in large structures (Fig. 3-28). Four microphase measurements of displacement and four local rotation angle measurements from an optical system are available (Table XVII). A proof-mass actuator is used for excitation. Three data records have been processed:

RECORD 1: OPEN LOOP

RECORD 2: CLOSED LOOP (LOW GAIN)

RECORD 3: CLOSED LOOP (HIGH GAIN)

This section describes the results from each of these data sets.

Fig. 3-29 shows the sine-sweep applied to the plate, as well as the eight measurements. The disturbance drives the left pivoted proof-mass (PPM) actuator while the remaining PPM and the contactless actuators are used for control. Note that controls U2, U3 and U4 are small, indicating that no feedback control is applied.

Detailed analysis of data shows that channels 5 and 6 have acceptable signal-to-noise ratios. A detailed plot of applied excitation and the measured output is shown in Fig. 3-30. Note that there is a significant bias and low-frequency drift. At least three modes can be clearly identified from the plots. Figure 3-31 shows the magnitude of the Fourier transforms of the

*This brassboard is discussed in detail in Section 4.

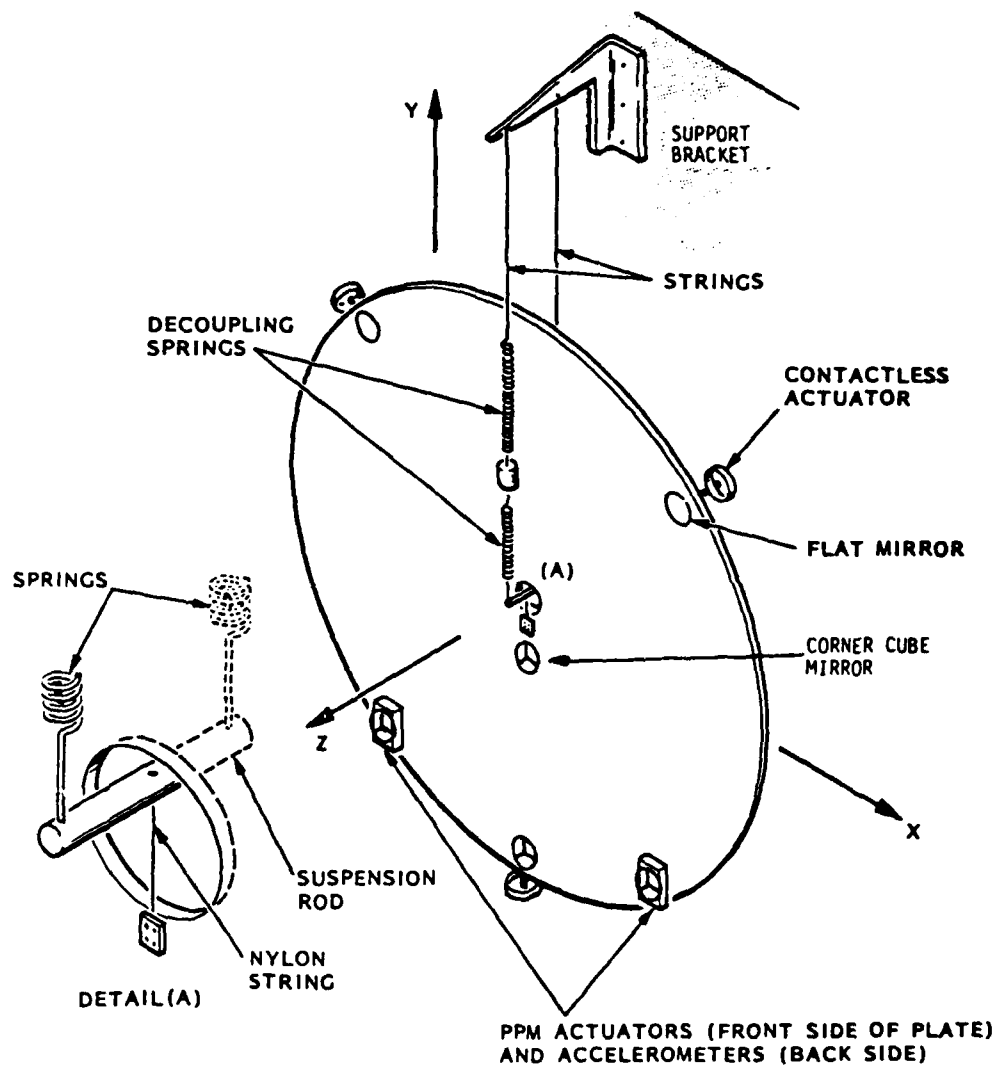


Figure 3-28 Plate Experiment Details

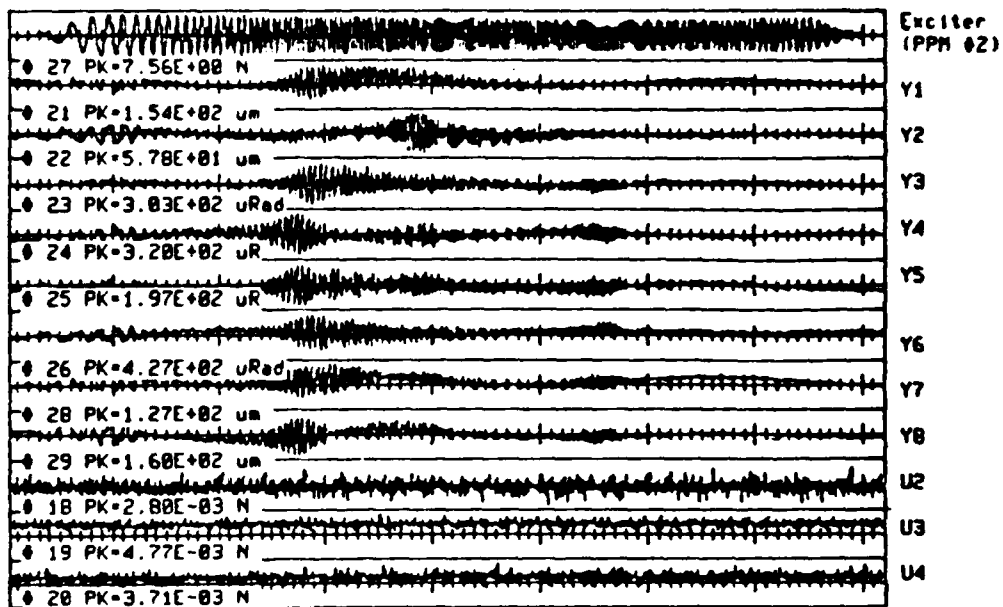


Figure 3-29 Record 1: Open-Loop Test Data

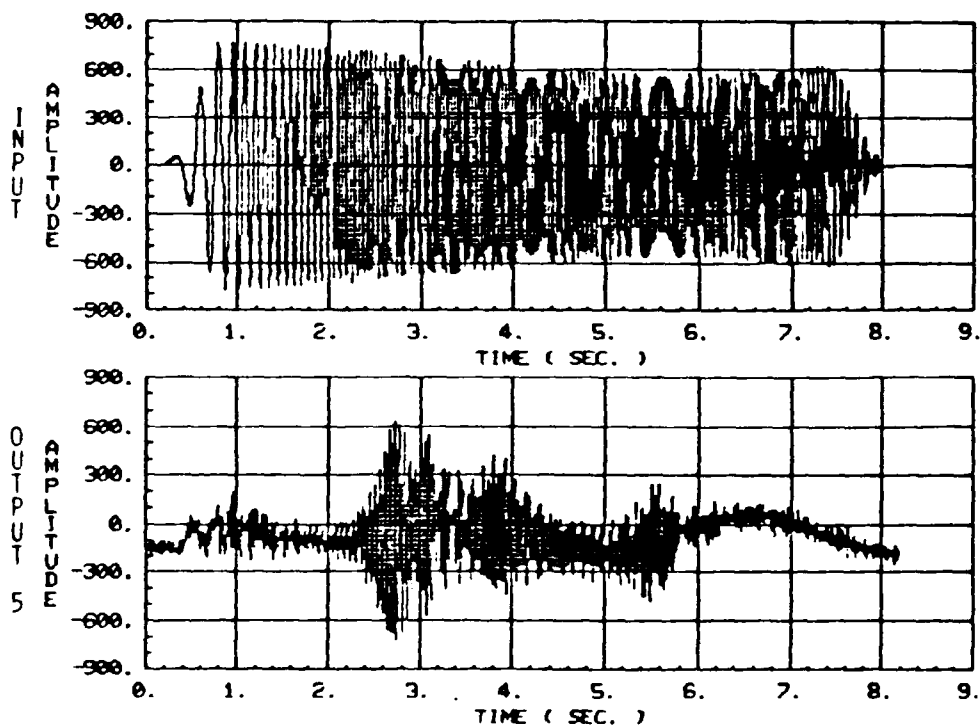


Figure 3-30 Input and Output at Channel 5 (Rotation at Right)

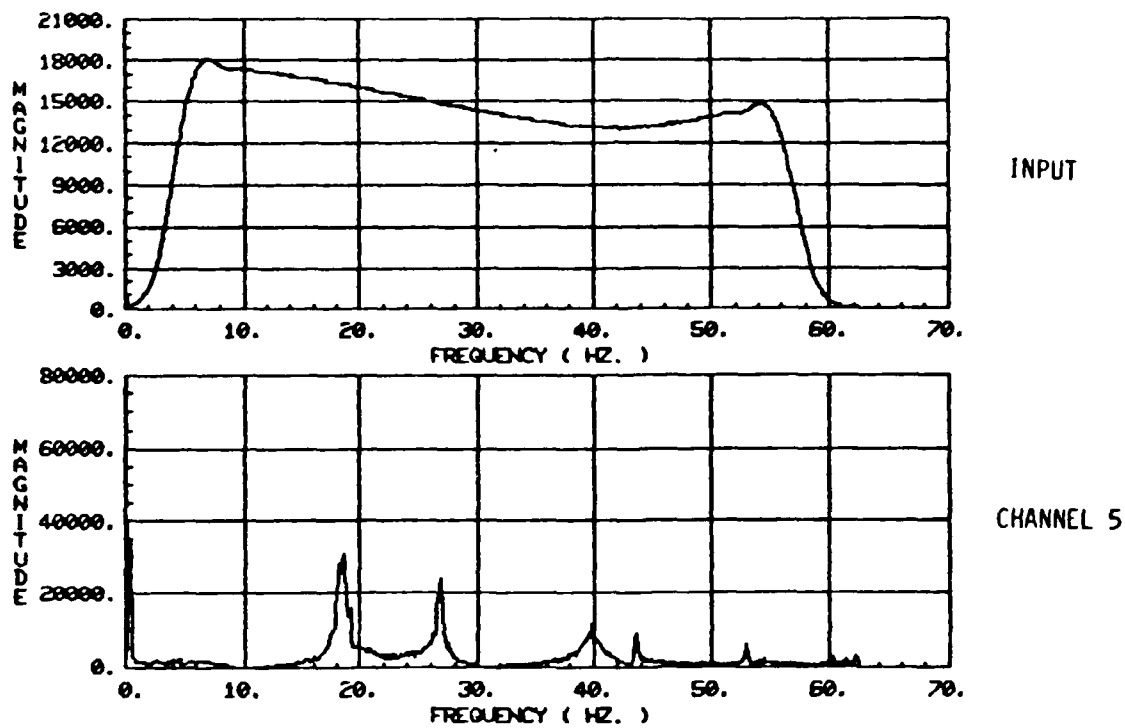


Figure 3-31 Input and Output Spectrum

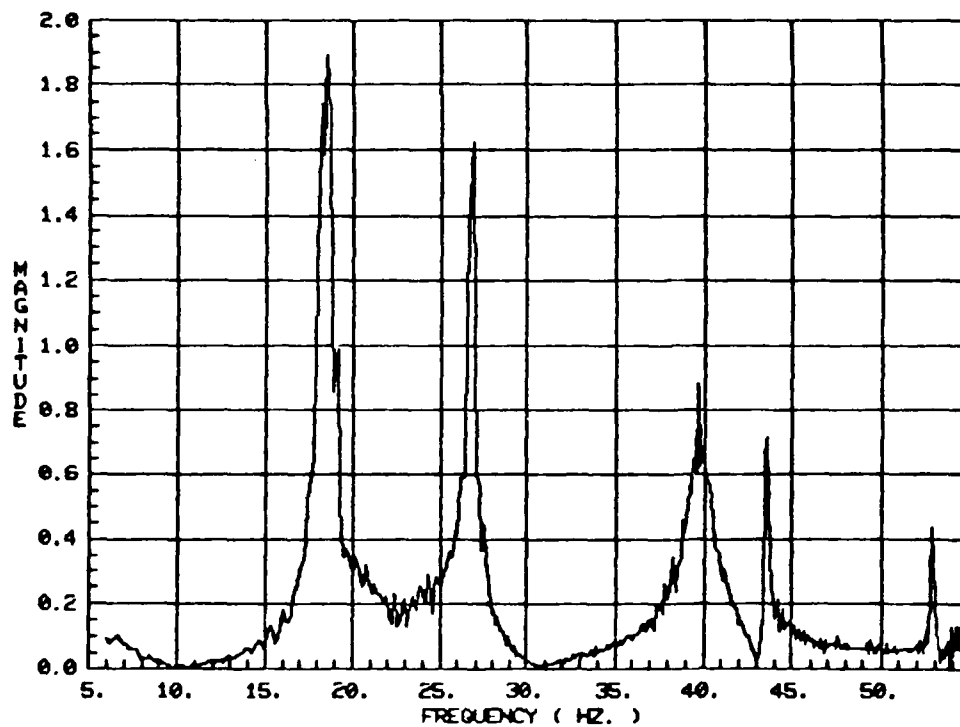


Figure 3-32 Measured Transfer Function

TABLE XVIII Description of Channels

CHANNEL NO.	DESCRIPTION	SCALING PER UNIT OUTPUT
E1	PROOF-MASS EXCITATION INPUT	31. N
Y1	MICROPHASE SENSOR AT THE BOTTOM	0.943 m
Y2	MICROPHASE SENSOR AT THE CENTER	SAME
Y3	ROTATION AT LEFT	2.24 rad
Y4	ROTATION AT LEFT	0.271 rad
Y5	ROTATION AT RIGHT	0.138 rad
Y6	ROTATION AT RIGHT	0.186 rad
Y7	MICROPHASE (LEFT LOWER)	0.943 m
Y8	MICROPHASE (LEFT UPPER)	0.943 m
U1-U4	FEEDBACK CONTROL ACTUATORS	244. N

excitation and the measured output. Note that the input power is mostly in the 5 Hz to 55 Hz region, and that there is a large amount of noise at low frequency.

The measured transfer function in Fig. 3-32 is obtained by dividing the output transfer function by the input transfer function. Five modes are clearly seen, although the modes at 43 Hz and 53 Hz do not appear to have the shape that is typical of a mode. The small peak near the 19 Hz frequency may be a mode or simply noise induced by measurements.

The following identification approach is used:

- Model to be identified is represented as at 16 state, discrete in modal and observable forms
- Maximum likelihood method and recursive prediction error (RPEM) method are used
- Residues of the poles are computed to explore feasibility of model reduction
- Results are compared with analytical models

Poles and zeros identified by the more accurate maximum likelihood approach are shown in Fig. 3-33. The pole locations are very close to those predicted by analytical finite-element analysis.

Figure 3-34 compares the measured time history with that predicted from the identified model on Fig. 3-33. Note the excellent fit and small error. The error spectrum shown in Fig. 3-35 is mostly white with a few peaks. A comparison of the measured and estimated transfer functions is given in Fig. 3-36. The accuracy of the identified model is demonstrated by the excellent fit. Differences in the transfer functions at high frequency are due to foldover and other sampling effects.

3.8.5.2 Closed-Loop Data with Low Gain. Figure 3-37 shows the time histories for a closed-loop experiment. The closed-loop control law was designed using modern control theory and frequency shaping methods. The excitation applied for identification is again a sine-sweep. The response of the fifth channel (top right rotation sensor) is shown in nondimensional form in Fig. 3-38. The three prominent modes as well as the low-frequency drift are easily seen. The data from 2 sec. to 4 sec. have been expanded to show two of the modes and the drift (Fig. 3-39). Note that the second mode is very noisy.

The spectrum of the input and channel 1 are shown in Fig. 3-40. The signal-to-noise ratio is poor. Channel 5 has a much better signal quality (Fig. 3-41). The two peaks below 5 Hz represent primarily noise. Figure 3-42 shows the ratio of the output to the input spectrum. Five modes can be clearly seen.

The maximum likelihood method is used to estimate parameters of a 16-state model. The identified and the analytical pole locations are given in Table XVIII. Figure 3-43 compares the measured transfer function and the transfer function based on estimated poles and zeros. The identified model appears to be reasonably good.

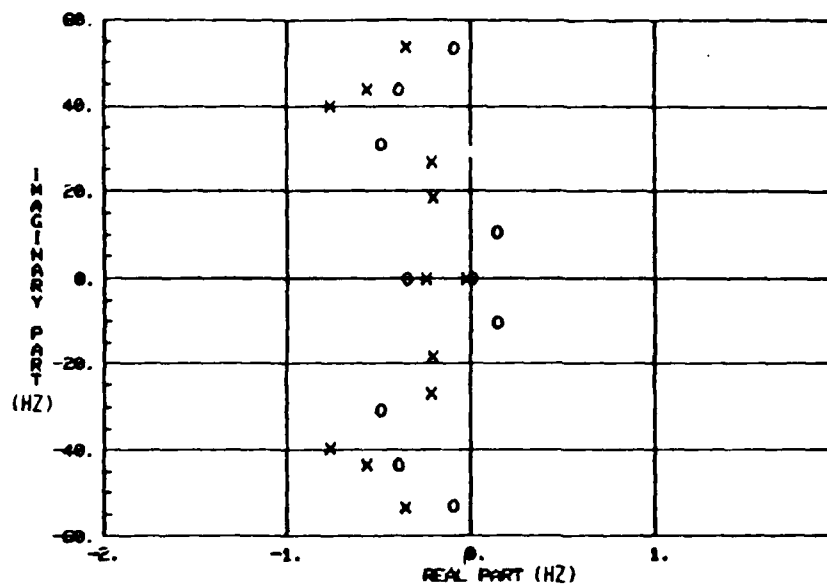


Figure 3-33 Estimated Poles and Zeros

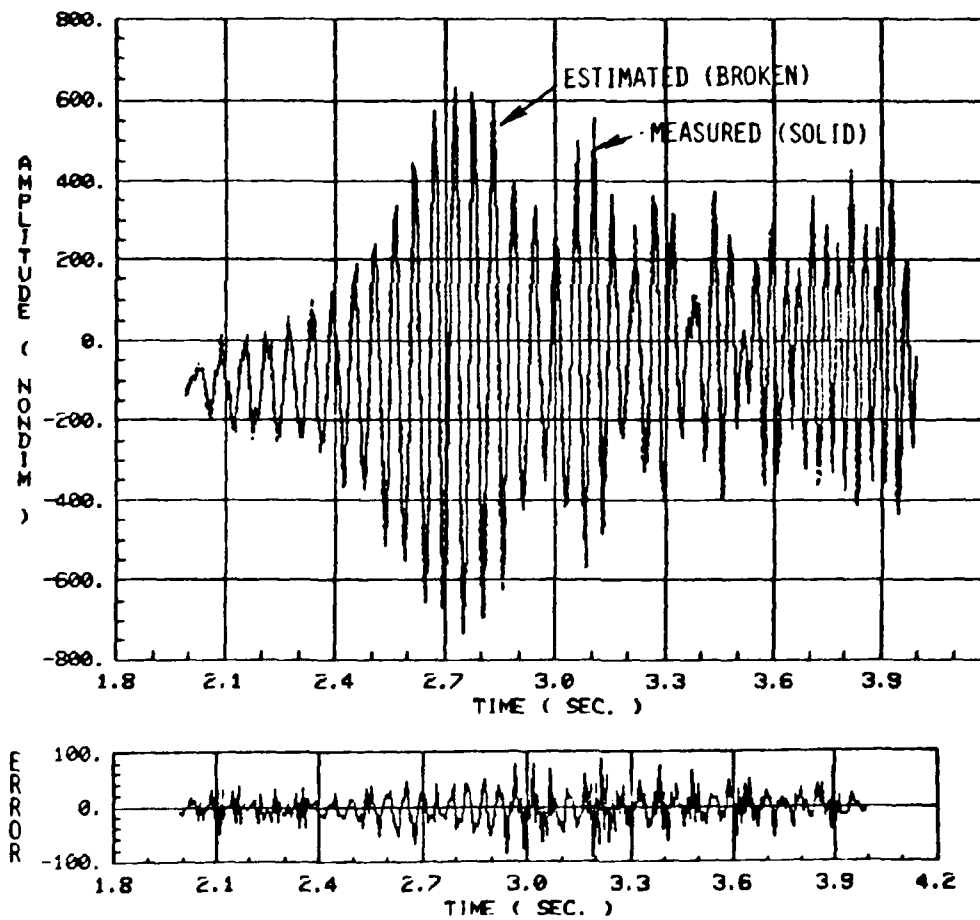


Figure 3-34 Measured and Estimated Time History Comparisons

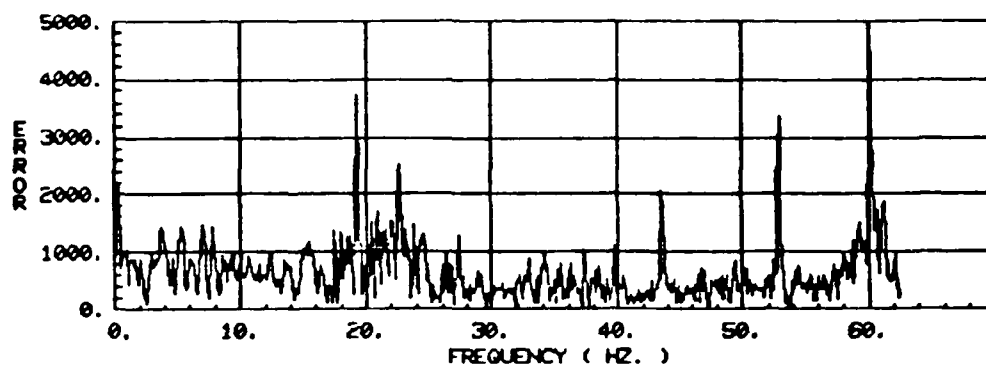


Figure 3-35 Output Error Spectrum

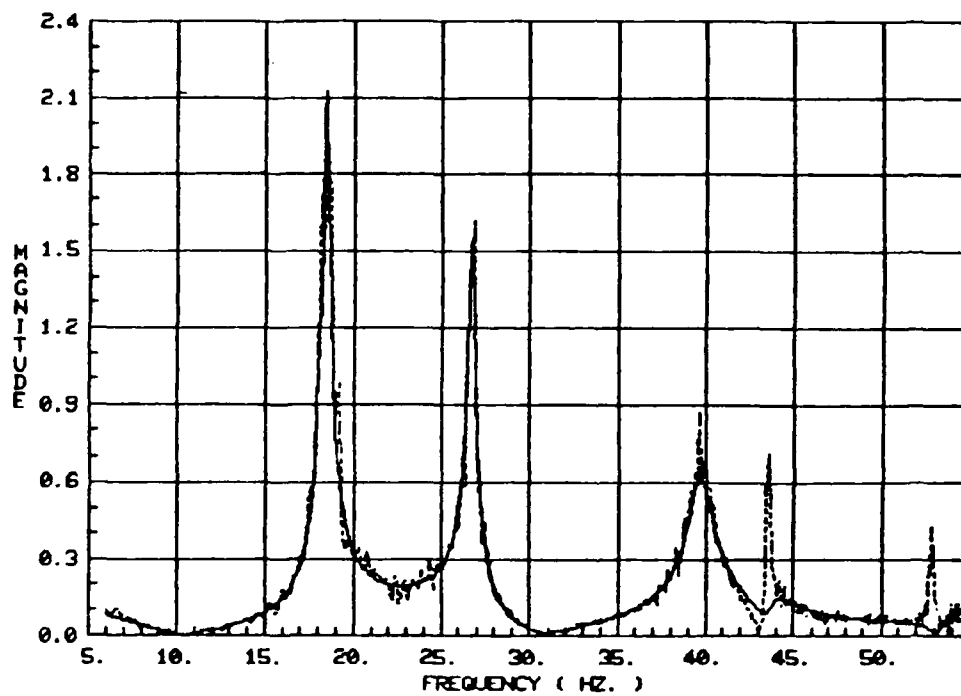


Figure 3-36 Comparison of Measured and Estimated Transfer Functions

TABLE XIX Results (Using Recursive Maximum Likelihood)

FREQUENCY OF MODE (HZ)	ANALYTICAL (CLOSED-LOOP) BASED ON DESIGN	IDENTIFIED CLOSED-LOOP	IDENTIFIED OPEN-LOOP
19.3*	5%	4.8%	1.12%
26.7	1%	.797%	.801%
39.7	1%	1.86%	1.92%
43.9	1%	1.3%	1.3%
53.8	1%	.7%	.7%

* CONTROLLED MODE

CIRCULAR PLATE CONTROL WITH MICROPHASE SENSORS
TEST OF CONTROLLER 306

HDA:29-AUG-82
HTI:17:15:27

TIME SCALE= 8.19 SEC.--FREQUENCY SCALE= 62.5 HZ. DA:29-AUG-82
TI:20:00:03

CLOSED-LOOP TEST FOR SYSTEM IDENTIFICATION

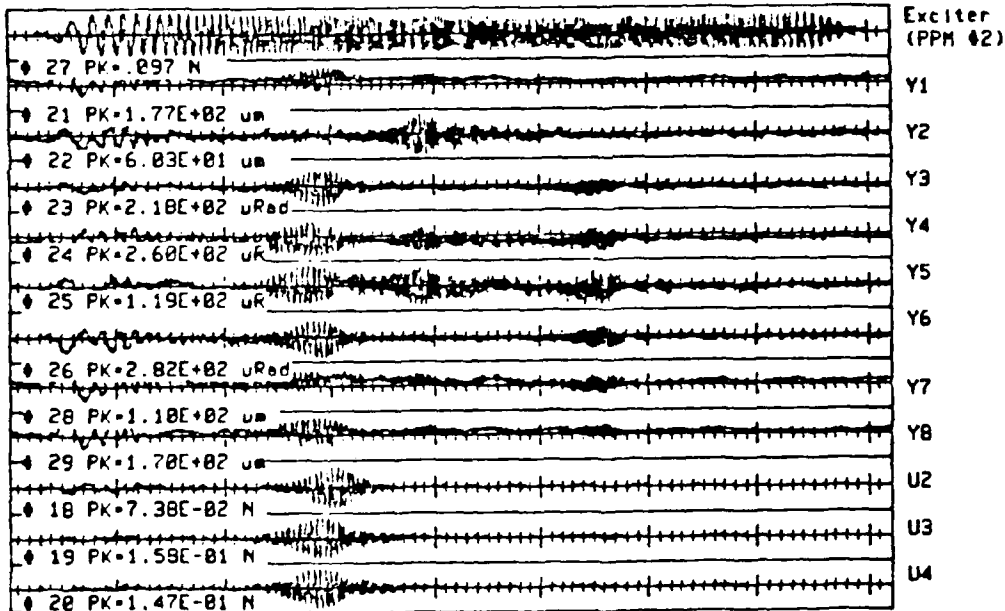


Figure 3-37 Closed Loop Data (Low Gain)

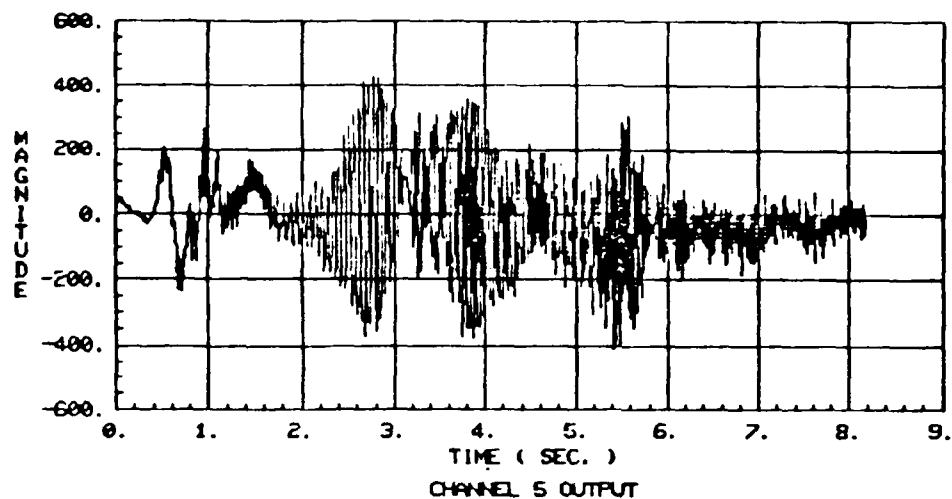


Figure 3-38 Channel 5 Time History (Closed Loop-Low Gain)

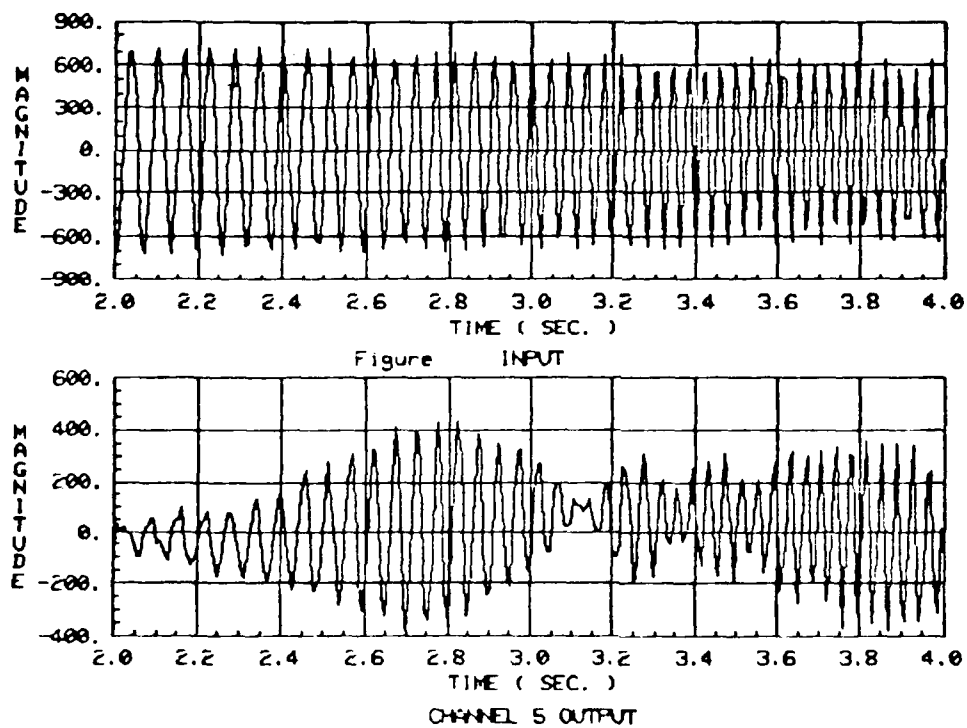


Figure 3-39 Two Significant Modes

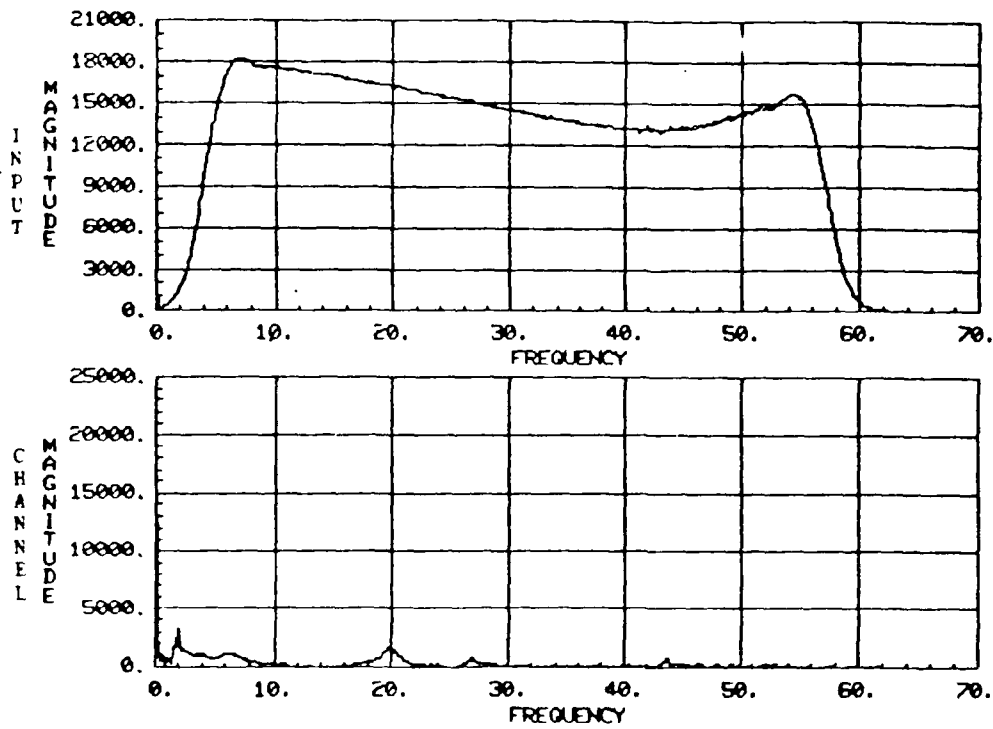


Figure 3-40 Input Spectrum and Channel 1 Spectrum

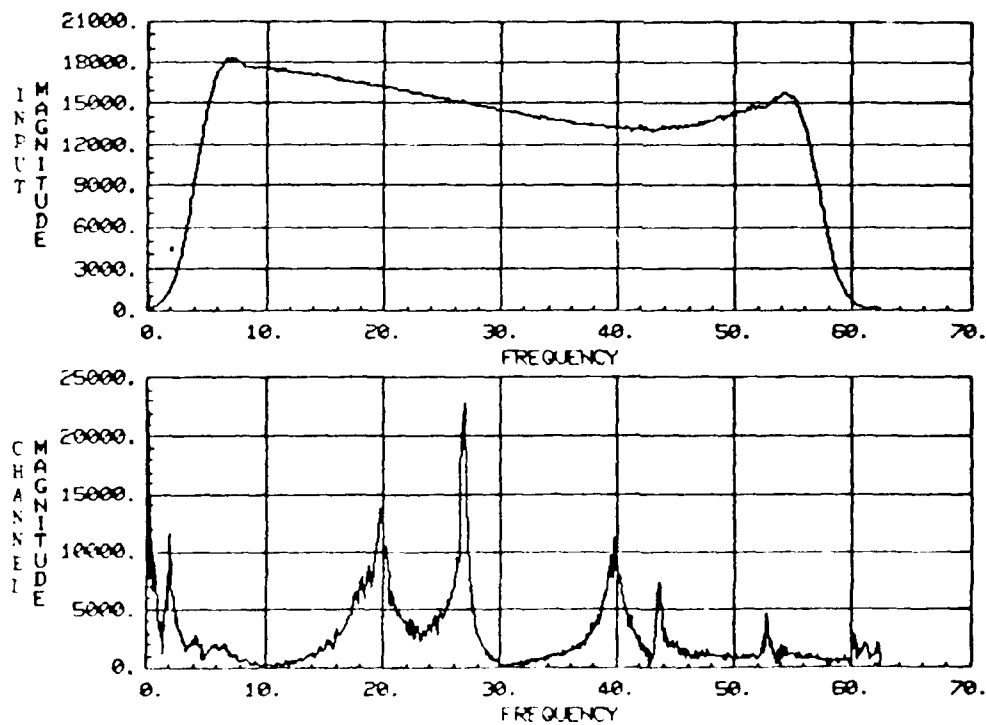


Figure 3-41 Input Spectrum and Channel 5 Output Spectrum

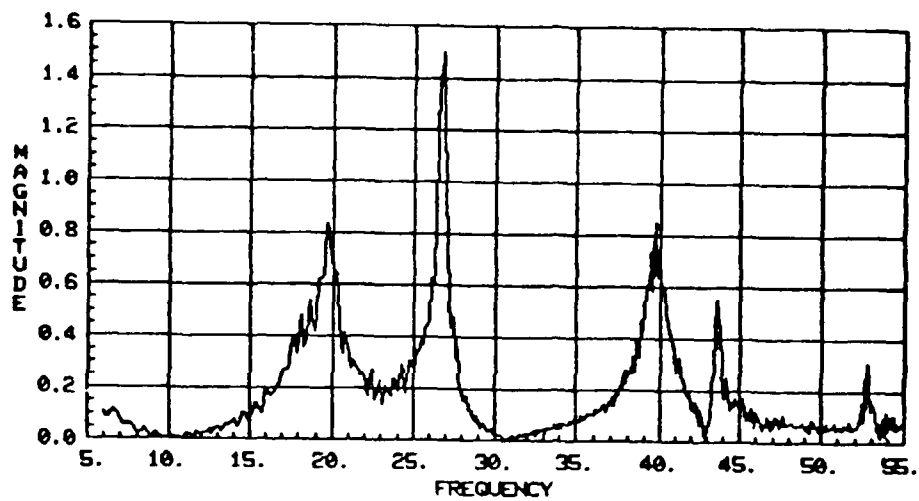


Figure 3-42 Transfer Function Between Channel 5 and Input

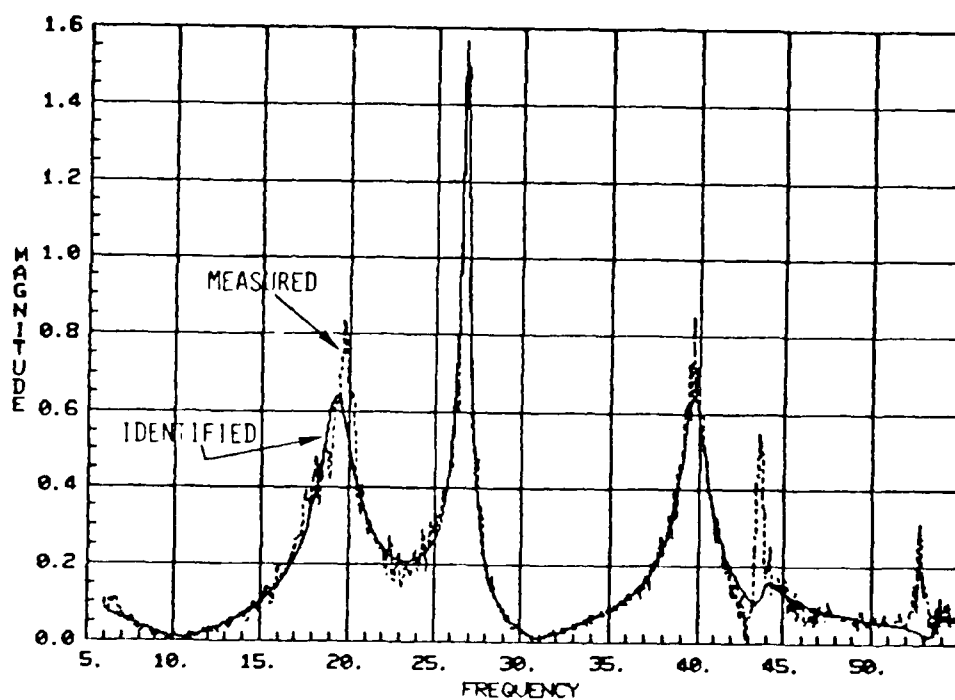


Figure 3-43 Comparison of Identified and Measured Transfer Functions

In Fig. 3-44 is plotted the real-part of the channel 5-to-input transfer function vs. the imaginary part (this is the Kennedy Pancu plot). Each of the polygons should be ideally a circle. The damping ratios and frequencies will be difficult to estimate from such plots. Therefore, for complex systems like the large space structures, classified techniques can provide only qualitative results (e.g., number of active modes). It appears that modern estimation methods are needed for maximizing accuracy and to determine the entire system of equations.

3.8.5.3 Closed Loop (High Gain). Figure 3-45 shows the input and channel 5 output time histories for the high-gain closed-loop system, with the corresponding spectrum shown in Fig. 3-46. The input spectrum is not uniform, partly because the closed-loop controller can remove energy from the structure. In fact, the input spectrum dips near the pole locations. The identified poles and zeros are shown in Fig. 3-47. Figure 3-48 compares the measured spectrum to the estimated spectrum. Note the excellent fit.

Table XIX compares the analytically predicted pole locations and those estimated by the maximum likelihood approach. There are significant discrepancies, probably indicating that the analytical study did not encompass all significant factors, e.g., actuator/sensor dynamics, rate limits, etc. More work is needed on the problem.

3.8.6 Conclusion and Summary

The maximum likelihood technique with appropriate modifications appears to be suitable for identification of control design models for large structures. The techniques appear to be applicable for developing open-loop as well as closed-loop models.

Further work is needed to study the robustness of the procedure to quantify the estimation accuracy. Much more experimental data must be processed to understand convergence characteristics of the maximum likelihood approach and to further extend the methodology.

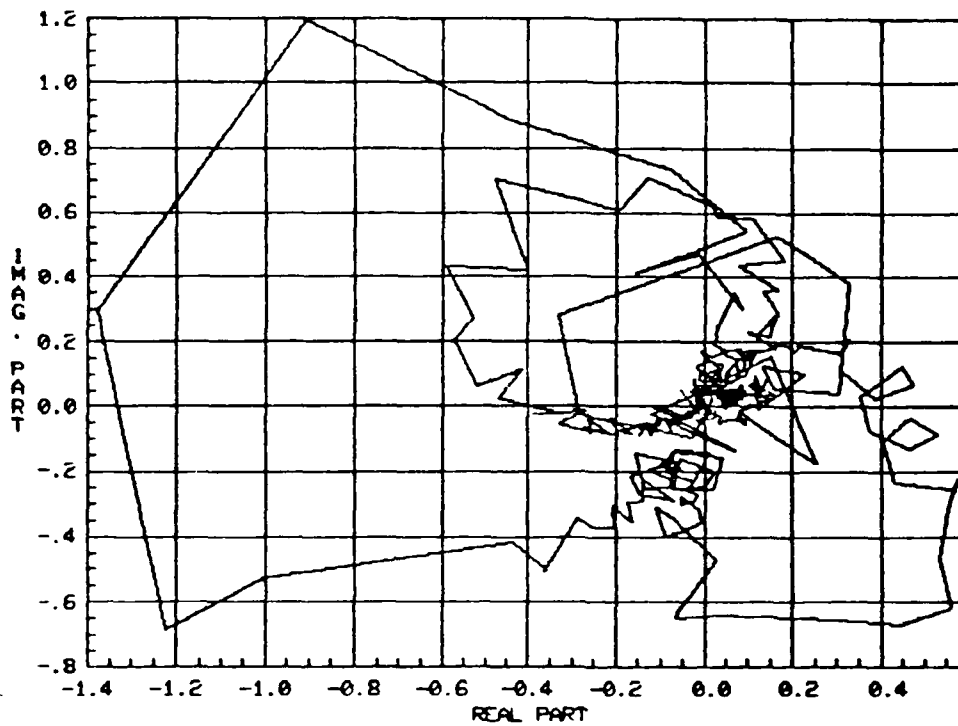


Figure 3-44 Channel 5 Transfer Function Cross Plot

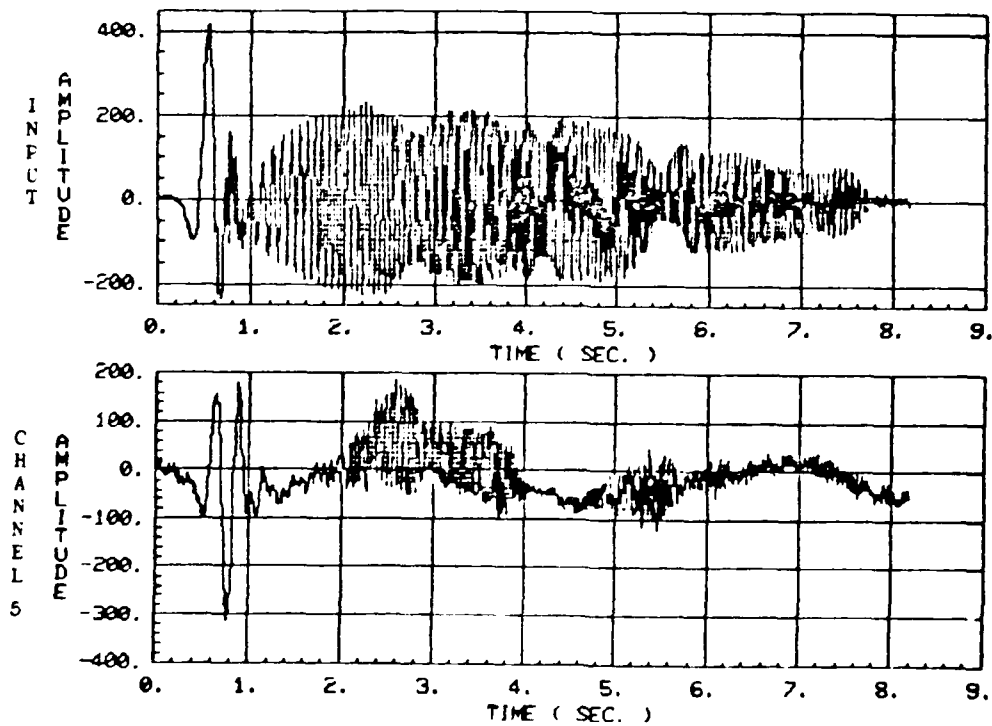


Figure 3-45 High Gain Closed Loop Data Time Histories

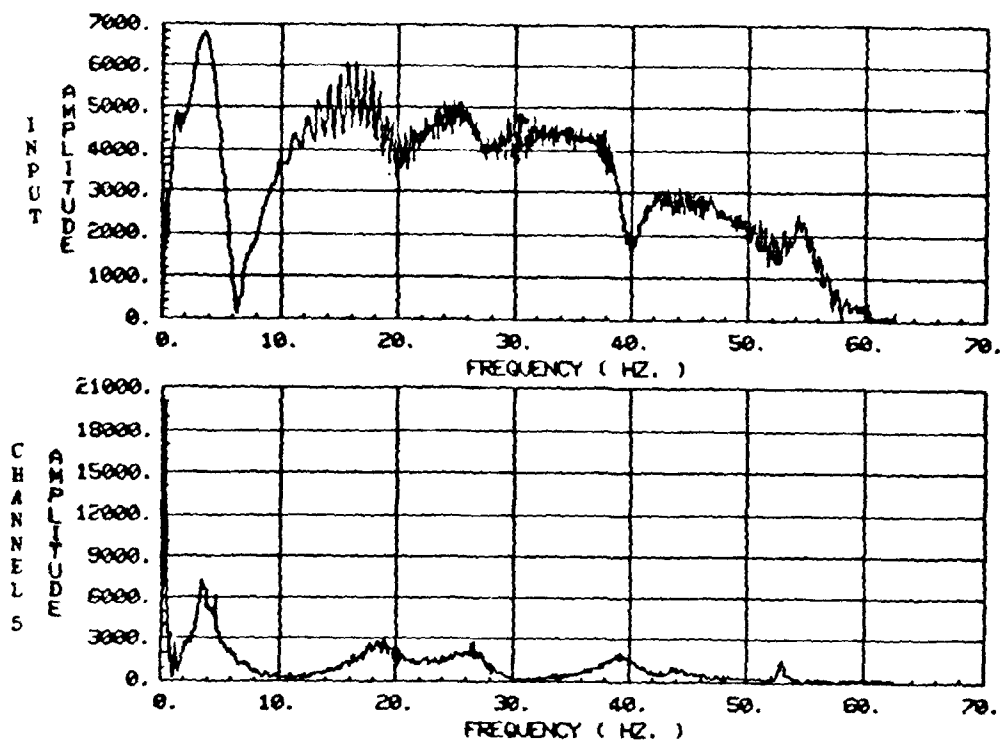


Figure 3-46 Input and Output Spectra for High Gain Closed Loop System

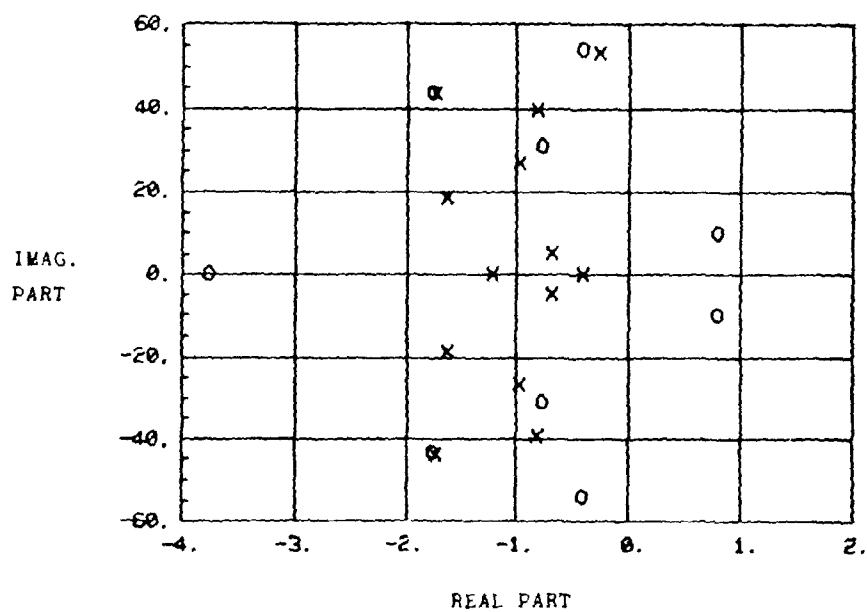


Figure 3-47 Identified Poles and Zeroes

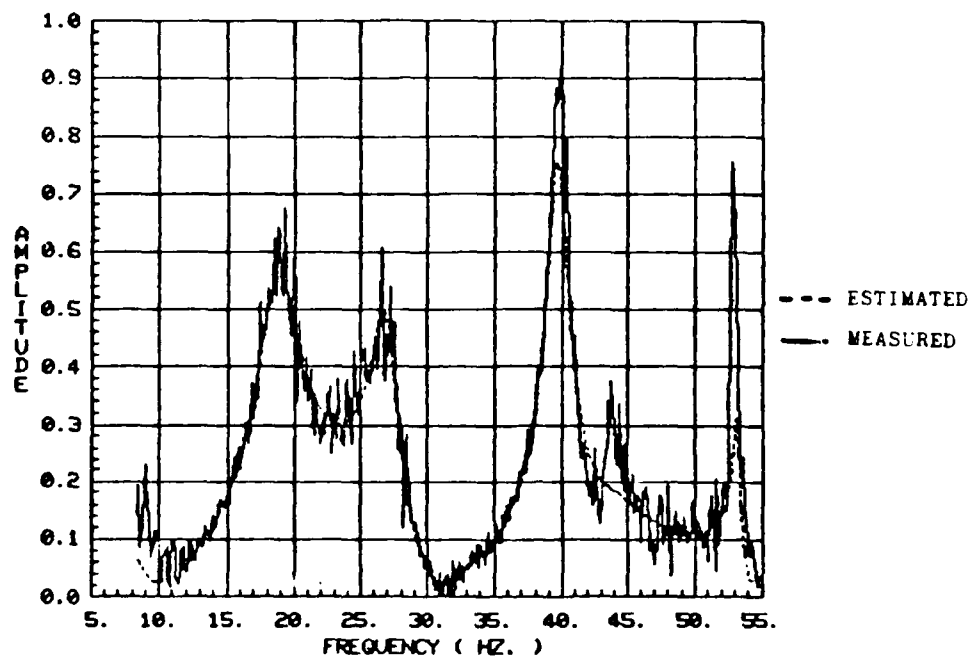


Figure 3-48 Measured and Estimated Transfer Functions

TABLE XX Closed-Loop Poles

LAC ONLY		HAC AND LAC			
Analytical		Analytical Predicted		Measured Max. Likelihood	
Frequency	Damping	Frequency	Damping	Frequency	Damping
.194	.005	c 0.55	.22		
		f 0.64	.41		
.324	.005	c 2.52	.70		
		f 2.52	.71		
.519	.005	c 2.68	.70		
		f 2.62	.70		
18.15	.018	c 18.60	.15		
		f 18.30	.15	18.7	.095
19.07	.009	c 19.57	.15		
		f 19.18	.12	19.94	.071
26.63	.008	c 26.95	.10	26.95	.036
		f 26.62	.10	26.66	.048
39.50	.010	c 39.59	.04	39.73	.019
		f 39.51	.05	39.62	.021
43.40	.001	c 43.43	.02	43.78	.022
		f 43.42	.04	43.89	.040

(c: controller, f: filter)

More work is also needed to treat

- Multi-input/multi-output responses
- Nonlinearities
- Poor signal-to-noise-ratio channels
- Modeling errors

It would also be desirable to have techniques which can optimally select input waveforms and spectra as well as sampling rate and other test variables.

Section 4

EXPERIMENTAL VERIFICATIONS

4.1 OBJECTIVES AND APPROACH

The fundamental objective of the ACOSS 12 experimental program was to validate the full ACOSS control methodology through ground laboratory experiments. A secondary objective was to include space-like or space qualified hardware in these experiments to develop confidence in real flight implementations.

To accomplish these objectives, test structures were designed to replicate some or most of the characteristics found in actual large space structures, principally, low natural damping and closely distributed modal frequencies. The ACOSS control methodology was applied to these structures, whereby finite elements were constructed and state-space models derived from them for control synthesis and evaluation.

The control laws were then mechanized in real-time on high-speed array processors and implemented on the test structures. Closed-loop characteristics were measured and compared with analytical predictions.

Because of the multidimensional nature of the problem, these characterizations required the use of adequate system identification techniques and advanced digital data processing. Verification of the proper performance of the state estimators was also a very important part of these tests. Incorrect estimates are usually a more severe cause of performance degradation than are direct model errors.

4.2 EXPERIMENT DESCRIPTION OVERVIEW

Three experiments were conducted:

- 1) The circular plate experiment (CP)
- 2) The Proof of Concept experiment (POC), and
- 3) The Truss-wheel experiment (TW)

The first two were the major experiments in structural control, while the third one was a first attempt to understand and model truss-like structures with high modal density.

The CP experiment had three objectives. First, the validation of the HAC/LAC approach on a highly resonant structure with nearly repeated modal frequencies, with a control system including both attitude and vibration control; second, the demonstration of the use of two new pieces of hardware: the Pivoted Proof Mass actuator (PPM) and the micro-phase optical sensor (u-phase sensor), which were both included for the first time in an optimal control scheme; finally, the demonstration of high-speed digital mechanizations (125 Hz sampling rate) and the use of almost full Nyquist range by the controller.

The main objective of the POC experiment was to demonstrate the control methodology on a three-dimensional, large-scale structure, having some likeness to a spacecraft configuration. Existing flight hardware (such as the Control Moment Gyros (CMGs) for both attitude and vibration control, or rate gyros for local sensing) was used in this experiment, which made it as close as it could be at this time to an actual space system. Obviously, it is a simple structure compared to any projected or existing real vehicle, but the important point was to apply all the steps of the modeling, control synthesis and analysis, and to be able to predict the results with some accuracy. The control mechanization was also done on a digital processor and digital control laws were synthesized directly (as opposed to being synthesized in the continuous domain and then being digitally implemented with a high enough

sampling rate). This procedure was even more important here than in the CP experiment because the maximum sampling rate was low (60 Hz).

Finally, a third experiment involved the so-called truss-wheel, a three-dimensional star-like truss structure, which was designed to have low damping and closely packed modes. The goal was to perform open loop characterizations of the structure and compare then to finite element model results. Only then could a state estimator be constructed in view of further control design.

Photographs of the experimental set-ups for these three experiments are shown in Figs 4-1, 4-2 and 4-3, respectively.

4.3 CIRCULAR PLATE EXPERIMENT

4.3.1 Description

The structure to be controlled is a flat aluminum circular plate, 1.2 in diameter and about 3 mm (1/8") thick. It is suspended vertically by a system of springs and strings attached near its center as shown in Fig. (4-4). This device provides nearly unrestrained boundary conditions for the plate, with the first three rigid body modes (x and y rotation, z translation) around or below 0.3 Hz, while the first bending mode occurs at about 19 Hz. The suspension system is attached to a frame mounted on a 14 foot long optics table to provide further insulation from ground vibrations. (The whole table can actually be floated on air bags. This feature was not exercised, however). The frame and the plate are enclosed in a sound-proof cabinet with a front plexiglass window to further reduce disturbances due to acoustic vibrations and air currents.

Sensors and Actuators

The sensing system is purely optical. Although two accelerometers were used in preliminary tests, they were abandoned because of adverse characteristics.

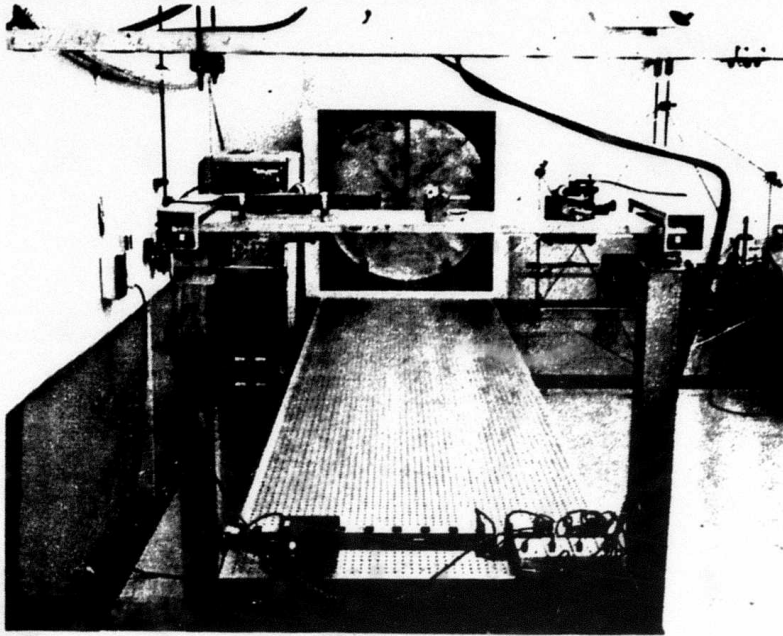


Figure 4-1. Circular Plate Experiment

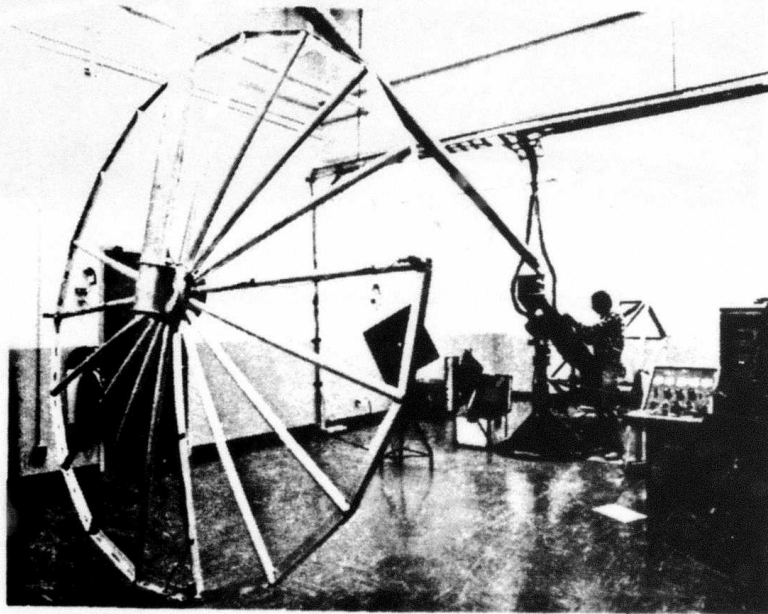


Figure 4-2. Proof-of-Concept Experiment

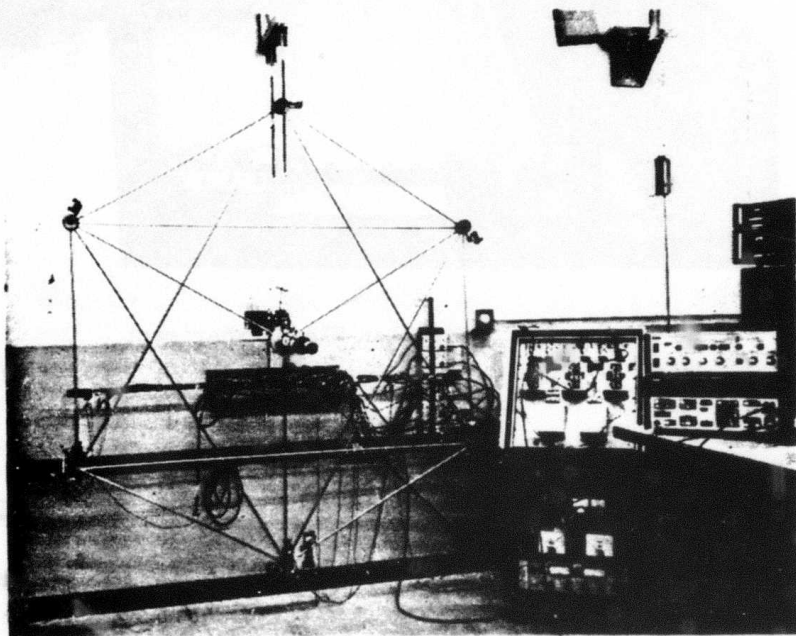


Figure 4-3. Truss-Wheel Experiment

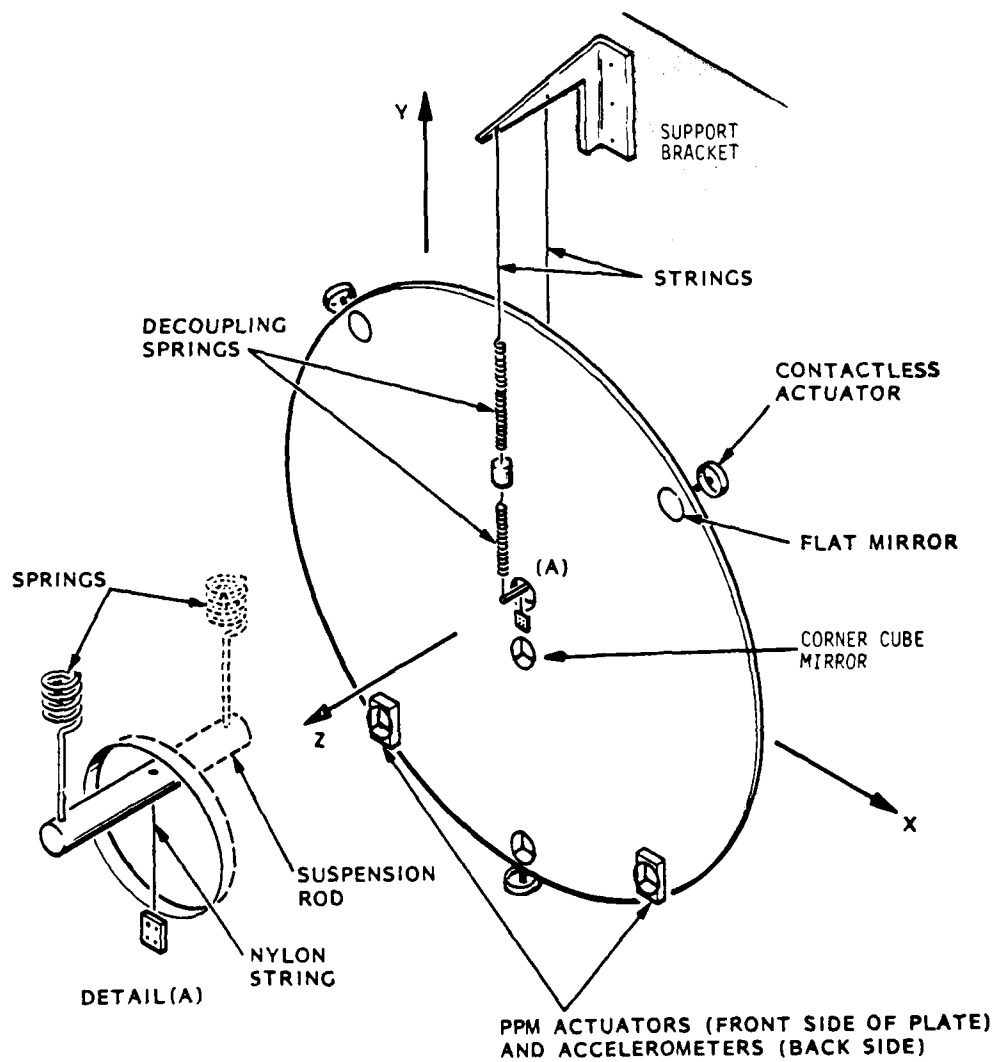


Figure 4-4 Plate Experiment: General Schematic

Instead, four corner-cube mirrors have been mounted on the plate and are used in conjunction with the μ -phase sensor which measures their position along the z axis by comparing the phase between outgoing and reflected laser beams. Also, two flat mirrors on the top reflect laser beams which are sensed by two two-dimensional linear photo-detectors (Fig. 4-5). Each detector measures the rotations about the y' and x' axes of the plate (x'y' are rotated by $\pm 45^\circ$ from the x/y axes).

Actuation is provided by three contactless actuators (for attitude and vibration control) and two PPM actuators (for vibration control or disturbance injection). These actuators were described in detail in the ACOSS 5 final report [1].

In Fig. 4-6 is shown a recapitulation of the actuator/sensor system with a nomenclature and numbering which will be used throughout this report. Table XXI shows the participation of these actuators and sensors in the control system and evaluation procedure. Six sensors and four actuators were used for control purposes. The remaining actuator (PPM) was used to excite the specimen with various disturbances, and the last two optical sensors provided supplementary information for evaluation purposes and an independent check of the system.

Control Synthesis Model

From the SPAR finite element model obtained during Phase II, system matrices were generated corresponding to the state equations.

$$\begin{aligned}\dot{x} &= Fx + Gu \\ y &= Hx\end{aligned}\tag{33}$$

(The state vector x is described in Table XXI, along with the vectors u and y.)

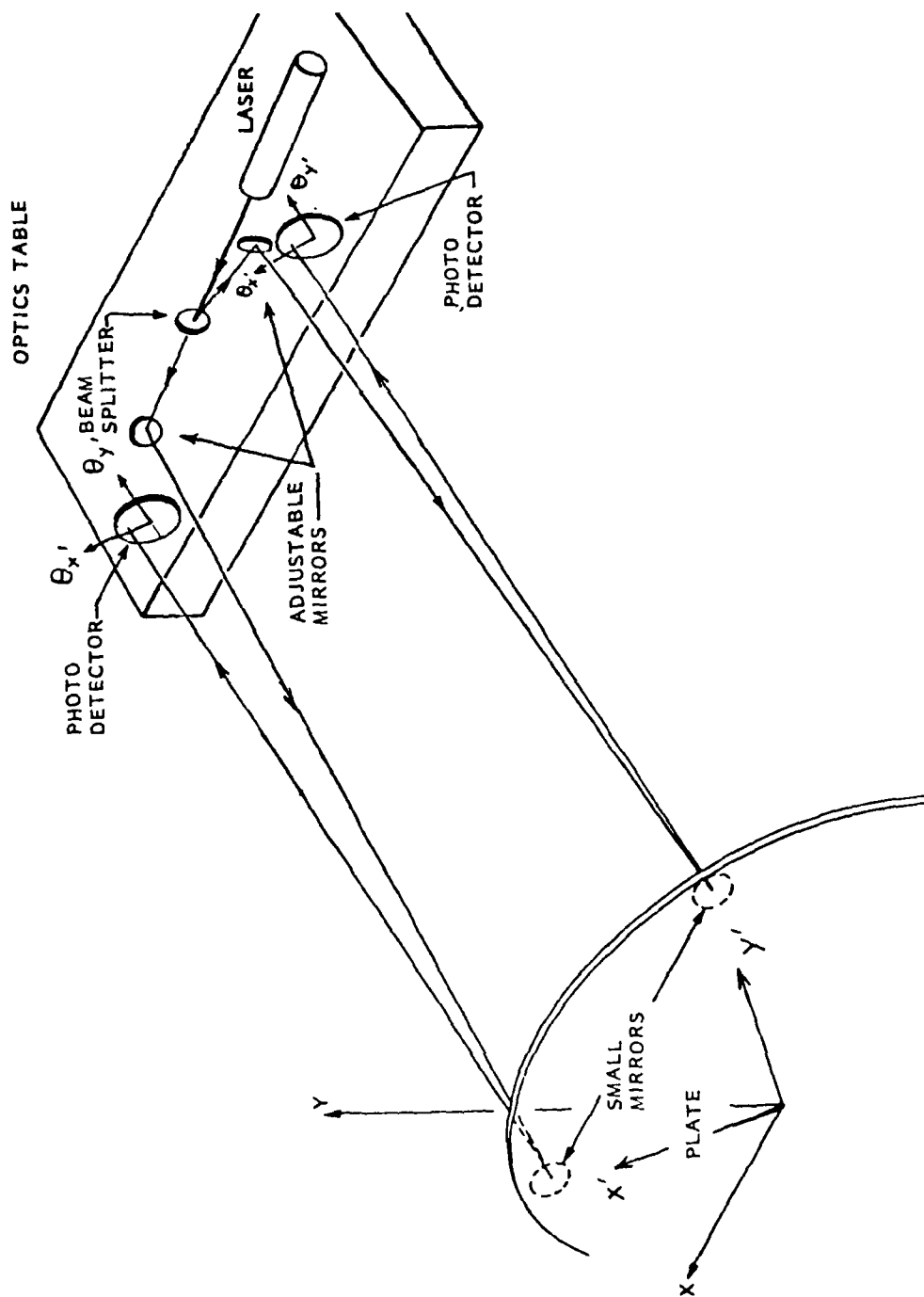


Figure 4-5 Circular Plate Experiment: Angular Optical Sensing System

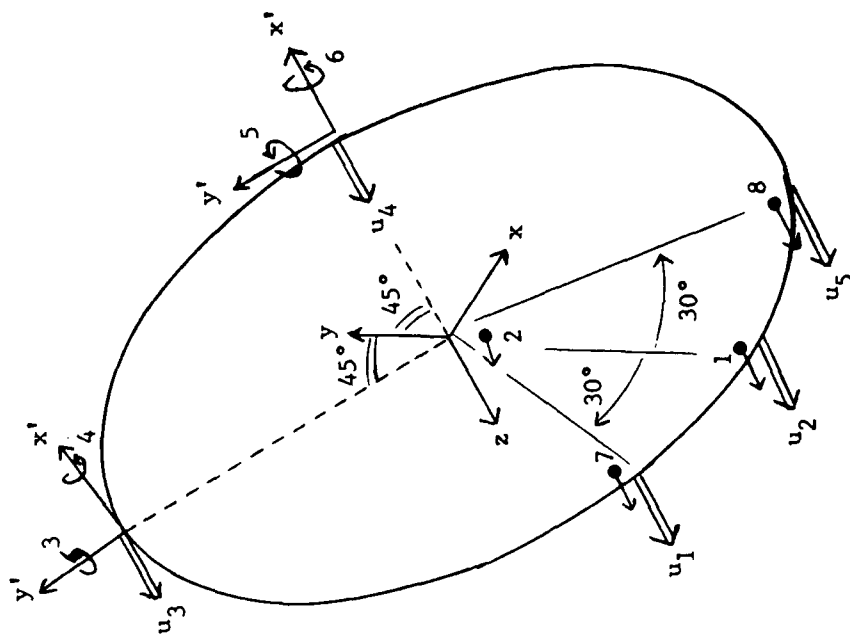


Figure 4-6 Circular Plate Experiment
Sensors and Actuators Definition

SENSORS

- 3, 4, 5 & 6 Angular (optical)
1, 2, 7 & 8 Displacement (μ Phase)

ACTUATORS

- u_1 & u_5 Proof-Mass (PPM)
 u_2, u_3 & u_4 Contactless (CEM)

TABLE XXI Control, Measurement and State Vectors Definition

<u>Control Vector</u>	<u>Actuator Number</u>	<u>Type</u>	<u>Action</u>	<u>Comments</u>
u_1	1	PPM	z-force	Control inputs provided by the controller
u_2	2	CEM	z-force	
u_3	3	CEM	z-force	
u_4	4	CEM	z-force	
u_5	5	PPM	z-force	
				used for excitation only
<u>Measurement Vector</u>	<u>Sensor Number</u>	<u>Type</u>	<u>Sensed Quantity</u>	
y_1	1	μ -phase	z-motion	Sensor inputs to the controller
y_2	2	μ -phase	z-motion	
y_3	3	angular	x' rotation	
y_4	4	angular	y' rotation	
y_5	5	angular	x' rotation	
y_6	6	angular	y' rotation	used for characterization only
y_7	7	μ -phase	z-motion	
y_8	8	μ -phase	z-motion	
<u>State Vector</u>	<u>Variable</u>	<u>Definition</u>		
x_1	$\dot{\theta}_x$	x-rotation rate		Rigid-body modes
x_2	θ_x	x-rotation		
x_3	$\dot{\theta}_y$	y-rotation rate		
x_4	θ_y	y-rotation		
x_5	\dot{z}	z-translation velocity		
x_6	z	z-translation		Bending mode amplitudes and rates
x_7	\dot{q}_1	1st (rate)		
x_8	q_1	(amplitude)		
x_9	\dot{q}_2	2nd "		
x_{10}	q_2	"		
x_{11}	\dot{q}_3	3rd "		
x_{12}	q_3	"		
x_{13}	\dot{q}_4	4th "		
x_{14}	q_4	"		
x_{15}	\dot{q}_5	5th "		
x_{16}	q_5	"		

The natural vibration modes of the plate are shown in Fig. (4-7). Note that for certain modes, some actuators or some sensors are situated on a nodal line, making them uncoupled from these particular modes.

The goal of the experiment was the control of the modes shown on the top line, the sampling rate limitation to 125 Hz making it impossible to control the higher modes. Three more degrees of freedom of the plate had to be controlled also: the two rotations and the translation along the z axis. Thus, a total of $3 + 5 = 8$ degrees of freedom was used, making up a 16-state control synthesis model. This model, rewritten in discrete form, is given by:

$$x_{n+1} = \phi x_n + \Gamma u_n \quad (34)$$

$$y_n = Hx_n$$

Thus, the state observer equations are

$$\hat{x}_{n+1} = \phi \hat{x}_n + \Gamma u_n + k (y_n - H \hat{x}_n) \quad (35)$$

and the control laws take the form

$$u_n = C \hat{x}_n \quad (36)$$

The control synthesis process consists of finding the values of K and C, the filter and control gain matrices respectively. Then equations 4.3 and 4.4 can be implemented in a microprocessor (in this case the CPSI 300 Array 3Y Processor). The AP receives the vector of measurements, y_n , as an input, and delivers the vector of actuation commands, u_{n+1} , according to an internal algorithm described by the matrix-vector multiplication:

$$\begin{bmatrix} \hat{x}_{n+1} \\ u_{n+1} \end{bmatrix} = A \begin{bmatrix} \hat{x}_n \\ u_n \\ y_n \end{bmatrix} \quad (37)$$

where

$$A = \begin{bmatrix} \phi - KH & \Gamma & K \\ C(\phi - KH) & C\Gamma & CK \end{bmatrix}$$

(ATTACHED SENSORS AND ACTUATORS PRODUCE SMALL "SEPARATION"
OF CLASSICAL "DOUBLE-ROOT" MODES)

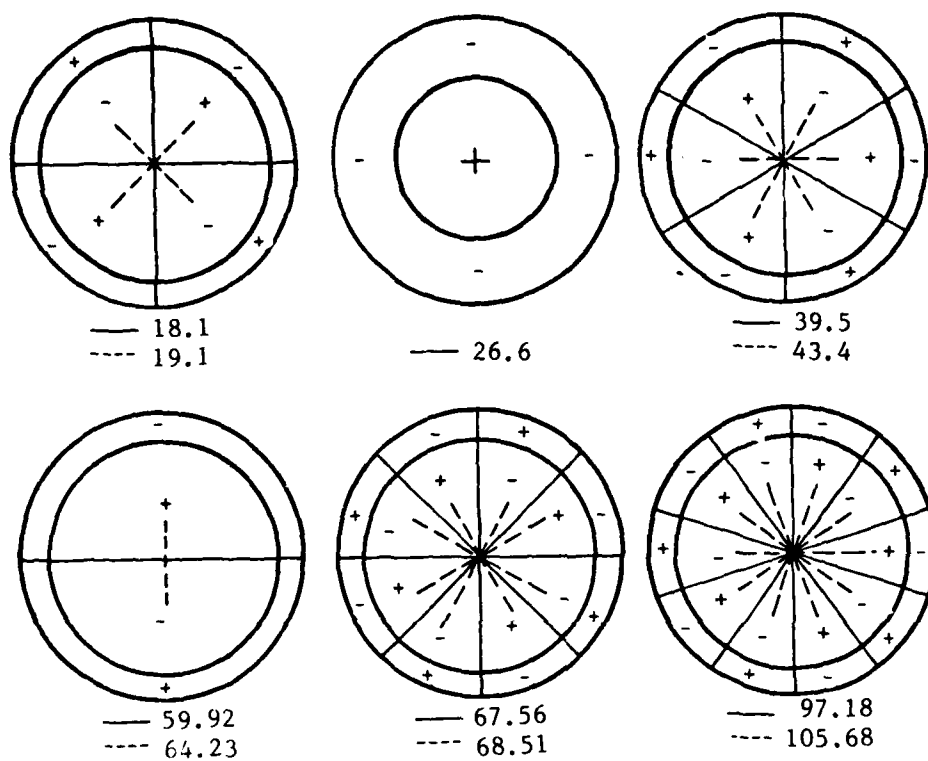


Figure 4-7. Modal Frequencies (Hz) and Patterns
for Circular Plate Experiment

It is easily shown that (4.5) is equivalent to Eqs. 4.3 and 4.4, however this formulation is a more efficient way for programming the AP.

Because of the importance of determining the behavior of the state estimator, it is required that the time histories of the full input vector $[\hat{X}_n, U_n, Y_n]^T$ be examined. This program, however, slows down considerably the algorithm and thus sampling rates were limited to 125 Hz.

The general configuration of the system is shown in Fig. 4-8, where the links between the different processors are shown. Because of the independence of the AP relative to the host processor, the latter can be used to characterize the system independently during closed-loop operations without affecting the control algorithm.

4.3.2 Test Plan. A test plan was originally established and included control based on the use of two accelerometers. However, due to inherent difficulties that revealed themselves during the tests, some of these tests had to be cancelled and, instead, more tests were performed with the μ -phase sensor which turned out to be a very reliable and precise sensor. Table (XXII) shows a matrix overview of the test plan and the modifications that were made during the course of the study. As can be seen, tests 5 and 6 were dropped to the benefit of 7 and 8 which have been successfully accomplished. The chart shows the different types of controllers to be tested and the objectives of each of them. The actuators in use in each case are listed as CEM (contact less electromagnetic) or PPM (pivoted proof-mass). Check marks denote performed tests.

Tests 1 to 4 were discussed in the interim report [25] and thus will not be detailed in the present report, except for the significant conclusions.

Test 8 constitutes the main achievement of this study since it includes all the features of the ACROSS methodology and will be discussed in the following section. Within the modifications made necessary by the experimental findings, the test plan has been followed and executed successfully. The actual experimental results are discussed next.

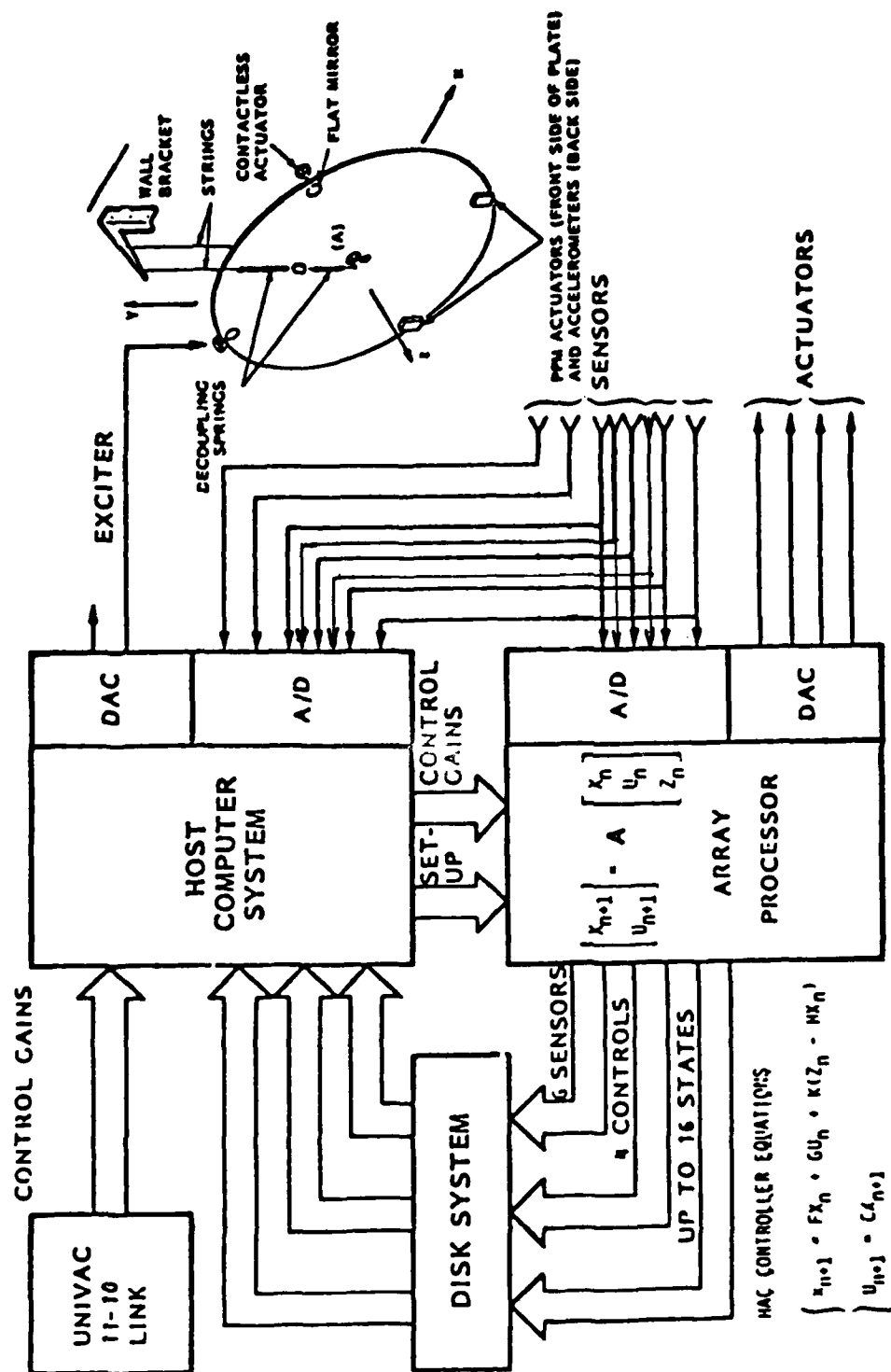


Figure 4-8 Plate Experiment - Overall Configuration

TABLE XXII Circular Plate Test Matrix Control Experiments

TEST #	PURPOSE	CONTROLLER TYPE	ACTUATORS NUMBER & TYPE	MODES CONTROLLED	DISTURBANCE TYPES	REMARKS
1	SYSTEM AND CALIBRATIONS CHECK OUT	CLASSICAL (P.I.D.)	2 CEM	2 RIGID	1, 2	DIGITAL IMPLEMENTATION OF ANALOG STABILIZER; 2 OPTICAL SENSORS ONLY. TOTAL OF 4 STATES
2	FILTER ALGORITHM & ACCELEROMETERS CHECKOUT	HAC	2 CEM	3 RIGID	1, 2	4 OPTICAL SENSORS & 2 ACCELEROMETERS
3	EFFECTS OF LAC	HAC + LAC				TOTAL OF 6 STATES
4	DEMONSTRATION OF MODAL CONTROL	HAC + LAC	2 CEM	3 RIGID 2 BENDING	1, 2	
5	DEMONSTRATION OF S.S. DISTURBANCE REJECTION EFFECTS OF DISTURBANCE VARIATION	HAC + LAC	2 CEM 2 PPM 1 CEM EXCITER	3 RIGID 2 BENDING	1, 2, 3	TOTAL OF 15 STATES
6	MULTIMODE CONTROL	HAC + LAC	2 CEM 2 PPM	3 RIGID 5 BENDING	1, 2	TOTAL OF 19 STATES
7	MICROPHASE OPTICS CHECK OUT	HAC/LAC	3 CEM	3 RIGID	1.2	1 μ PHASE SENSOR FOR TRANSLATIONAL MODE
8	MICROPHASE OPTICS DEMONSTRATION FOR MULTIMODE CONTROL	HAC/LAC	3 CEM 1 PPM	3 RIGID 5 FLEXIBLE	1.2	16 STATES 6 SENSORS

NOT PERFORMED

DISTURBANCES: 1 ENVIRONMENTAL NOISE
 2 STEP FUNCTION
 3 SINUSOIDAL

4.3.3 Results.

Control Experiment Procedure. The various operations involved in the structural control experiments are shown in Fig. 4-9. From the finite element analysis, a linear model is derived which is used as a basis for control synthesis programs. These programs generate a set of gain matrices which are stored in the 11-23 and may be manually updated if needed. The appropriate set is loaded into the array processor. Then the control algorithm is started and the AP controls the specimen and may acquire data. These data are stored on disk and can be analyzed off-line by the 11-23 or transmitted to a larger computer (VAX, UNIVAC 1110) for further processing. Also, while the AP is running, dynamic characterizations may be carried out by the 11-23.

Implementation of the LAC System.

Because of the inner velocity servo-loop that is used on the PPM actuators, they automatically provide some active damping, without any other external loop. In fact, their dynamics mimics a passive inertial damper. For this reason, their inner loop damping capability is limited, but is nevertheless sufficient to stabilize most of the HAC control laws. Therefore, as long as the PPM actuators were used in the control scheme, they were automatically introducing a LAC type of stabilization. The only way to study the HAC system by itself is to utilize only the CEM actuators in the control synthesis. In all cases studied, whether attitude control only or full attitude and vibration control was employed, the HAC system alone always showed instabilities due to spillover. These instabilities would disappear as soon as the PPMs were turned on (whether or not they were included in the control scheme).

Early Experimental Results

The first test that utilized the AP (test 1) was meant to be a check of the correct functioning of the different subsystems, actuators, sensors, microprocessors and the calibration factors. A simple classical attitude controller was implemented successfully and controlled the two rotations about the X and Y axes within a few microradians (5 μ rad RMS).

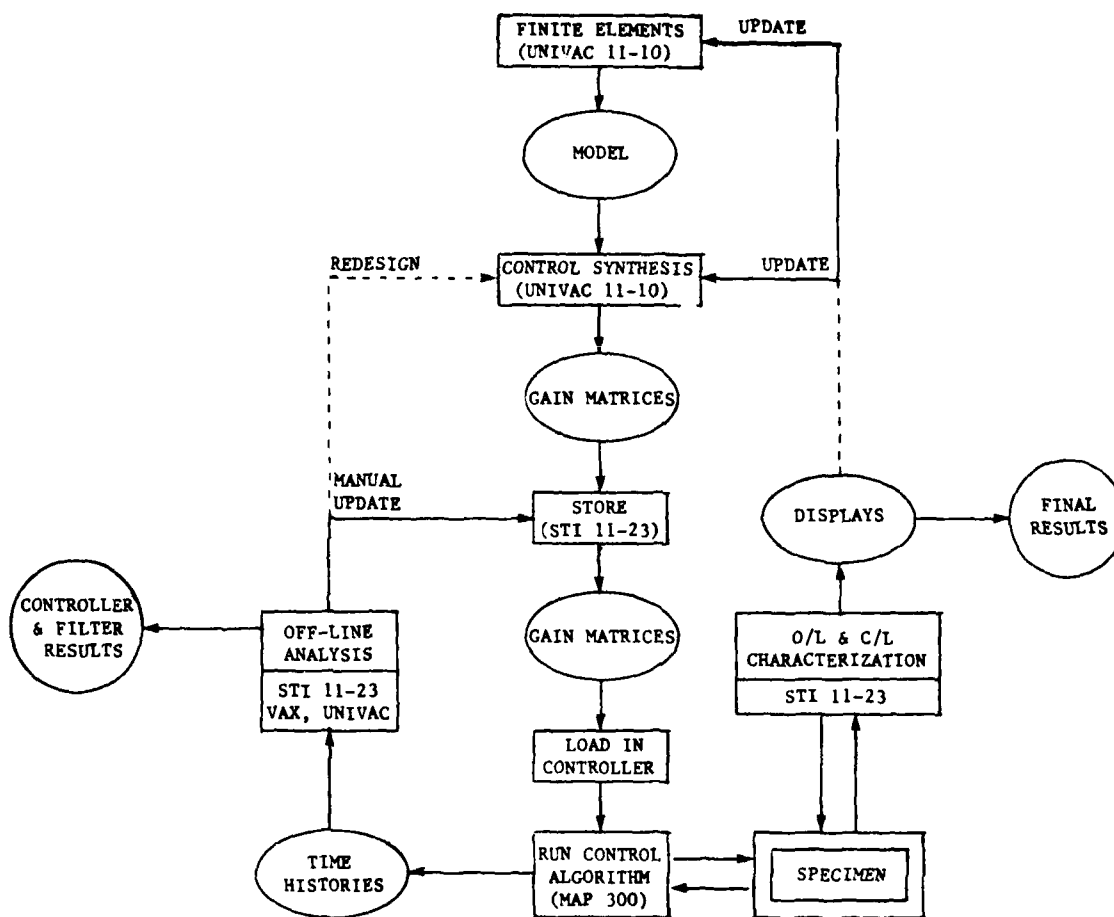


Figure 4-9 Control Experiment Procedure

An optimal controller was then synthesized to control the same two rotations plus the Z-translation, to which the accelerometers were sensitive. Finally, control of the first two bending modes was added to this controller's function. In all these cases, the only actuators being used for HAC were the two top CEM actuators, while, as explained previously, the PPM actuators were providing the LAC stabilization.

These last two tests were only partially successful in that the performance obtained was very low and not in good agreement with predictions. Table XXIII summarizes the main difficulties encountered and the steps that were taken to alleviate them and continue the experiments.

Static Observer Implementation

The introduction of the two μ -phase measurements, namely the bottom and center Z-displacements, made possible the construction of a static-observer. Indeed, 6 measurements were now available (4 local rotations, 2 local displacements) and thus one could reconstruct from them the two rigid body rotations, the Z-translations and the next three bending modes. If one assumes that no other mode is excited, the following relation is true:

$$y = [z_1, z_2, \theta_1, \theta_2, \theta_3, \theta_4] = H_o [\theta_x, \theta_y, z, q_1, q_2, q_3] \quad (38)$$

where this H_o is a 6 x 6 matrix. Because of the particular choice of sensors, the matrix is invertable (i.e, the quantities $(\theta_x, \theta_y, \dots, q_3)$ are statically observable and thus their estimates can be obtained by

$$[\theta_x, \theta_y, z, q_1, q_2, q_3] = H_o^{-1} y \quad (39)$$

TABLE XXIII Results of the First Series of Tests

EXPERIMENTAL DIFFICULTIES	CORRECTIVE STEP TAKEN
(1) Poor rigid body controllability with the 2 top CEM only	Use a third CEM at bottom of plate
(2) Bad characteristic of accelerometer at low frequency \Rightarrow rigid body problems	Replace accelerometers by μ phase displacement sensors
(3) Unverified plate model	Identification of critical elements
(4) Filter evaluation	Use of static observer. Add two more sensors for cross-check.

Of course this estimate is corrupted by sensor calibration errors, sensor noise and the fact that Eq. 4.6 is a truncation since the right hand side should contain all the other modal amplitudes q_4, q_5 etc. However, the static observer defined by Eq. 4.7 is still very useful to make a rough check of the Kalman filter.

Filter Study

The critical part of an optimal controller is usually the filter, or state observer, and thus it needs to be carefully studied first. An HAC controller was designed, after modifications 1 and 2 of Table XXIII were implemented. This controller was to control the 3 rigid body modes plus the first two bending modes, introducing about 5% damping in these modes. The experiment showed severe instabilities which were removed when no modal control was applied. A semi-open-loop test was thus made to check the behavior of the filter. Figs. 4-10, 4-11 and 4-12 show the main result obtained. In Fig. 4-10 a static observer determined these five modal responses to an excitation at the first bending frequency. The top trace shows the excitation; next are the three rigid-body and two lowest bending responses. As one would expect, the input excites primarily the first bending mode. Only the rigid-body mode could be controlled in this test, because feeding back the bending states caused instability.

The output of the filter is shown in Fig. 4-11. The state estimates of the optimal filter must match the previous statically observed states for the controller to work. X_{rot} , Y_{rot} , and Z_{trans} are the three controlled rigid-body state estimates, and Q_1 and Q_2 , the two uncontrolled bending-state estimates (18.1 and 19.1 Hz). The rigid-body estimates match the corresponding states in the preceding figure, indicating correct frequencies and mode shapes for the rigid-body modes. The optimal estimate histories show how the filter attenuates the measurement noise in the statically observed states.

CIRCULAR PLATE CONTROL WITH MICROPHASE SENSORS
TEST OF CONTROLLER 3C1 1 (NO MODAL CONTROL)

STATIC OBSERVER OUTPUT

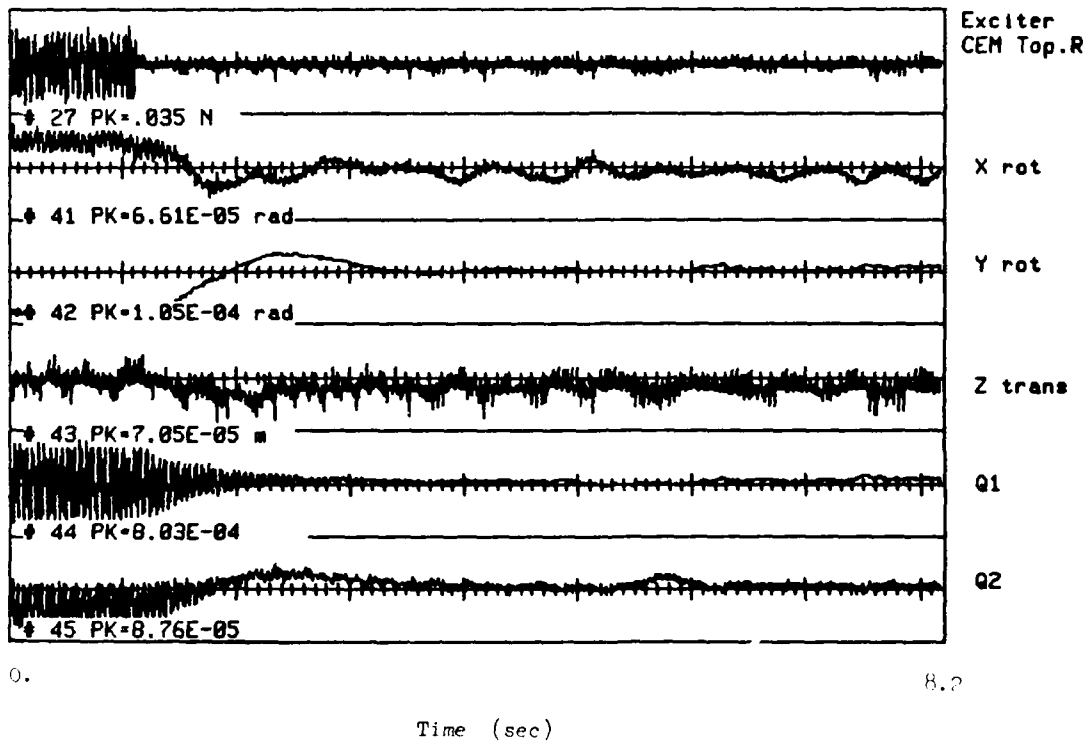


Figure 4-10. Circular Plate Experiment Response to
Excitation at First Bending Frequency

CIRCULAR PLATE CONTROL WITH MICROPHASE SENSORS
TEST OF CONTROLLER 3C1 1 (NO MODAL CONTROL)

FILTER OUTPUT

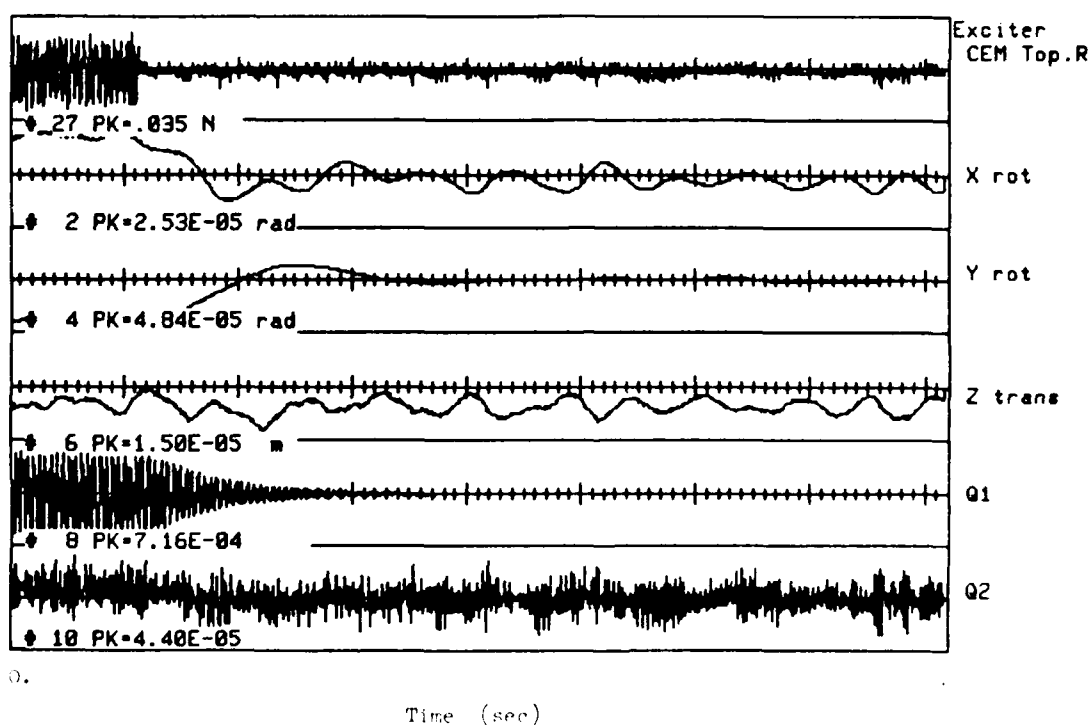


Figure 4-11. Circular Plate Experiment Optimal State Estimate
After Excitation at First Bending Frequency

CIRCULAR PLATE CONTROL WITH MICROPHASE SENSORS
TEST OF CONTROLLER 3C1 1 (NO MODAL CONTROL)

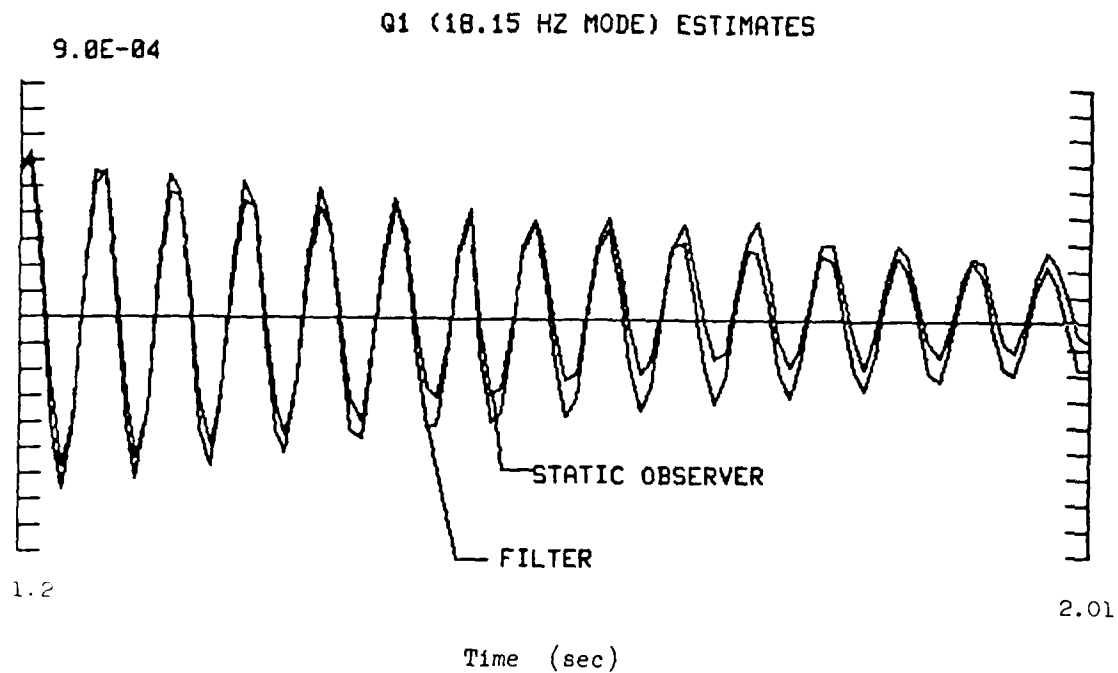


Figure 4-12. Circular Plate Experiment - Actual and Estimated Uncontrolled Bending Response to Excitation at the Resonant Frequency

Finally, as shown in Fig. 4-12, the filter seems to correctly estimate the first bending mode when no attempt is made to control the latter. The fact that this mode becomes unstable in closed-loop indicates the possibility of errors in the value of the control input matrix G.

Another effect was discovered which appears to be fundamental for this type of controller. Since the optimized filter was suspected of giving wrong answers in closed-loop, the static observer was used instead, with the additions of band pass filters to reduce the noise and discriminate between the states. Basically, the pseudo-static observer was defined by:

$$\ddot{\tilde{x}}_i + 2\zeta_i\omega_i\dot{\tilde{x}}_i + \omega_i^2\tilde{x}_i = H_{ij}^{-1}y_j \quad (40)$$

The instability disappeared with this filter, although the performance was still poor. Further tests showed that the instability was caused by the rigid body states being improperly driven by the modal states, due to insufficient rejection of these states by the optimal filter. A comparison of the transfer functions for the optimal filter with the quasi-static observer shows this phenomenon more clearly. The transfer functions compared are from an actual rigid body state (X_2 , the Y-rotation angle) to the estimate of a modal state (X_{10} , the second bending mode amplitude). In Fig. 4-13 is shown the response of the optimal filter. This open-loop frequency response explains the sensitivity of controller stability to model error. The bending state estimation puts a notch at a rigid-body resonant frequency to eliminate the irrelevant state's contribution to the measurements. This allows low filter gains that minimize transmission of broadband measurement noise. The rejection of signals at non-resonant frequencies is low so the system stability is sensitive to errors in the modelled open or closed-loop resonant frequencies.

By contrast, the response of the quasi-static observer shown in Figure 4-14 shows a very significant rejection of irrelevant modes, at all frequencies.

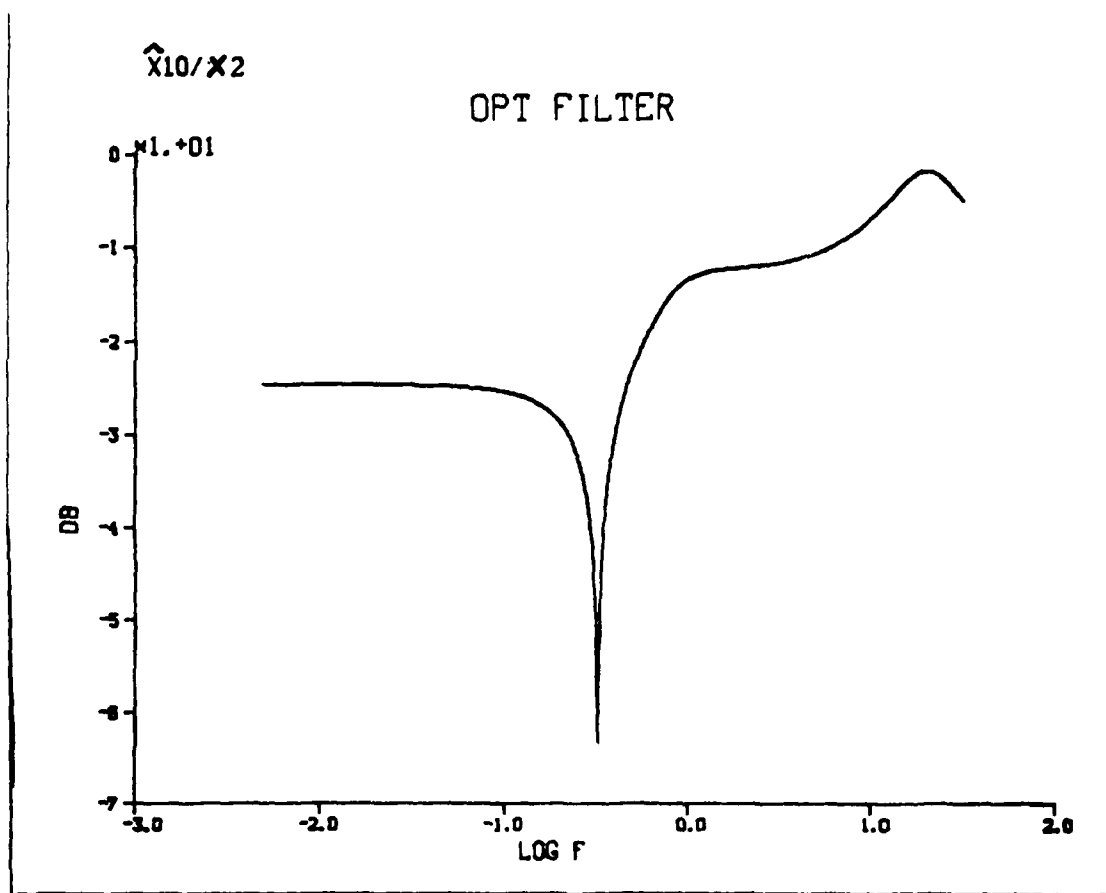


Figure 4-13 Circular Plate Experiment - Optimal Filter Frequency Discrimination Against Irrelevant Modes

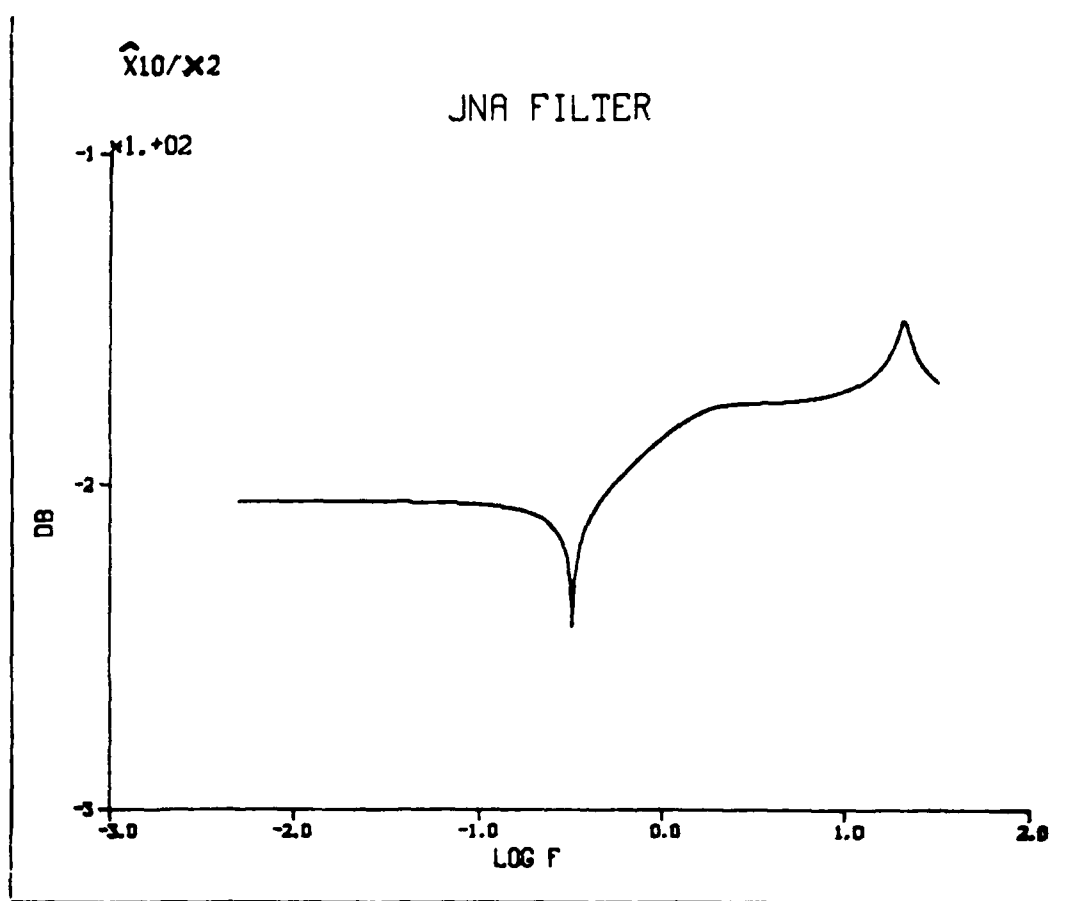


Figure 4-14 Circular Plate Experiment - Quasi-Static Observer

This filter indeed makes use of spatial discrimination much more than the optimal filter does. The drawback of such a filter, however, is its low performance in terms of sensor noise rejection. The optimal filter reduces this noise by relying on the exact knowledge of the modal frequencies, thus its increased sensitivity to errors.

Model Refinement

In order to progress in the experiment, it was decided to proceed to a limited parameter identification to improve the accuracy of the matrices G and H. Direct measurements were performed using sine-wave excitations at the various modal frequencies and the model was updated. The final model, which included the three rigid body and the first five bending modes, is shown in Table XXIV, where the matrices F and G have been converted to their discrete equivalent Φ and Γ .

The 16-States HAC Control Experiment

From the model described above, a full 16th order controller was designed. The gain matrices C and K corresponding to the controller and the filter respectively are given in Table XXV. These gains were loaded in the AP along with the coefficient matrices Φ , Γ and H. The control actuators were the left PPM actuator and the 3 CEM actuators. No anti-aliasing filtering was performed on the sensor signal because of unacceptable phase rotations that this filtering produces. However, a mild second order filter was used on the control inputs to avoid excessive roughness in the actuator output forces which otherwise would tend to excite a wide spectrum of higher frequency modes.

The closed-loop tests were conducted by exciting the actuator #5 (PPM) with a chirp (fast frequency sweep) between 1 and 60 Hz.

TABLE XXIV 16 States Control Synthesis Model

***F MATRIX IS 16X 16 NON-ZERO ELEMENTS FOLLOW

1, 1,	9.9971-01,	1, 2,	-3.3148-02,	2, 1,	7.9930-03,	2, 2,	9.9987-01
3, 3,	9.9985-01,	3, 4,	-1.1887-02,	4, 3,	7.9995-03,	4, 4,	9.9995-01
5, 5,	9.9940-01,	5, 6,	-8.5019-02,	6, 5,	7.9980-03,	6, 6,	9.9966-01
7, 7,	5.8806-01,	7, 8,	-8.8732+01,	8, 7,	6.8229-03,	8, 8,	6.1607-01
9, 9,	5.6279-01,	9, 10,	-9.7237+01,	10, 9,	6.7728-03,	10, 10,	5.7703-01
11, 11,	2.2018-01,	11, 12,	-1.6107+02,	12, 11,	5.7547-03,	12, 12,	2.3558-01
13, 13,	-4.0377-01,	13, 14,	-2.2275+02,	14, 13,	3.6166-03,	14, 14,	-3.8600-01
15, 15,	-5.7308-01,	15, 16,	-2.2296+02,	16, 15,	2.9984-03,	16, 16,	-5.7162-01

***G MATRIX IS 16X 4 NON-ZERO ELEMENTS FOLLOW

1, 1,	-2.7125-03,	1, 2,	-3.1460-03,	1, 3,	2.3814-03,	1, 4,	2.3814-03
2, 1,	-1.0850-05,	2, 2,	-1.2585-05,	2, 3,	9.5259-06,	2, 4,	9.5259-06
3, 1,	1.6719-03,	3, 2,	-2.1199-12,	3, 3,	2.3646-03,	3, 4,	-2.3646-03
4, 1,	6.6877-06,	4, 2,	-8.4796-15,	4, 3,	9.4585-06,	4, 4,	-9.4585-06
5, 1,	5.5186-04,	5, 2,	5.5186-04,	5, 3,	5.5186-04,	5, 4,	5.5186-04
6, 1,	2.2077-06,	6, 2,	2.2077-06,	6, 3,	2.2077-06,	6, 4,	2.2077-06
7, 1,	3.6175-03,	7, 3,	-5.8336-03,	7, 4,	5.8336-03,	8, 1,	1.5652-05
8, 3,	-2.5241-05,	8, 4,	2.5241-05,	9, 1,	9.9831-04,	9, 2,	5.7908-03
10, 1,	4.3425-06,	10, 2,	2.5189-05,	11, 1,	2.0924-03,	11, 2,	1.2603-03
11, 3,	1.9681-03,	11, 4,	1.9681-03,	12, 1,	9.9300-06,	12, 2,	5.9810-06
12, 3,	9.3401-06,	12, 4,	9.3401-06,	13, 1,	3.6166-08,	13, 3,	2.5316-03
13, 4,	-2.5316-03,	14, 1,	2.2504-10,	14, 3,	1.5753-05,	14, 4,	-1.5753-05
15, 1,	1.1124-04,	15, 2,	3.0584-03,	15, 3,	1.9430-03,	15, 4,	1.9430-03
16, 1,	7.8412-07,	16, 2,	2.1558-05,	16, 3,	1.3696-05,	16, 4,	1.3696-05

***H MATRIX IS 6X 16 NON-ZERO ELEMENTS FOLLOW

1, 2,	-5.8635-01,	1, 6,	1.0000+00,	1, 10,	8.5500-01,	1, 12,	2.1900-01
1, 16,	1.0200+00,	2, 2,	-3.2908-02,	2, 6,	1.0000+00,	2, 10,	-1.1550-01
2, 12,	-5.1400-01,	2, 16,	-1.4140-02,	3, 2,	-7.0710-01,	3, 4,	7.0710-01
3, 8,	-6.7400-02,	3, 10,	-1.9000+00,	3, 12,	-2.5600-01,	3, 14,	-2.1520+00
3, 16,	2.3930+00,	4, 2,	7.0710-01,	4, 4,	7.0710-01,	4, 8,	-7.0500-01
4, 10,	4.4350-01,	4, 12,	1.1400+00,	4, 14,	1.5810+00,	4, 16,	1.5563+00
5, 2,	-7.0710-01,	5, 4,	7.0710-01,	5, 8,	-4.9000-01,	5, 10,	-5.4040-01
5, 12,	-1.0500+00,	5, 14,	1.2600+00,	5, 16,	-1.2400+00,	6, 2,	7.0710-01
6, 4,	7.0710-01,	6, 8,	-5.6100-02,	6, 10,	2.3600+00,	6, 12,	3.6000-01
6, 14,	-2.5100+00,	6, 16,	-2.8014+00				

TABLE XXV 16 States HAC Controller

***C MATRIX IS 4X 16 (CONTROLLER GAINS)

1, 7,	-8.0143+00,	1, 8,	3.1746+02,	1, 9,	-3.0186+00,	1, 10,	2.9813+02
1, 11,	-2.2741+01,	1, 12,	2.1335+03,	1, 15,	7.0675-01,	1, 16,	-6.1011+02
2, 1,	2.2580+01,	2, 2,	2.3043+02,	2, 3,	4.2301-02,	2, 4,	1.2149+00
2, 5,	-8.0580+00,	2, 6,	-5.4139+00,	2, 7,	9.5711-01,	2, 8,	-6.8076+00
2, 9,	-3.2153+01,	2, 10,	1.1389+03,	2, 11,	-1.0589+01,	2, 12,	6.0269+02
2, 13,	-1.8406-01,	2, 14,	-1.3200+02,	2, 15,	-3.7400+00,	2, 16,	1.4535+03
3, 1,	-1.9161+01,	3, 2,	-2.0442+02,	3, 3,	-3.5128+01,	3, 4,	-3.8688+02
3, 5,	-4.9838+00,	3, 6,	-3.6438+00,	3, 7,	1.2046+01,	3, 8,	-1.6907+02
3, 9,	2.8698+00,	3, 10,	4.1339+02,	3, 11,	-2.0727+01,	3, 12,	2.5775+03
3, 13,	-5.9945+00,	3, 14,	1.4256+03,	3, 15,	-2.4859+00,	3, 16,	1.0485+03
4, 1,	-1.9292+01,	4, 2,	-2.0585+02,	4, 3,	3.4959+01,	4, 4,	3.8600+02
4, 6,	-3.7899+00,	4, 7,	-1.1272+01,	4, 8,	2.0306+02,	4, 9,	3.3141+00
4, 10,	3.6721+02,	4, 11,	-2.1264+01,	4, 12,	1.8654+03,	4, 13,	5.6083+00
4, 14,	-1.6902+03,	4, 15,	-2.4749+00,	4, 16,	1.0184+03,		

***K MATRIX IS 16X 6 (FILTER GAINS)

1, 1,	-5.4020-01,	1, 2,	3.0760-02,	1, 3,	-5.0296-01,	1, 4,	5.0935-01
1, 5,	-5.2185-01,	1, 6,	4.8587-01,	2, 1,	-4.8365-02,	2, 2,	5.7741-03
2, 3,	-4.9480-02,	2, 4,	5.0145-02,	2, 5,	-5.0875-02,	2, 6,	4.8257-02
3, 1,	-8.0557-03,	3, 2,	4.4646-03,	3, 3,	6.5006-01,	3, 4,	5.3580-01
3, 5,	5.8599-01,	3, 6,	6.4061-01,	4, 1,	-8.0697-04,	4, 2,	4.6836-04
4, 3,	6.4048-02,	4, 4,	5.4350-02,	4, 5,	5.8701-02,	4, 6,	6.3399-02
5, 1,	1.8188-02,	5, 2,	2.1916-02,	5, 3,	-3.1850-03,	5, 4,	3.4430-03
5, 5,	-3.4781-03,	5, 6,	3.0506-03,	6, 1,	1.1680-02,	6, 2,	1.4316-02
6, 3,	-2.3486-03,	6, 4,	2.4914-03,	6, 5,	-2.5053-03,	6, 6,	2.2712-03
7, 1,	1.1203-01,	7, 2,	9.4937-02,	7, 3,	-4.2036-02,	7, 4,	1.5184+01
7, 5,	1.0757+01,	7, 6,	-5.6227-01,	8, 1,	3.7197-03,	8, 2,	-4.5848-03
8, 3,	-2.3674-02,	8, 4,	-1.1699-01,	8, 5,	-9.8171-02,	8, 6,	-2.3207-02
9, 1,	-1.9204+00,	9, 2,	1.7580-01,	9, 3,	3.1287+00,	9, 4,	-3.0911-01
9, 5,	5.3617-01,	9, 6,	-3.8630+00,	10, 1,	8.2535-03,	10, 2,	1.9964-03
10, 3,	-1.9745-02,	10, 4,	2.1622-03,	10, 5,	-2.5164-03,	10, 6,	2.3384-02
11, 1,	-2.7771+00,	11, 2,	6.7458+00,	11, 3,	1.2731+00,	11, 4,	-1.2492+01
11, 5,	1.3033+01,	11, 6,	-1.9679+00,	12, 1,	2.3230-03,	12, 2,	-8.1305-03
12, 3,	-1.5041-02,	12, 4,	2.3977-02,	12, 5,	-1.7514-02,	12, 6,	1.8949-02
13, 1,	1.0374-01,	13, 2,	4.0077-03,	13, 3,	4.7717+00,	13, 4,	-2.8962+00
13, 5,	-2.6341+00,	13, 6,	4.8204+00,	14, 1,	-3.4239-04,	14, 2,	-5.6593-06
14, 3,	8.5517-03,	14, 4,	-5.2532-03,	14, 5,	-4.0111-03,	14, 6,	9.9023-03
15, 1,	-1.9225+00,	15, 2,	-3.2375-02,	15, 3,	-4.3681+00,	15, 4,	-2.7782+00
15, 5,	2.4529+00,	15, 6,	4.9200+00,	16, 1,	-5.4845-03,	16, 2,	-4.5929-04
16, 3,	-1.1506-02,	16, 4,	-6.5950-03,	16, 5,	7.2200-03,	16, 6,	1.1133-02

The system was stable and the time histories of the various responses are shown in Figs. 4-15 to 4-18. This series of charts shows the characteristics of a successful controller for the plate that acts on three rigid-body modes and the five lowest bending modes (18.1, 19.1, 26.2, 40 and 43.4 Hz). Fig. 4-15 shows the four actuator responses to a wide-band chirp excitation by one proof-mass actuator (PPM). Control activity appears as the excitation frequency sweeps through plate resonances. Most of the activity is in the first five modes where the controller increases damping significantly. The PPM actuator participates significantly in controlling the bending modes.

The time histories of the excitation and the six sensor signals used by the optimal filter are shown next in Fig. 4-16. Modal excitations are seen occurring at different times in different channels as the input frequency sweeps through the various resonances of the plate. The varied modal response among the sensors reflects the various observability of each mode by each sensor.

The traces of Fig. 4-17 are those of the complete sensor system: 6 for control plus two for independent checking and characterization. Since the rigid body translation was only lightly controlled, the displacement sensors (1, 2, 7 & 8) show more low frequency activity than the other sensors. Finally, the static observer output is shown in Fig. 4-18. Higher frequency modes, not modelled by this observer, corrupt these modal responses. Thus a Kalman filter is absolutely necessary in this case (where the number of modes to be controlled exceeds the number of sensors) to properly estimate all the bending modes to be controlled.

From the previous data, more specific information may be obtained by further processing. For instance, transfer functions such as the one shown in Fig. 4-19 where phase and amplitude are displayed, give a quick estimation of resonances and damping.

CIRCULAR PLATE CONTROL WITH MICROPHASE SENSORS

1P3C16-4 16-STATE CONTROLLER CLOSED-LOOP TEST

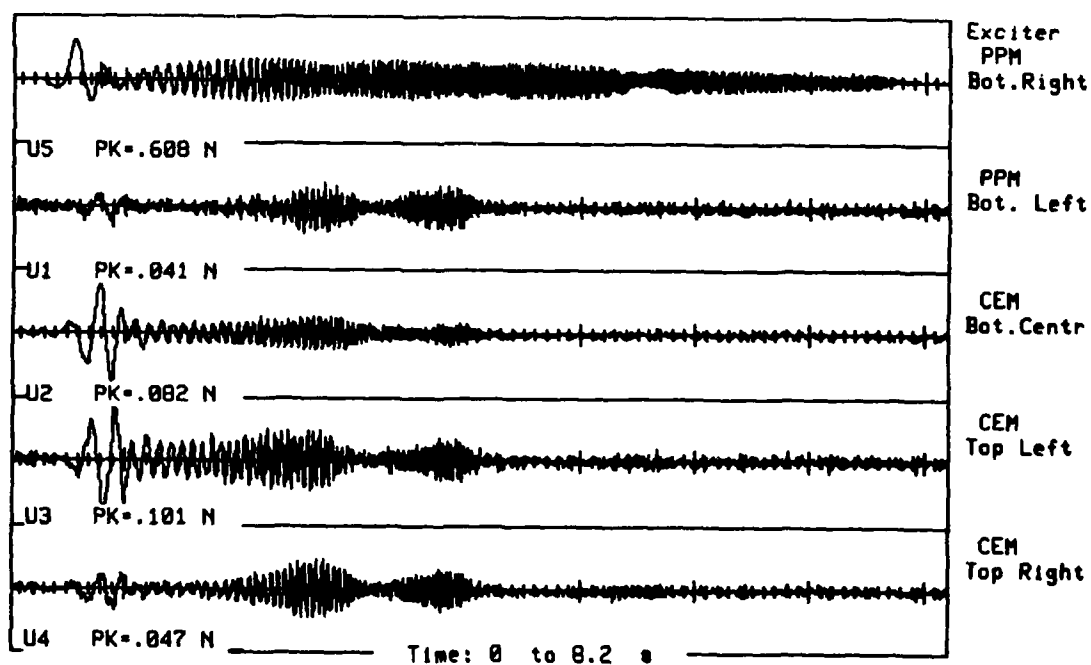


Figure 4-15 Circular Plate Experiment
Excitation & Control Inputs

CIRCULAR PLATE CONTROL WITH MICROPHASE SENSORS

1P3C16-4 16-STATE CONTROLLER CLOSED-LOOP TEST

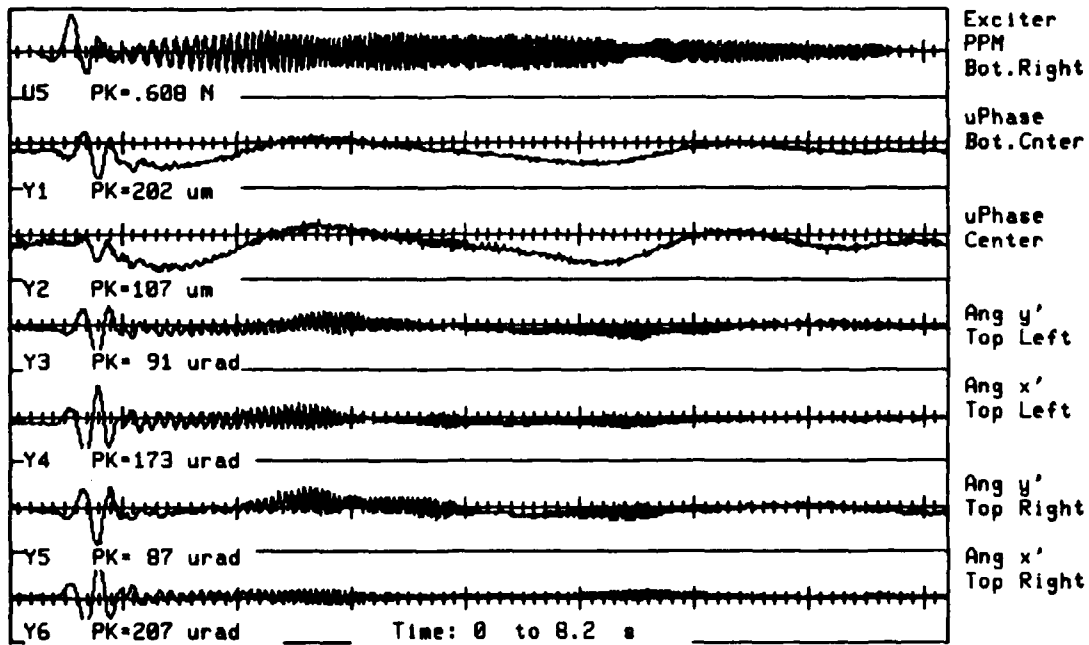


Figure 4-16 Circular Plate Experiment
Excitation and Sensor Outputs

CIRCULAR PLATE CONTROL WITH MICROPHASE SENSORS

1P3C16-4 16-STATE CONTROLLER CLOSED-LOOP TEST

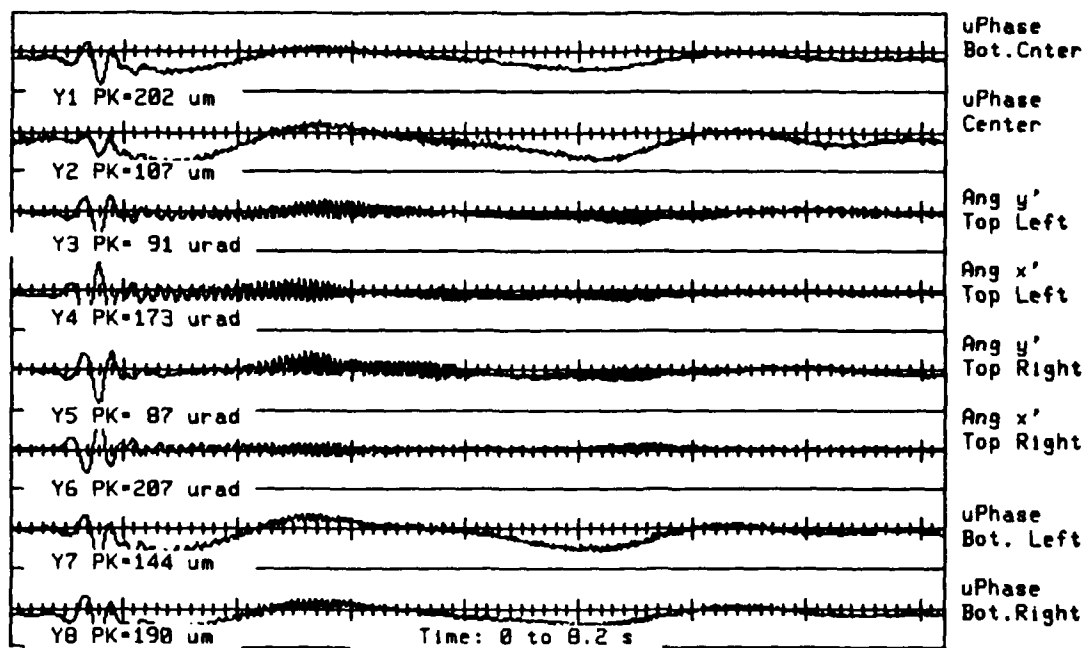


Figure 4-17 Circular Plate Experiment
Control and Evaluation Sensors Output

CIRCULAR PLATE CONTROL WITH MICROPHASE SENSORS
 1P3C16-4 16-STATE CONTROLLER CLOSED-LOOP TEST

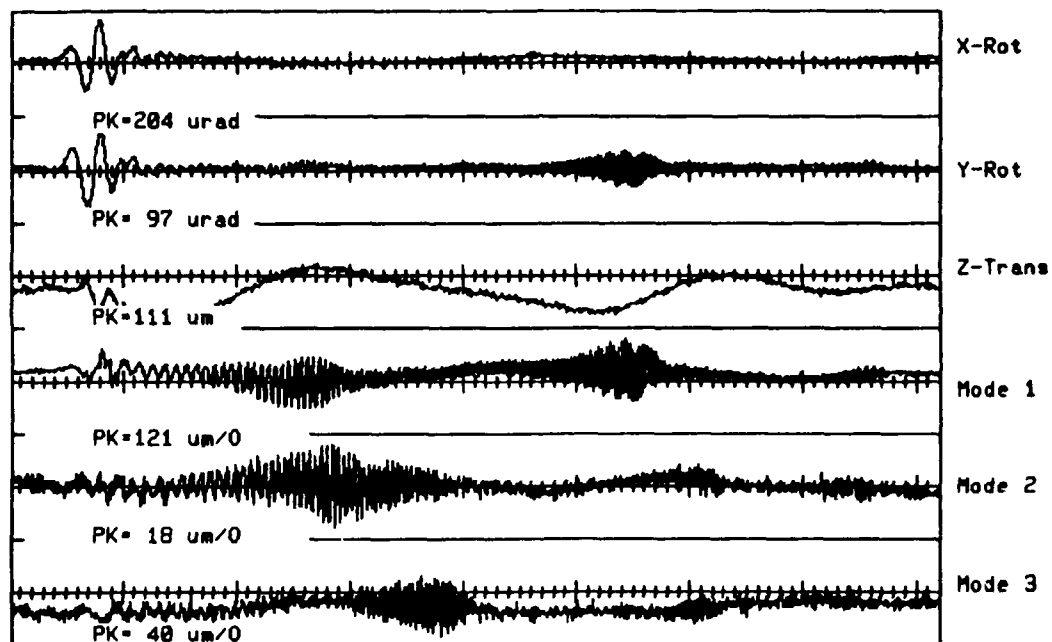


Figure 4-18 Circular Plate Experiment
 Static Observer Output (Chirp Input)

CIRCULAR PLATE CONTROL WITH MICROPHASE SENSORS

1P3C16-4 16-STATE CONTROLLER CLOSED-LOOP TEST

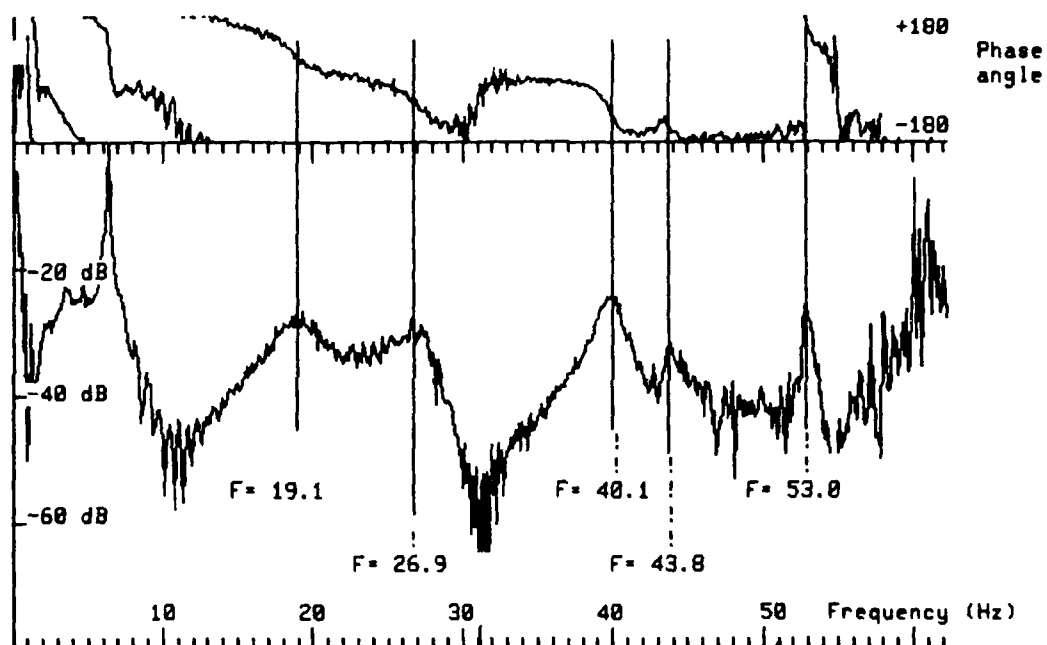


Figure 4-19 Circular Plate Experiment
Transfer Function Plot Y5/U5

Quantitative values can be obtained by curve-fitting techniques, and Fig. 4-20 shows an example of such methods. In the case shown, a function of the form

$$T(\omega) = \sum_{n=1}^4 \frac{A_n + j B_n}{\omega_n^2 - \omega^2 + 2j\zeta_n \omega_n}$$

(represented by the continuous lines) was fitted to the measured transfer function (dotted line) by adjusting the parameters A_n , B_n , ω_n , and ζ_n . Sensor #5 was close to a nodal line for the 19.75 Hz mode and thus no response could be observed at that frequency for this particular sensor. Thus data from other sensors was needed to identify the 19.75 Hz mode, as shown in Fig. 4-21. The above identification of modal frequencies and dampings was performed using the VAMP program. The results of the closed-loop identification of the previous figures is summarized in Table XXVI showing an excellent agreement with the predicted frequencies and dampings. The purely open-loop results are not shown because they differ only slightly in frequency from the LAC case (the damping ratios, however, were quite different, one to two orders of magnitude lower). Where the LAC brings only around 1% damping, the HAC system achieves more than 10% as predicted. The doubling-up in the predicted frequencies is due to the addition of the filter roots (denoted by f) to the controller roots (denoted by c). While the uncontrolled structure was of order 16, the closed-loop system becomes truly a 32nd order system and mode shapes can be significantly affected by this coupling with the filter. The damping ratios were subsequently re-evaluated using the more precise maximum likelihood method (ML). They are listed in the table and turned out to be lower than those obtained with VAMP. This difficulty of estimating damping ratios larger than 10% is typical of the identification problem of closed-loop structures.

CIRCULAR PLATE CONTROL WITH MICROPHASE SENSORS

1P3C16-4 16-STATE CONTROLLER CLOSED-LOOP TEST

Transfer function Y5/U5

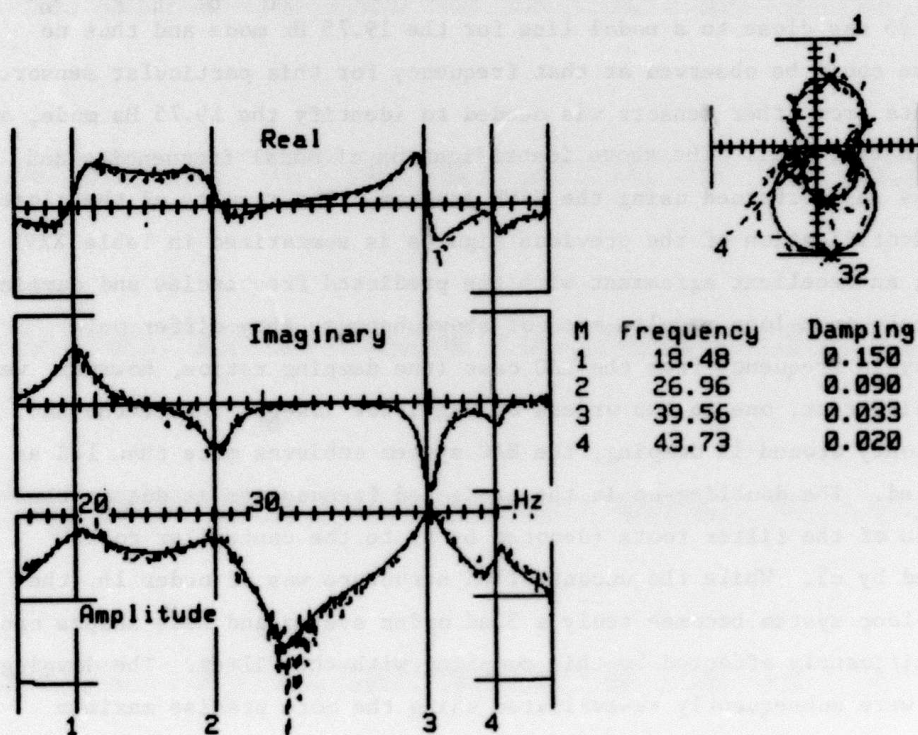


Figure 4-20 Circular Plate Experiment
Modal Identification by
Curve Fitting (VAMP)

CIRCULAR PLATE CONTROL WITH MICROPHASE SENSORS

1P3C16-4 16-STATE CONTROLLER CLOSED-LOOP TEST

Transfer function Y6/U5

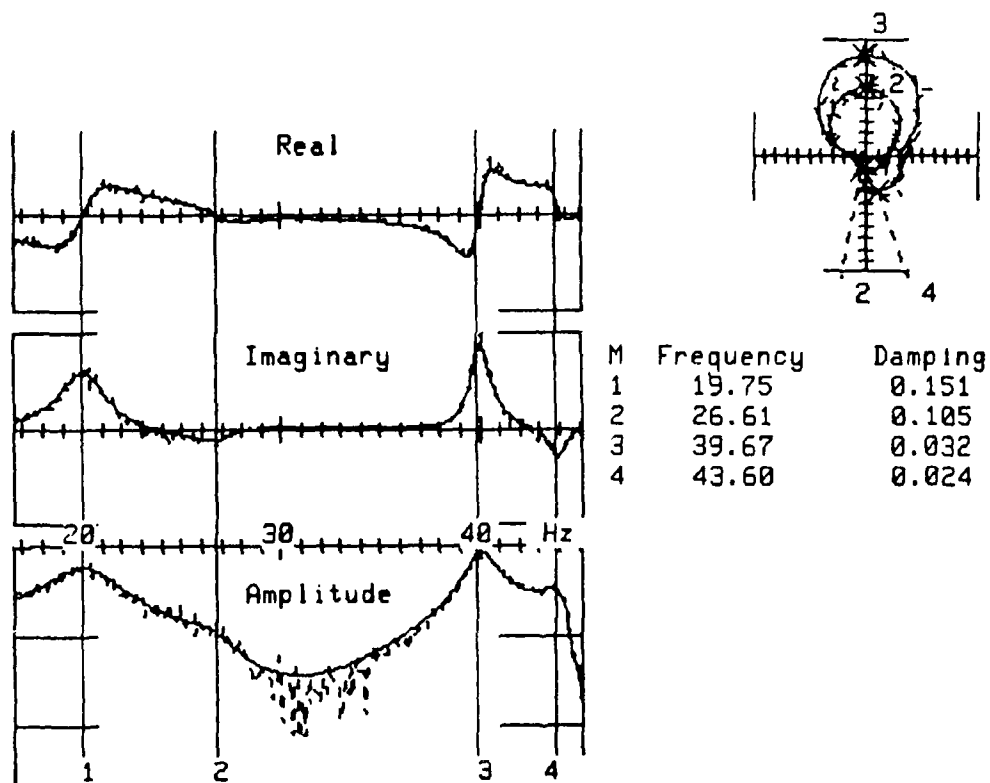


Figure 4-21 Circular Plate Experiment
Modal Identification by Curve
Fitting (VAMP)

TABLE XXVI Closed-Loop Poles

C L O S E D - L O O P P O L E S

L A C O N L Y		H A C a n d L A C				MAX. LIKELIHOOD Freq. Damping
Frequency	Damping	P R E D I C T E D		M E A S U R E D		
		Frequency	Damping	Frequency	Damping	
.194	.005	c 0.55	.22	-	-	
		f 0.64	.41			
.324	.005	c 2.52	.70	-	-	
		f 2.52	.71			
.519	.005	c 2.68	.70	-	-	
		f 2.62	.70			
18.15	.018	c 18.60	.15	18.48	.15	18.7 .095
		f 18.30	.15			
19.07	.009	c 19.57	.15	19.75	.15	19.94 .071
		f 19.18	.12			
26.63	.008	c 26.95	.10	26.96 26.61	.09 .11	26.95 .036 26.66 .048
		f 26.62	.10			
39.50	.010	c 39.59	.04	39.67 39.56	.03 .03	39.73 .019 39.62 .021
		f 39.51	.05			
43.40	.001	c 43.43	.02	43.73	.03	43.78 .022 43.89 .040
		f 43.42	.04			

(c : controller f : filter)

(c : controller f : filter)

A final overview of the effect of the control system is shown in Fig. 4-22 where the open-loop and closed-loop response of the plate is described by the response of the combined output from sensors #5 and 6 (this combination was used so that both modes at 18 and 19 Hz could be seen at once). This result was obtained using a spectrum analysis and a slow sine sweep of the exciter. The rigid body (low frequency side) is not behaving as expected, showing low damping characteristics. However, the frequency has been pushed up to about 3 Hz as predicted. This rigid body behavior seems to be a recurring problem and was observed in other experiments as well (see Section 4.5). It is not determined at this time what kind of model error contributes to it.

Significant Results of the Plate Experiment

Table XXVII describes the most significant results and achievements of the plate experiment. The main and most significant achievement for the ACOSS Program is that it was possible to close the loop on a very lightly damped two-dimensional structure with a relatively high order (16th) optimal controller and to obtain significant amounts of damping (up to 10%) as theoretically predicted. Because the rigid body modes were part of the controlled variables and because of the high performance characteristics of this system (10 μ -radians accuracy range), this experiment sets the program one step further toward real space applications. Also, the use of newly developed actuators and sensors is quite significant.

Conclusions

These experiments have been very successful in that they achieved their purpose of validating the control methodology. They also indicated that improvement in system performance will require progress in the following areas:

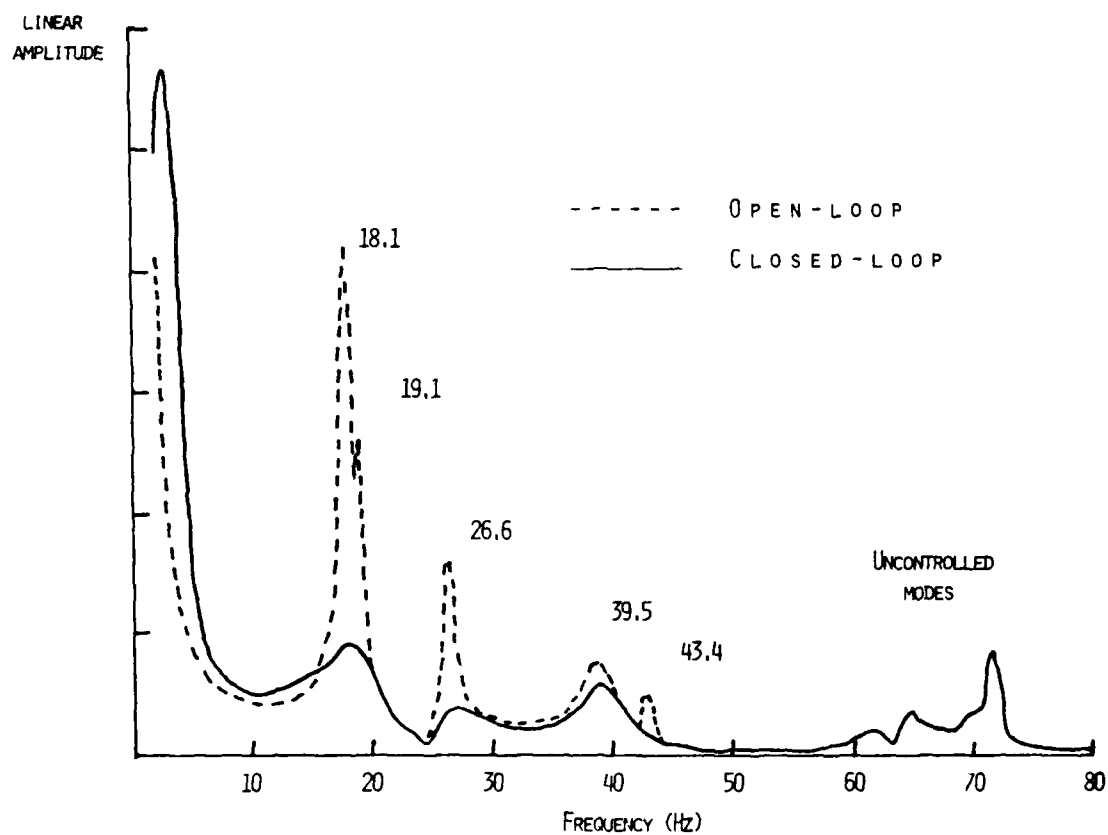


Figure 4-22 Circular Plate Experiment
Combined O/L & C/L Frequency
Responses of Sensors #5 & 6

TABLE XXVII Circular Plate Experiment Significant Results

Experimental validation of ACOSS technology achieved in the following areas:

- HAC/LAC control methodology verified
- Significant amounts of modal damping obtained
- Proof-mass actuators used in HAC schemes
- Multichannel μ -phase sensor applied to structural control
- Digital implementation demonstrated on high-order system

- System Identification & Modeling
- Filter Design
- Rigid Body Interactions
- Digital Mechanizations
- Actuator/Sensor Accuracy

From the experimental results, performance limitations and problems require more attention in the areas mentioned above. Performance is strongly related to model accuracy, thus identification is of prime importance. Filter design is also a gray area because of its dependence upon model errors and more theory is needed. The rigid body effects are not yet well understood and have been noticed both in the lab and in simulations. Finally better architecture is needed for microprocessor implementation of fast, high order, control algorithms.

4.4 TRUSS WHEEL EXPERIMENT

4.4.1 Description

This truss structure is about 2m across and made of thin stainless steel tubing (10 mil thickness). Lead weights are located at the vertices and the center hub contains a laser and beam splitter to provide sensing of the outside vertices rotations, via flat mirrors and linear photo detectors (Fig. 4-22a). This test setup is installed also in the Palo Alto Laboratory. The bracket holding the wheel suspension system is mounted on a concrete wall. Four optical detectors have been installed on the wheel, six accelerometers and four Pivoted Proof Mass (PPM) Actuators. Figure 4-23 shows the general nomenclature used for this system of actuators and sensors. The PPMs driving electronics has been installed in a mobile bay.

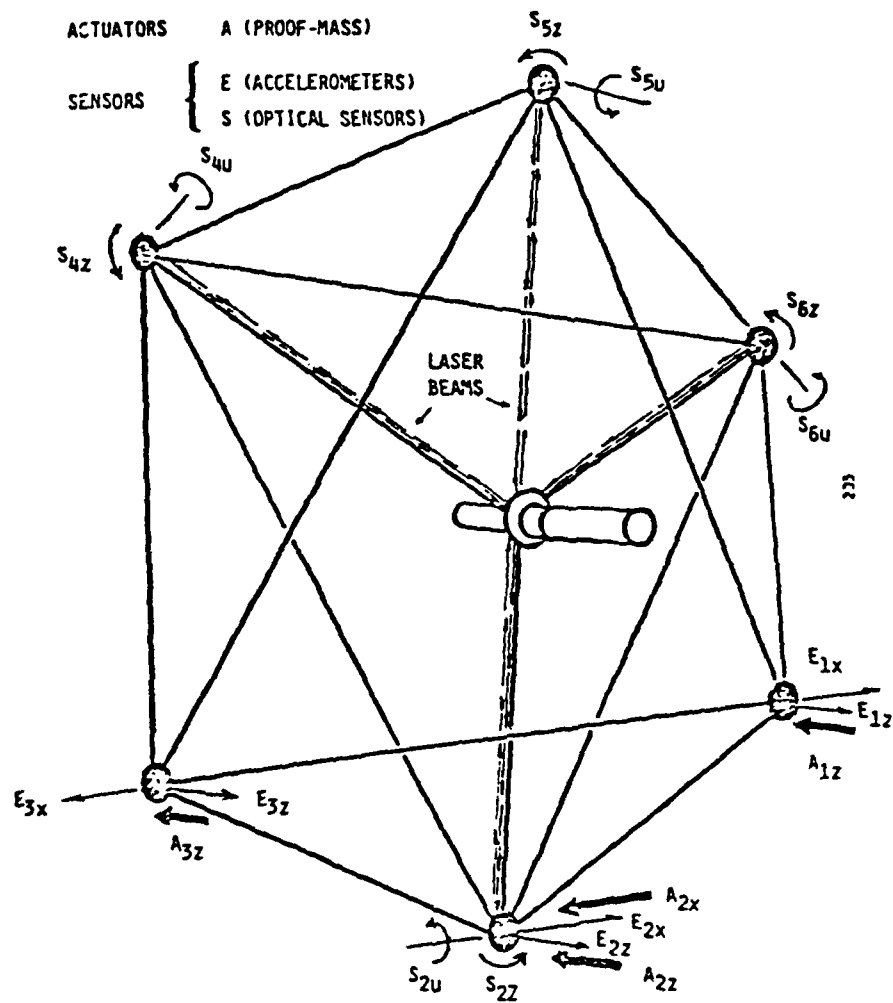


Figure 4-22a Wheel Actuators and Sensors

For the open-loop characterization test, 15 measurement channels were connected to the 11-23 processor, comprising 8 optical channels, 6 accelerometers and a force measurement channel corresponding to an accelerometer mounted in lieu of the proof-mass on the PPM actuator chosen for exciting the structure. In order to be able to characterize the wheel in a truly open-loop sense, it was necessary to disconnect the velocity servo-loop around the exciting PPM. Since then the actual force produced by the actuator was no longer known exactly (because of the actuator dynamics itself), it was necessary to measure this force, and this was done using an accelerometer mounted at the proof-mass location.

Wheel Finite Element Model

A finite element model was constructed which included 636 degrees of freedom. Front and side views of this model are shown in Fig. 4-22b. The center hub consists of a laser tube with balance weights at one end and it is modelled as a rigid bar with tip and central masses to match the main mass properties of the actual hub (i.e., mass, inertia, center of mass). The model includes details of the mirror mounted off the end of the PPM actuators. A perspective view of the complete model is shown in Fig. 4-22c. The total weight is 36.4 lbs. which matches exactly the measured weight.

Optical Sensor Model

The signals observed on the photo detectors result from various deformations of the wheel parts and need to be related to the modal amplitudes for the construction of a state-space model of the wheel. The picture shown in Figure 4-23 is a rough portrayal of one of the four optical systems. Motions of the spot (z) on the detector give rise to a pair of signals which may be used for estimation and control. These motions depend upon the various rotations and translations of the rigid hub (supporting both laser and detector) and of the mirror. Since these

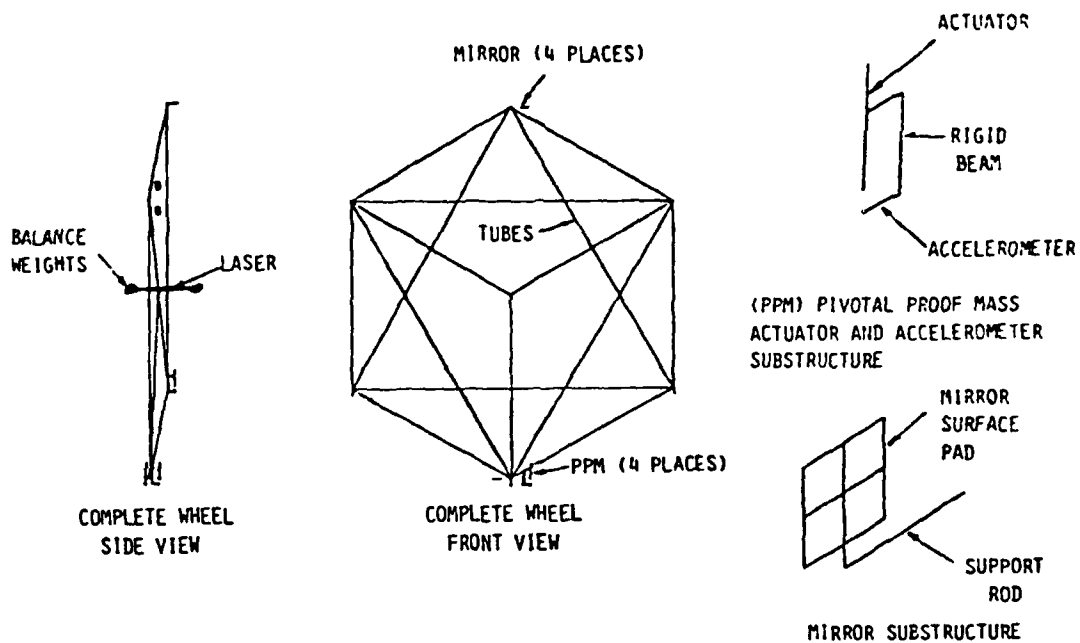


Figure 4-22b Components of the Wheel Finite Element Model

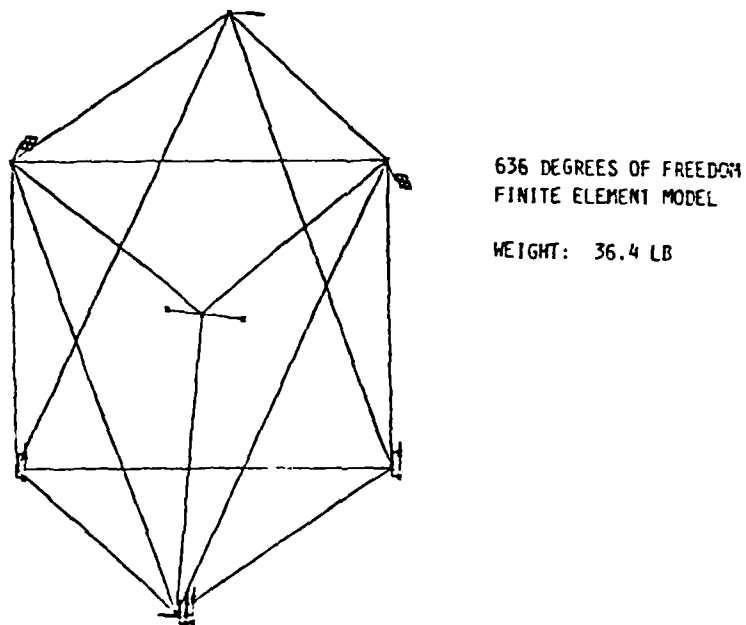
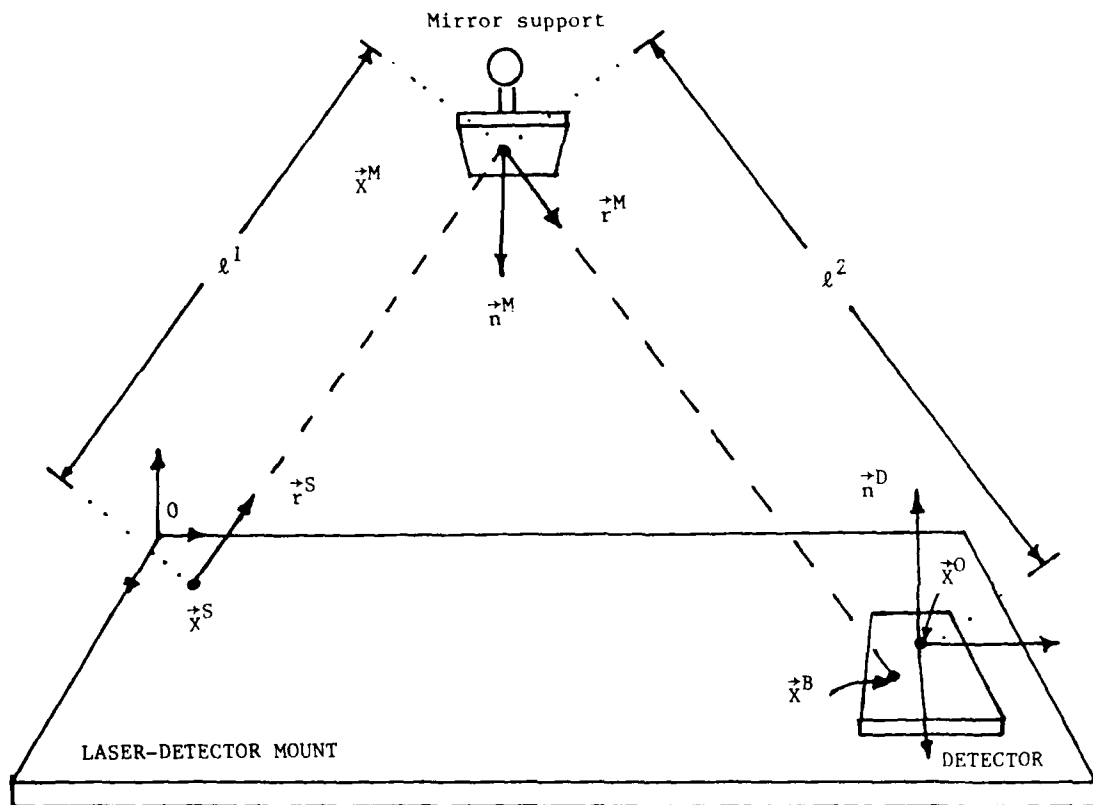


Figure 4-22c Complete Wheel Model



$$\vec{Z} = [\vec{X}^S + \vec{R}^S + \vec{R}^M] - \vec{X}^0 = \vec{X}^B - \vec{X}^0$$

Figure 4-23 Truss Wheel Experiment Optical System Model for Truss-Wheel

rotations and translations can be expressed in terms of vibration mode shapes, a relation of the type $y = M q$ may be obtained, where q is the vector of modal amplitudes, M a constant coefficient matrix and y the vector of voltage outputs from the detectors. For displacements of the spot compatible with the detector range (~ 30 mm), the linear approximations were accurate to better than 2% for the first 22 modes studied.

4.4.2 Test Plan

A matrix representation of the original test plan is shown in Fig. 4-24. The first test was to perform an open-loop characterization and compare the results to the finite element model. Because of the serious difficulties encountered in this comparison, test #4 was not conducted. The complex modal behavior exhibited by this structure will require more sophisticated tests and analyses. Since only a few modes were correlated with the model, a limited effort was made to synthesize a state estimator for this structure.

4.4.3 Results

Open Loop Characterization

The major difficulties encountered in this task were due principally to (a): the low natural damping (less than .3% of critical) and (b): the close packing of the modes. Item (a) made it necessary to use a very slow frequency sweep technique to make measurement near and at resonance. In fact, a "sweep and dwell" type of operation was required to obtain valid steady-state responses. This made the testing very time consuming at the low frequency end of the spectrum. Item (b) required that many sensors be used so that the mode shapes could be separated spatially rather than temporarily. However hardware failures and poor signal/noise ratios in some sensors reduced this capability. The "sweep & dwell" logic (also named SWIFT) is shown in Fig. 4-25 while the test setup is shown in

<u>TEST #</u>	<u>PURPOSE</u>	<u>EXCITER LOCATIONS</u>	<u>METHOD</u>	<u>RESULTS</u>
1	OPEN-LOOP MODAL CHARACTERIZATION	AZ1	NEW VAMP (SLOW SWEEP)	FREQUENCIES, DAMPING TRANSFER FUNCTIONS
2		AX1		
3		AZ3		
4	MODAL CHARACTERIZATION WILL LAC	AZ3	NEW VAMP INST. VAR. & MAX. LIKELIHOOD	SAME
5	STATE ESTIMATION	AZ3	OPTIMAL FILTER	FIRST 5 BENDING MODES

Figure 4-24 Wheel Test Matrix

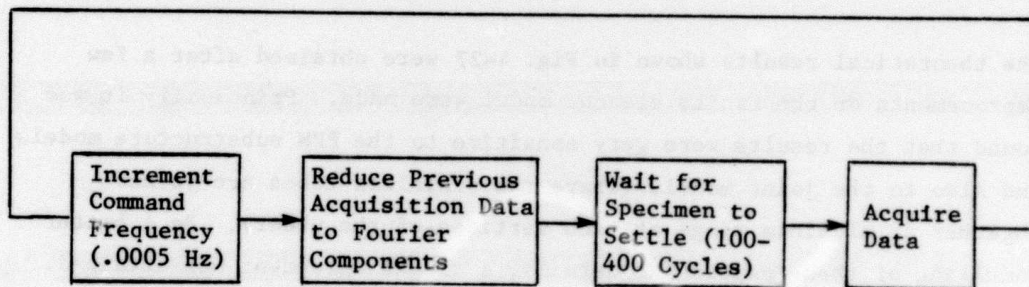


Figure 4-25 Sinewave Integration Fourier Transform
SWIFT
(VAMP Implementation)